THE EFFECTS OF FLOW ON RESISTIVE INSTABILITIES IN MAGNETOHYDRODYNAMICS

LEI HOU

A thesis submitted in partial fulfilment of the requirements of the University of Abertay Dundee for the degree of Doctor of Philosophy.

This research programme was carried out in collaboration with Dublin City University; the project was funded by EC Contract EUR FU 89/CCFP, EC, Brussels.

May, 1994

I certify that this thesis is the true and accurate version of the thesis approved by the examiners.

Signed [redacted] Date 6/10/94

(Director of Studies)

It looks like a butterfly's wing but with power of fusion in the sun; it sounds like symphonic music.

It is an unstable beauty!

This painting "The butterfly" was done by myself five years ago in China on my leaving for Western Europe to begin my overseas study. It has accompanied me during my postgraduate research and has been put beside my computer. It is a window of imagination different from the real and sophisticated computational work. After three years' PhD study during the writing-up process of my thesis, the computer figures presented here for the eigen-mode loci show a very surprisingly similar pattern to the painting besides the real computer window. Accordingly, I have entitled these complicated loci pattern figures as "the Butterfly's Wing"---they move on the paper driven by the various parameters.

Mathematics is no longer a collection of symbols, it is full of life. One may feel the power inside these operators; the dynamics which are represented by these variables; the capability and accuracy of these solutions for practical problems. It represents nature.

I would like to say that this is a combination or fusion of ART and SCIENCE which might supply nuclear energy for human civilization.

DECLARATION

I, Lei Hou, hereby certify that this thesis has been composed by myself, that it is a record of my own work and that it has not been presented in partial or complete fulfilment for any other degree or professional qualification.

Signed: [redacted] Date: 21 Oct. 1994

Certificate

I hereby certify that the candidate, Lei Hou, has fulfilled the conditions of the Resolution and Regulations appropriate to the degree of PhD.

Signature of supervisor: [redacted] Date: 21/10/94

Copyright

Acknowledgements

I would like to express my deep gratitude to my supervisor, Dr Richard B Paris, for his constant supervision, encouragement and invaluable assistance towards the completion of this thesis. I would also like to thank Professor Alastair D Wood and Dr Alan W Hood for advice on the project. Thanks also go to the Computer Centre in the University for their consistent useful technical help.
My sincere thanks to all friends for being there, and especially to my parents in China for their hearty support during my overseas study.
Finally, financial support from the Contract EUR FU 89/CCFP, EC, Brussels and the Department of Mathematical and Computer Sciences, University of Abertay Dundee are gratefully acknowledged.

SUMMARY

Resistive instabilities in MHD have been understood as one of the most important problems in astrophysical and controlled thermonuclear fusion research during the past four decades. This class of instability results from the introduction in the ideal MHD equations of a small but finite electrical resistivity. The addition of this term results in a relaxation of the "flux-freezing" constraint thereby enabling the plasma to change its magnetic field topology to a state of lower energy.

The model studied in this thesis is the plane magnetic current layer in which a gravitational acceleration acting normally to the magnetic surfaces is introduced to simulate the effects of magnetic field line curvature of more realistic geometries. The two main types of resistive instability considered are the resistive tearing mode and the resistive (gravitational) interchange (or G-) mode. The equations describing the linearized set of MHD equations have been derived for a viscous plasma in the presence of a sub-Alfvénic equilibrium flow along the confining magnetic field. In the limit of small electrical resistivity, the analysis of the stability problem follows the standard procedure of division of the current layer into a narrow resistive boundary layer about the "resonant" plane, where dissipative effects are important, together with an ideal, infinitely-conducting outer region where flux-freezing is a good approximation.

The determination of the normalized growth rate P of the instability presents itself in the form of a non-standard eigenvalue problem where the (complex) eigenvalue P appears both in the governing differential equation and in the boundary conditions. The dependence of P on the various parameters of the problem has been determined by two different methods of numerical solution. The first method employs a Fourier transform approach to reduce the boundary-layer equation to a third-order ordinary differential equation. The second approach applies to the boundary-layer equation directly and appeals to residue calculus. This alternative method of solution provides a means of verification of the numerical results.

A detailed investigation of the eigenvalue loci in the complex P-plane as a function of the equilibrium flow parameter and other physical parameters has been carried out. This study is supported by an asymptotic analysis of the boundary-layer equation for large values of the flow parameter and comparison is made with the numerical results.

The main contributions in this study include:

(i) A detailed understanding of the physical model and the derivation of the differential equations. The linearized stability of the plane current layer configuration has been carefully analysed.

(ii) For high temperature thermonuclear fusion plasmas, the magnetic Lundquist number is high and solution of the MHD system has been carried out by means of a standard boundary layer analysis to determine the dependence of the growth rate of the instability on the other parameters.

(iii) Numerical solution of the system of equations valid in the boundary layer has been initially carried out using Fourier transform techniques. An alternative method of solution of the boundary-layer equations has been implemented as a means of verification.

(iv) To explore the complicated eigen-loci structure, a very delicate numerical investigation has been undertaken. We obtain a good understanding on the loci spectrum bifurcation, visco-G mode exchange behaviour.

(v) By using a singular perturbation technique we have estimated the growth rate analytically in the large flow limit which confirms the numerical results and predicts the asymptotics of the growth rate.

THE EFFECTS OF FLOW ON RESISTIVE INSTABILITIES IN MAGNETOHYDRODYNAMICS

CONTENTS page

CHAPTER I

INTRODUCTION

Magnetohydrodynamics (MHD) is a macroscopic theory of describing a plasma (or ionised gas) as an electrically conducting fluid in the presence of magnetic fields; the subject is also sometimes called hydromagnetics or magneto-fluid mechanics. In the presence of a magnetic field an electric field is defined with respect to a particular frame of reference. From relativity theory, we know the transformation laws for the electric and magnetic fields in a frame of reference which moves with a velocity $\underline{V}$ with respect to a stationary frame of reference in which the electric and magnetic fields are $\underline{E}$ and $\underline{B}$ respectively. If a magnetised fluid moves, then an electric field is produced given by $\underline{E}+\underline{V}\times\underline{B}$. Since a plasma is highly electrically conducting, the current is proportional to the electric field $\underline{j}=\underline{E}/\eta$. Here $\underline{j}$ is the current density and η is the specific resistivity, which is independent of density ρ and proportional to $(KT_e)^{-3/2}$, where $K=1.38\times10^{-16} erg/^{o}K$ is Boltzmann's constant and T_e is the electron temperature. The electric current induced in the fluid as a result of its motion modifies the magnetic field and produces forces which can modify the motion of the fluid.

To describe a plasma in the magnetohydrodynamic approximation, we need the fluid equations for conservation of mass, momentum and energy, together with Maxwell's equations and constitutive relations. The addition of resistivity to the ideal MHD equations would dissipate away electric currents. However, it is important to realize that the addition of dissipation can produce new instabilities by removing constraints from the ideal equations.

1.1 Resistive Instabilities in MHD

The study of resistive magnetohydrodynamic instabilities (referred to as MHD instability modes thereafter) in high temperature plasmas is of great theoretical importance in controlled

thermonuclear fusion research, where it is required to magnetically confine a hot hydrogen plasma from all material contact for a sufficiently long period. The various kinds of experimental devices constructed have all been found to suffer to a greater or lesser degree from several types of plasma instabilities which impose severe limitations on the amount of current and pressure which can be confined by the magnetic field. Instabilities due to finite resistivity are also of considerable interest in astrophysics, where their application has been found in the study of solar flares, geomagnetic phenomena and in star formation theory.

The introduction of a small, but finite, electrical resistivity provides the plasma with an additional degree of freedom to reduce its potential energy. In an ideal, infinitely conducting plasma, magnetic lines of force that are initially distinct must remain so during any perturbation. This follows from the well-known flux-freezing constraint which states that the fluid must remain attached to the magnetic field lines. A resistive plasma, however, will have a density gradient, so that the plasma will tend to diffuse across the magnetic surfaces towards regions of lower density. The flux-freezing constraint will be relaxed in a resistive plasma and lines of magnetic force can "snap" and reconnect to change the magnetic field topology, giving rise to a new class of instabilities known as "resistive instabilities". This class of instabilities is analogous to the new modes of instability in hydrodynamics when the constraint of conservation of vorticity is relaxed by the introduction of finite viscosity.

The definition of instability is that an equilibrium is unstable if any small perturbation of the equilibrium grows in time. Different types of perturbation are possible and when they are studied separately it can be said that an equilibrium is stable or unstable to a particular mode. There are three basic types of resistive instability:

(i) a long wave-length "tearing mode" driven by a non-uniform equilibrium current density $j'\neq 0$, which corresponds to break up of the current layer along current flow lines;

(ii) a short wave-length "rippling mode" from an equilibrium resistivity gradient $\eta'\neq 0$; and

(iii) a short wave-length "gravitational interchange mode" (or G-mode), driven by the interaction of a gravitational acceleration with an inverted plasma density gradient $\rho'\neq 0$.

The gravitational acceleration introduced into the model can either be regarded as a means of simulating, in the simple plane slab model, magnetic field line curvature effects of more realistic laboratory confinement configurations, such as Tokamak machines, or may be

thermonuclear fusion research, where it is required to magnetically confine a hot hydrogen plasma from all material contact for a sufficiently long period. The various kinds of experimental devices constructed have all been found to suffer to a greater or lesser degree from several types of plasma instabilities which impose severe limitations on the amont of current and pressure which can be confined by the magnetic field. Instabilities due to finite resistivity are also of considerable interest in astrophysics, where their application has been found in the study of solar flares, geomagnetic phenomena and in star formation theory.

The introduction of a small, but finite, electrical resistivity provides the plasma with an additional degree of freedom to reduce its potential energy. In an ideal, infinitely conducting plasma, magnetic lines of force that are initially distinct must remain so during any perturbation. This follows from the well-known flux-freezing constraint which states that the fluid must remain attached to the magnetic field lines. A resistive plasma, however, will have a density gradient, so that the plasma will tend to diffuse across the magnetic surfaces towards regions of lower density. The flux-freezing constraint will be relaxed in a resistive plasma and lines of magnetic force can "snap" and reconnect to change the magnetic field topology, giving rise to a new class of instabilities known as "resistive instabilities". This class of instabilities is analogous to the new modes of instability in hydrodynamics when the constraint of conservation of vorticity is relaxed by the introduction of finite viscosity.

The definition of instability is that an equilibrium is unstable if any small perturbation of the equilibrium grows in time. Different types of perturbation are possible and when they are studied separately it can be said that an equilibrium is stable or unstable to a particular mode. There are three basic types of resistive instability:

(i) a long wave-length "tearing mode" driven by a non-uniform equilibrium current density $j'\neq 0$, which corresponds to break up of the current layer along current flow lines;

(ii) a short wave-length "rippling mode" from an equilibrium resistivity gradient $\eta'\neq 0$; and

(iii) a short wave-length "gravitational interchange mode" (or G-mode), driven by the interaction of a gravitational acceleration with an inverted plasma density gradient $\rho'\neq 0$.

The gravitational acceleration introduced into the model can either be regarded as a means of simulating, in the simple plane slab model, magnetic field line curvature effects of more realistic laboratory confinement configurations, such as Tokamak machines, or may be

regarded as resulting from a gravitational field, as would be appropriate in certain astrophysical applications. This latter gravitational interchange mode has an analogue in the Rayleigh-Taylor instability in hydrodynamics, where a heavy fluid is supported by a lighter fluid in a gravitational field or in an accelerating system.

The full set of MHD equations is a complicated non-linear system. MHD instability theory deals with small perturbations. It is however possible to expand the variables in the governing equations to obtain equations which are linear in the perturbed variables. The resulting theoretical problem can then be solved using the various techniques applicable to linear equations.

The two principal uses of MHD instability theory are the design and the analysis of experiments. Linear theory enables us to rule out strongly unstable configurations but does not by itself rule out the use of weakly unstable (usually nonlinear) systems. Instabilities are often observed in experiments. The central problem in controlled thermonuclear fusion is to minimize the instabilities (i.e. the rate of resistive diffusion) by using a well-designed magnetic field. In particular the experimental results help to decide which of a number of possible nonlinear effects are important. Conversely, the resulting theoretical models suggest useful experimental investigations.

In a typical laboratory plasma with density about 10^{13}~10^{14} ion-electron pairs per cm^3, each of these particles follows a complicated trajectory and it is necessary to follow each of these; prediction of the plasma's behaviour would then be a hopeless task. Fortunately, this is not usually necessary because, surprisingly, the majority-perhaps as much as 80%-of plasma phenomena observed in real experiments can be explained by a rather crude model. This model is that used in fluid mechanics, in which the identity of the individual particles is neglected as in an ordinary fluid; frequent collisions between particles keep the particles in a fluid element moving together. In the case of plasmas, the fluid contains electrical charges. It is surprising that such a model works for plasmas, which generally have infrequent collisions.

1.2 Basic MHD Equations

For a quasineutral plasma with singly charged ions, we can define the mass

density ρ, mass velocity $\underline{V}$, and current density $\underline{j}$ as follows

$$\rho =: n_i m_i + n_e m_e \approx n(m_i + m_e) \tag{1.1}$$

$$\underline{V} =: \frac{1}{\rho}(n_i m_i \underline{V_i} + n_e m_e \underline{V_e}) \approx \frac{m_i \underline{V_i} + m_e \underline{V_e}}{m_i + m_e} \tag{1.2}$$

$$\underline{j} =: ec(n_i \underline{V_i} - n_e \underline{V_e}) \approx nec(\underline{V_i} - \underline{V_e}) \tag{1.3}$$

where m_i, m_e denote the ion and electron masses, n_i, n_e the ion and electron number densities with $n_i \approx n_e = n$, $\underline{V_i}, \underline{V_e}$ are ion and electron velocities, c is the speed of light(mixed Gaussian units) and e is the electric charge. In the equation of motion, we shall add a term $m_i n \underline{g}$ for a gravitational force. This term can be used to represent any nonelectromagnetic force applied to the plasma. The ion and electron equations can be written as

$$m_i n \frac{d\underline{V_i}}{dt} = en(\underline{E} + \underline{V_i} \times \underline{B}) - \nabla p_i + m_i n \underline{g} + \underline{P_{ie}} \tag{1.4}$$

$$m_e n \frac{d\underline{V_e}}{dt} = -en(\underline{E} + \underline{V_e} \times \underline{B}) - \nabla p_e + m_e n \underline{g} + \underline{P_{ei}} \tag{1.5}$$

where $d/dt = \partial/\partial t + \underline{V} \cdot \nabla$ is the convective rate of change and $\underline{P_{ie}} = -\underline{P_{ei}} = \eta e^2 n^2 (\underline{V_e} - \underline{V_i})$ is the collision term. The combination of (1.4) and (1.5) yields, in the notations of (1.1)-(1.3),

$$n \frac{d}{dt}(m_i \underline{V_i} + m_e \underline{V_e}) = en(\underline{V_i} - \underline{V_e}) \times \underline{B} - \nabla \overline{p} + n(m_i + m_e)\underline{g}, \tag{1.6}$$

where $\overline{p} = p_i + p_e$ is the pressure. The electric field has cancelled out and leaves a simple momentum equation

$$\rho \frac{d\underline{V}}{dt} = \frac{\underline{j} \times \underline{B}}{c} - \nabla \overline{p} + \rho \underline{g}, \tag{1.7}$$

where $d\underline{V}/dt$ contains a nonlinear term $(\underline{V} \cdot \nabla)\underline{V}$. This is the single-fluid equation of motion describing the mass flow. The electric field does not appear explicitly because the

density ρ, mass velocity $\underline{V}$, and current density $\underline{j}$ as follows

$$\rho =: n_i m_i + n_e m_e \approx n(m_i + m_e) \tag{1.1}$$

$$\underline{V} =: \frac{1}{\rho}(n_i m_i \underline{V_i} + n_e m_e \underline{V_e}) \approx \frac{m_i \underline{V_i} + m_e \underline{V_e}}{m_i + m_e} \tag{1.2}$$

$$\underline{j} =: ec(n_i \underline{V_i} - n_e \underline{V_e}) \approx nec(\underline{V_i} - \underline{V_e}) \tag{1.3}$$

where m_i, m_e denote the ion and electron masses, n_i, n_e the ion and electron number densities with $n_i \approx n_e = n$, $\underline{V_i}, \underline{V_e}$ are ion and electron velocities, c is the speed of light(mixed Gaussian units) and e is the electric charge. In the equation of motion, we shall add a term $m_i n \underline{g}$ for a gravitational force. This term can be used to represent any nonelectromagnetic force applied to the plasma. The ion and electron equations can be written as

$$m_i n \frac{d\underline{V_i}}{dt} = en(\underline{E} + \underline{V_i} \times \underline{B}) - \nabla p_i + m_i n \underline{g} + \underline{P_{ie}} \tag{1.4}$$

$$m_e n \frac{d\underline{V_e}}{dt} = -en(\underline{E} + \underline{V_e} \times \underline{B}) - \nabla p_e + m_e n \underline{g} + \underline{P_{ei}} \tag{1.5}$$

where $d/dt = \partial/\partial t + \underline{V} \cdot \nabla$ is the convective rate of change and $\underline{P_{ie}} = -\underline{P_{ei}} = \eta e^2 n^2 (\underline{V_e} - \underline{V_i})$ is the collision term. The combination of (1.4) and (1.5) yields, in the notations of (1.1)-(1.3),

$$n \frac{d}{dt}(m_i \underline{V_i} + m_e \underline{V_e}) = en(\underline{V_i} - \underline{V_e}) \times \underline{B} - \nabla \overline{p} + n(m_i + m_e)\underline{g}, \tag{1.6}$$

where $\overline{p} = p_i + p_e$ is the pressure. The electric field has cancelled out and leaves a simple momentum equation

$$\rho \frac{d\underline{V}}{dt} = \frac{\underline{j} \times \underline{B}}{c} - \nabla \overline{p} + \rho \underline{g}, \tag{1.7}$$

where $d\underline{V}/dt$ contains a nonlinear term $(\underline{V} \cdot \nabla)\underline{V}$. This is the single-fluid equation of motion describing the mass flow. The electric field does not appear explicitly because the

fluid is neutral. The fluid dynamic theory is applicable to (1.7).

A less obvious equation is obtained by taking a different linear combination of the two-fluid equations. Let us multiply (1.4) by m_e and (1.5) by m_i and subtract the latter from the former. The result is

$$m_i m_e n \frac{d}{dt}(\underline{V}_i - \underline{V}_e) = en(m_i+m_e)\underline{E} + en(m_e\underline{V}_i + m_i\underline{V}_e)\times\underline{B} - m_e\nabla p_i$$

$$+ m_i\nabla p_e - (m_i+m_e)\underline{P}_{ei}. \qquad (1.8)$$

With the help of (1.1) and (1.3), (1.8) becomes

$$\frac{m_i m_e n}{e}\frac{d}{dt}\left(\frac{\underline{j}}{nc}\right) = e\rho\underline{E} - (m_i+m_e)ne\eta\frac{\underline{j}}{c} - m_e\nabla p_i + m_i\nabla p_e$$

$$+ en(m_e\underline{V}_i + m_i\underline{V}_e)\times\underline{B}. \qquad (1.9)$$

The last term can be simplified as follows:

$$m_e\underline{V}_i + m_i\underline{V}_e = m_i\underline{V}_i + m_e\underline{V}_e + m_i(\underline{V}_e - \underline{V}_i) + m_e(\underline{V}_i - \underline{V}_e)$$

$$= \frac{\rho}{n}\underline{V} - (m_i - m_e)\frac{\underline{j}}{nec}. \qquad (1.10)$$

Dividing (1.9) by $e\rho$, we now have the electron-magnetic constraint on the fluid

$$\underline{E} + \frac{\underline{V}\times\underline{B}}{c} - \frac{\eta\underline{j}}{c^2}$$

$$= \frac{1}{e\rho}\left\{\frac{m_i m_e n}{e}\frac{d}{dt}\left(\frac{\underline{j}}{nc}\right) + (m_i - m_e)\frac{\underline{j}\times\underline{B}}{c} + m_e\nabla p_i - m_i\nabla p_e\right\}. \qquad (1.11)$$

In the limit $m_e/m_i \to 0$ $(\rho \approx nm_i)$, this becomes

$$\underline{E} + \frac{\underline{V}\times\underline{B}}{c} = \frac{\eta\underline{j}}{c^2} + \frac{1}{en}\left(\frac{\underline{j}\times\underline{B}}{c} - \nabla p_e\right). \qquad (1.12)$$

This is the generalized Ohm's law. It describes the electrical properties of the conducting fluid. The $\underline{j}\times\underline{B}$ term is called the Hall current term. It often happens that this and the last

term are small enough to be neglected; in this case Ohm's law is then simply

$$\underline{E} + \frac{\underline{V}\times\underline{B}}{c} = \frac{\eta \underline{j}}{c^2}. \qquad (1.13)$$

The equation of continuity for the mass density ρ is easily obtained from the sum and difference of the ion and electron equations of continuity, namely

$$\frac{d}{dt}\rho + \rho\nabla\cdot\underline{V} = 0. \qquad (1.14)$$

In considering the truncated Maxwell equations we have

$$\underline{j} = \frac{c}{4\pi}\nabla\times\underline{B}, \quad \frac{\partial \underline{B}}{\partial t} = -c\nabla\times\underline{E}, \quad \nabla\cdot\underline{B} = 0 \qquad (1.15)$$

where $\underline{E}$, $\underline{j}$ are the electric field and current density, η is the isotropic electrical resistivity. Combining Ohm's law (1.13) with (1.15) yields the induction equation describing the rate of change of $\underline{B}$ due to fluid motions and resistive diffusion

$$\frac{\partial}{\partial t}\underline{B} = \nabla\times(\underline{V}\times\underline{B}) - \nabla\times\left(\frac{\eta}{4\pi}\nabla\times\underline{B}\right)$$

$$= \nabla\times(\underline{V}\times\underline{B}) + \frac{\eta}{4\pi}\nabla^2\underline{B}. \qquad (1.16)$$

The classical value of η is given by the Spitzer formula

$$\eta \sim 3.8\times10^3\, Z \ln\Lambda / T_e^{3/2}\ \Omega m\, cm,$$

where Z is the ionic charge, $\ln\Lambda$ is the Coulomb logarithm and T_e is the electron temperature in °K.

Note that (1.16) is analogous to the vorticity equation for an incompressible viscous fluid in hydrodynamics (obtained by taking the curl of the momentum equation)

$$\frac{\partial}{\partial t}\underline{W} = \nabla\times(\underline{V}\times\underline{W}) + \nu\nabla^2\underline{W}, \quad \underline{W}=\nabla\times\underline{V}$$

where ν is the uniform coefficient of kinematic viscosity. Comparing this with (1.16) when η is supposed uniform, shows the equivalence $\underline{W}\leftrightarrow\underline{B}$ and $\nu\leftrightarrow\eta/4\pi$. It follows that

when η is supposed uniform, shows the equivalence $\underline{W} \leftrightarrow \underline{B}$ and $\nu \leftrightarrow \eta/4\pi$. It follows that theorems on vorticity in hydrodynamics carry over to the behaviour of magnetic flux $\underline{B}$ in resistive MHD, with the viscous diffusion coefficient ν replaced by the resistive diffusion coefficient $\eta/4\pi$. Just as in hydrodynamics, one defines a Reynolds number Va/ν measuring the ratio of inertial to viscous forces, where V and a represent the characteristic speed and dimension of a particular problem, one defines a magnetic Reynolds number given by $4\pi aV/\eta$. This quantity provides a measure of the ratio of the convective and diffusion terms of (1.16)

$$\frac{|\nabla\times(\underline{V}\times\underline{B})|}{|\eta\nabla^2\underline{B}/4\pi|} \sim \frac{4\pi a}{\eta}V \equiv \text{magnetic Reynolds number.}$$

For $\eta=0$, the magnetic Reynolds number is infinite and (1.16) yields $\partial\underline{B}/\partial t = \nabla\times(\underline{V}\times\underline{B})$. In analogy with Kelvin's theorem in inviscid hydrodynamics, this equation represents the well-known flux-freezing equation; namely that in an infinitely conducting plasma, magnetic field lines are constrained to move with the plasma. If $4\pi aV/\eta \ll 1$, then (1.16) becomes essentially the resistive diffusion equation $\partial\underline{B}/\partial t \approx \eta\nabla^2\underline{B}/4\pi$, with the characteristic resistive diffusion time $\tau_R = 4\pi a^2/\eta$. This time scale can vary considerably according to the problem under consideration.

As a consequence of flux-freezing, a magnetic field line effectively has inertia and, in analogy with a stretched elastic string, leads to the possibility of transverse waves that propagate along the lines of force with the wave speed $V_A = B/(4\pi\rho)^{1/2}$. This speed is known as the Alfvén wave speed and defines another basic time scale, the hydromagnetic time scale $\tau_H = a(4\pi\rho)^{1/2}/B$ on which disturbances in the plasma propagate along the field. Again τ_H can vary enormously according to the parameters of the problem considered.

The ratio of the resistive diffusion to hydromagnetic time scales

$$S = \frac{\tau_R}{\tau_H} = \frac{4\pi a}{\eta}V_A$$

will be subsequently seen to be an important parameter in resistive instability theory. Of principal interest in this study is the case of high temperature plasmas for which η is small, so that the Lundquist (magnetic Reynolds) number S is large. Values of S for laboratory

thermonuclear fusion plasmas are typically in the range 10^3-10^7. In astrophysical applications, where the characteristic dimension a is extremely large, S is found similarly to be a large number. The significance of a high Lundquist number is that resistive diffusion effects are generally small and flux-freezing may be considered to hold to a good approximation. It will be seen in the following chapter that when $S>1$ resistive effects need only be taken into account in a narrow layer, known as a resistive boundary layer, in which strict flux-freezing is relaxed with the field decoupling from the plasma. Resistivity effects are then only important in this thin boundary layer.

In a highly conducting plasma confined by a sheared magnetic field (see Figure 1.1)

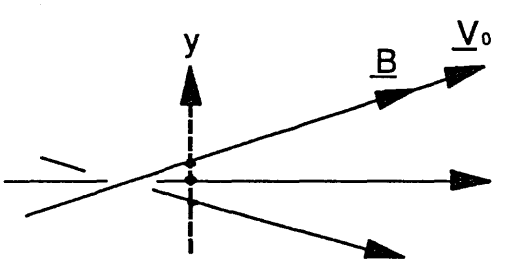

FIGURE 1.1 Sheared magnetic field. The direction of $\underline{B}_0$ changes with y. The flow $\underline{V}_0$ is along the magnetic field.

in the presence of a gravitational acceleration acting normal to the magnetic surfaces, the resistive modes---the so called tearing and G-modes---will be characterised by time scales which depend on the basic characteristic time scales τ_R, τ_H and the gravitational interchange

time scale τ_g of the problem. The time scale τ on which these modes grow in the linear regime is found to be scale like

$$\tau \sim \tau_R^a \tau_H^b \tau_g^c ,$$

where a, b and c are fractional powers with $|a|, |b| < 1$.

The G-mode is of importance in a variety of laboratory and astrophysical plasmas. The effective destabilizing 'gravitational' force in magnetic confinement devices may be interpreted as resulting from the interaction of an adverse plasma pressure gradient and weak magnetic field line curvature, or from the effects of plasma rotation. The simplest representation of this instability is the ideal, incompressible, magnetized plane plasma slab with a diffuse density profile $\rho_0(y)$ acted upon by a gravitational acceleration g in the positive y-direction. It is then well known that, for adverse density gradients $(\rho_0' > 0)$ and for short transverse wavelength perturbations about the equilibrium magnetic field, the linearized growth rate ω of Rayleigh-Taylor modes is characterized by $\tau_g \sim (-g\rho_0'/\rho_0)^{-1/2}$.

1.3 Review of Earlier Work on Resistive Instabilities

Resistive instabilities have been extensively studied both for laboratory and astrophysical applications. The first major theoretical study on the cases in the absence of equilibrium flow was presented by Furth, Killeen and Rosenbluth (1963) (hereinafter referred to as FKR) in their systematic and detailed investigation. Resistive instabilities have received much attention over the last three decades, both in linear and nonlinear regimes. On the other hand, it is necessary to determine the nonlinear effects of any instability to discover their ultimate consequences, particularly for the confinement properties of the plasma. Once an instability has grown to sufficiently large amplitude some or all of the nonlinear parts of the terms neglected in linear theory become important.

In the linear regime, the resistive tearing mode has been extended in several directions. In particular, a considerable number of analytical studies have been done on the effect of equilibrium flows on the inner problem using a constant internal field approximation. The order adopted in the asymptotic matching of the inner and outer solutions will be introduced in §2.2, in which the leading order solution in the resistive boundary layer is taken to be a

constant. A dispersion relation has been derived when the fluid and Alfvénic speed have approximately the same spatial profile. Hofmann (1975), Paris and Sy (1983) considered the influence of sub-Alfvénic flows parallel to the magnetic flux surfaces. Dobrott, Prager and Taylor (1977) showed that perpendicular flows, due to evolution of the equilibrium on the resistive time scale, must also be included in the linear stability problem. Dobrowolny and Paravano (1979) have shown the possible existence of a number of scalings with the resistivity that differ from the static case with and without viscosity. The effect of both parallel and perpendicular flows on the tearing mode was later studied in some detail by Bondeson and Persson (1986), who gave information about growth rates and marginal stability.

The effects of larger flows in the Alfvénic regime have been considered analytically by Chen and Morrison (1990a), numerically in linear calculations by Einaudi and Rubini (1986, 1989) and in non-linear calculations by Persson and Bondeson (1990) and Persson (1991). They found a stabilizing influence of flow when the flow shear is larger than the magnetic field shear in contrast to the results in the sub-Alfvénic regime (Paris and Sy, 1983; Bondeson and Persson, 1986). Paris, Wood and Stewart (1993) re-examined the effects of sub-Alfvénic equilibrium shear flow along the confining magnetic field. The investigation on the tearing mode yields that the ordering in the resistive boundary layer in the sub-Alfvénic regime is not the same as that of the Alfvénic regime; in the latter case, the matching condition of the outer solution is no longer independent of the equilibrium flow while in the sub-Alfvénic regime the matching condition is dependent upon the global structure of the equilibrium magnetic field rather than flow.

While the effects of flow on the inner problem have been studied in some detail, the effect of viscous flow on the outer problem is not well understood. Recently Chen and Morrison (1990b) showed analytically the influence of viscous flow in the outer region on the matching condition in slab geometry. This has been extended to cylindrical geometry using numerical techniques by Wessen and Persson (1991).

Substantial flows along the confining magnetic field have been observed in the laboratory in many Tokamaks, particularly during neutral beam injection. It is commonly believed that resistive modes are a likely source of Tokamak disturbance, especially the tearing and "gravitational interchange" modes. It is for this reason that the current study to investigate the

effects of equilibrium plasma flow along the equilibrium magnetic field has been undertaken.

1.4 Recent Study on Resistive Instabilities in MHD

As we know so far, the simplest theoretical model for the study of resistive instabilities is the MHD approximation. However, despite the simplicity of the model, the MHD theory of real situations is complicated by three basic sources. First, the geometries of interest in fusion research tend to be complicated. Secondly, there arise in the analysis resonant or singular surfaces which require some care in their treatment to the boundary layer problem and thirdly it is often necessary also to solve problems in the nonlinear development of instabilities. We should therefore pursue the linear theory in slab geometry to establish some of the foundations from the previous investigations on the tearing mode and flowless G-mode and, then solve a non-standard complex eigenvalue problem for the mixed tearing-G-mode. The recent study involves analytic and numerical investigations on a third-order differential equation which governs the behaviour of the mixed visco-tearing-gravitational interchange (or G-) modes. The equations describing the linearized set of MHD equations have been derived for a viscous plasma in the presence of a sub-Alfvénic equilibrium flow along the confining magnetic field. In the limit of small electrical resistivity, the analysis of the stability problem follows the standard procedure of division of the current layer into a narrow resistive boundary layer about the "resonant" plane, where dissipative effects are important, together with an ideal, infinitely-conducting outer region where flux-freezing is a good approximation. A substantial computation enables us to obtain the eigen-loci of viscous tearing and gravitational modes, which presents a detailed comparison with the hydrodynamic stability theory, such as the dual role played by viscosity; the bifurcation and the G-mode instability exchange behaviour. Finally, by use of singular perturbation theory, we estimate asymptotically the dominant behaviour of the instability growth rate in the large flow limit which might supply useful information of simulating the hydrodynamic Kelvin-Helmholtz instability.

1.4.1 Analogy with Hydrodynamic Stability

In dealing with resistive MHD instabilities, we are involved with a boundary-layer problem which has an analogy in hydrodynamic stability theory. The essential problems of

hydrodynamic stability were recognized and formulated in the nineteenth century, notably by Helmholtz, Kelvin, Rayleigh and Reynolds. Hydrodynamic stability has been considered as one of the central problems of fluid mechanics. It is concerned with *when* and *how* laminar flows break down, their subsequent development and their eventual transition to turbulence.

Broadly speaking, one may say that instability occurs because there is some disturbance of the equilibrium of the external forces, inertia and viscous stresses of a fluid. External forces of interest are buoyancy in a fluid of variable density, surface tension, etc. It is also convenient to regard centrifugal force as an external force when there is rotation of the whole system in which the fluid moves. If heavy fluid rests above light fluid it is clear that the fluid will tend to overturn under the action of gravity.

It might be conjected, from general physical arguments, that viscous forces will contribute a stabilizing effect by tending to damp out the disturbances. If one further observes that instability generally occurs at large Reynolds number, $S_R = \rho LV/\mu$, where ρ is the fluid density, L a characteristic length, V a characteristic flow velocity and μ is the viscosity, then one might reason that the principal features of the mechanism of instability may be obtained by first neglecting viscous forces, and incorporating them later as a stabilizing influence. There is also an obvious advantage of such an approach from the point of view of simplicity of analysis. Since viscous terms contain spatial derivatives of the highest order, their neglect would reduce the order of the differential equations.

Rayleigh (1883) found that, for parallel flows to be unstable, the velocity distribution must show a point of inflexion. Later, Tollmien (1935) showed that this condition is also sufficient for velocity distributions of certain general types. A physical mechanism for interpreting this result was described by Lin (1945), using an acceleration formula derived on the basis of von Kármán's mechanism of vorticity redistribution (1934).

However, a comparison of the conclusions in the viscous and non-viscous studies reveals the rather surprising result that viscous forces can serve as a cause of instability *viscous forces can serve as a cause of instability*. In the absence of viscosity, the motion is stable with respect to disturbances of a given wavelength, provided the Reynolds number is high enough. For wavelengths beyond a certain lower limit, there is always a finite range of Reynolds number for which the motion is unstable. Thus, an increase

of viscosity could actually induce instability. On the other hand, the motion is completely stable if the Reynolds number is sufficiently low, as one would expect from the damping influence of viscous forces. The viscous forces are shown to be capable of inducing a viscous stress when we consider a perturbed viscous flow, which is absent in the inviscid case. If this stress converts energy from the basic flow into the disturbance, it could induce instability. It will be discussed that this stress is possibly favourable to the conversion of energy into the disturbance motion.

1.4.2 Stability and Instability in MHD Analysis

The MHD instability problem we consider here is that of a sheared magnetic field confining a hot plasma with the equilibrium flow caused by neutral beam injection. The study follows the same manner as in hydrodynamics, the inviscid case first and then the viscous flow. We then investigate the growth rate of the perturbation. If the perturbed quantity tends to increase, the motion is defined as unstable; otherwise the motion is stable.

In considering a perturbation with a wave vector $\underline{k}=\{k_x, 0, k_z\}$, there are interactions between the wavefront and magnetic field line $\underline{B_0}$ and flow $\underline{V_0}$ which are parallel to the x axis. Here, the wave parallel to the magnetic field is called an Alfvén wave, which is a transverse disturbance propagating along the magnetic lines of force with the Alfvén speed $V_A=B_0/\sqrt{4\pi\rho}$, where ρ is the fluid density and B_0 is the magnetic field strength.

In MHD instability analysis, either a physical boundary or an interface between fluids occurs, across which different solutions should be matched. In this situation a geometrical surface is presumed to exist between the two regions in which the field variables are related by matching conditions which allow special kinds of discontinuities to take place in certain field variables when crossing the surface. Mathematically, it is necessary to give a precise definition for the jump occuring in the perturbed quantities to account this most obvious type of discontinuity in the boundary layer (ideal or resistive layers). The jump conditions for either a weak discontinuity, in which the perturbed quantity itself is continuous across the surface but where some derivative of it may be discontinuous, or a strong discontinuity occurs in the theory of magnetohydrodynamic shocks, where the incompressible fluid experiences discontinuity across the surface, they are treated as two different problems. We only consider weak discontinuities in this thesis. The ordering of the perturbed quantities adopted here

enables us to limit the analysis to a surface with weak discontinuity in a thin resistive boundary layer.

As the most recent study relevant to the problem is to shed further light on the complicated investigations in the long wavelength and short wavelength limits, we shall choose this type of mathematical definition of a perturbation and will use it to determine the behaviour of the perturbation itself and of the solutions behind it.

1.5 Structure of the Thesis

The study of the effects of flow on the resistive modes so far (see §1.3) has concentrated on the tearing mode, with or without viscosity. These previous investigations included all physical aspects of the conservational system except the external force acting on the system. The purpose of the present study is to attempt to extend these investigations to deal with the effects of both viscous and non-viscous plasma flow on the resistive gravitational mode which results from an external force as stated in §1.1. The possible instability (G-mode) is driven by an inverted density gradient or an inverted pressure gradient in a curved magnetic field. We shall see, however, that the gravitational mode cannot be studied separately from the tearing mode, but that a certain degree of mode-mixing is inevitable. The effects of gravitational acceleration on the flowing tearing mode, the mixing of the modes and instability exchange behaviour, will be examined in great detail in this investigation.

The model considered is the simple plane current layer with a plasma flow directed along the sheared magnetic field, with a 'gravitational' acceleration acting normal to the plane of the layer. The method we adopt is an analytical-computational approach using the standard division (in the limit of high magnetic Lundquist number) of the current layer into two regions: a concentration of the dynamics and dissipative effects in a narrow layer centred about the 'resonant' surface and an 'outer' infinitely conducting region where approximate flux-freezing holds. The problem thus takes on the form of a 'sheet pinch type' boundary layer problem with the instability growth rate being determined by asymptotically matching the solution in the boundary layer to that valid in the outer infinitely conducting regions. Therefore a systematic review and numerical estimates on finite-resistivity instabilities of a sheet pinch in the absence of equilibrium flow has been undertaken in Chapter 3. This study

is of fundamental importance in our investigation.

This thesis consists of seven chapters. Each chapter contains an introduction part. In Chapter 2 we introduce the fundamental derivation of the MHD bounday-layer equations and the standard physical scales. Chapter 3 contains a discussion of the flowless resistive modes based on the analysis of FKR. For non-zero values of the flow parameter, we present numerical methods in Chapter 4 to obtain the eigenvalue of the differential system, which is the growth rate of the instability for the inviscid case. We discuss the effects of viscosity in Chapter 5. In Chapter 6 a singular perturbation method has been employed to determine asymptotically the growth rate for large values of flow. Finally, we conclude the effects of flow on the leading behaviour of the mixed visco-resistive tearing and G-modes, and discuss the possible directions for further studies on MHD instability theory in Chapter 7.

CHAPTER III

FORMULATION OF THE BOUNDARY-LAYER EQUATIONS

Introduction

A fundamental derivation of the boundary-layer equation is to be carried out in this chapter for the investigation of the effects of flow on MHD visco-resistive instabilities. The combination of numerical-analytical method will be adopted in the limit of high magnetic Lundquist number to deal with a boundary-layer problem: a narrow layer centred about the "resonant" surface, in which a small but finite resistive diffusion is allowed to take place; and an external flux-freezing region where the Lundquist number approaches infinity. We then end up considering a boundary-layer problem where the instability growth rate is determined by asymptotically matching the solution in the narrow boundary-layer to that valid in the outer infinitely conducting region. The matching order of the balancing algebra is in the sub-Alfvénic regime. It will turn out that the instability growth rate appears in a non-standard way as the eigenvalue parameter in an ordinary differential equation boundary value problem. The location of this eigenvalue parameter in the complex plane, which we determine by asymptotically-induced numerical methods, will decide the stability, or otherwise, of the system.

2.1 Model and Governing Equations

We begin by considering the simple slab model consisting of an infinite plane current layer specified by the equilibrium sheared magnetic field

$$\underline{B}_0=\underline{e}_x B_{ox}(y)+\underline{e}_z B_{oz}(y)\ ,\ \underline{V}_0=\underline{e}_x V_{ox}(y)+\underline{e}_z V_{oz}(y)$$

subject to a gravitational acceleration $\underline{e}_y g$ acting in the positive y-direction. The equilibrium flow $\underline{V}_0$ is parallel to $\underline{B}_0$. The equilibrium density ρ is assumed to vary only in the y-

direction. We consider the resistive MHD equations for incompressible plasma, with uniform resistivity and including only the perpendicular component of the collisional part of the viscous tensor. The equations are

$$\nabla\times\rho\left(\frac{\partial \underline{V}}{\partial t}+\underline{V}\cdot\nabla\underline{V}\right)=\nabla\times\left[\frac{1}{c}(\underline{j}\times\underline{B})+\rho\underline{g}+\mu_{\perp}\nabla^{2}\underline{V}\right], \tag{2.1}$$

$$\frac{\partial \underline{B}}{\partial t}=\nabla\times(\underline{V}\times\underline{B})+\frac{\eta}{4\pi}\nabla^{2}\underline{B}, \tag{2.2}$$

$$\frac{\partial \rho}{\partial t}+\nabla\cdot(\rho\underline{V})=0, \tag{2.3}$$

$$\nabla\cdot\underline{B}=\nabla\cdot\underline{V}=0, \tag{2.4}$$

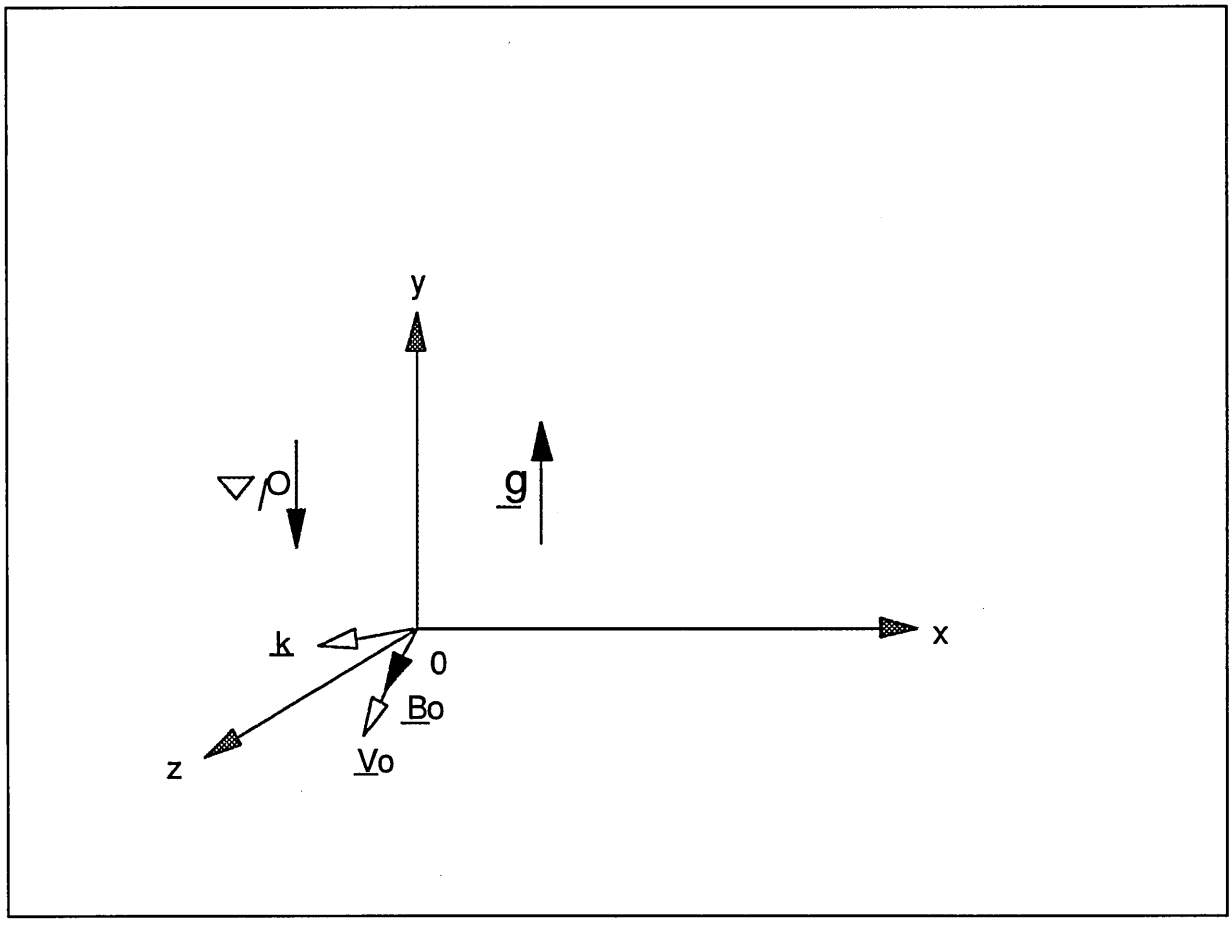

Figure 2.1 Slab geometry consisting of an infinite plane current layer specified by the equilibrium magnetic field $\underline{B}_0$, where $\underline{V}_0 \| \underline{B}_0$, $\underline{k} \perp \underline{B}_0$ on the plane y=0.

where η and $\mu_\perp$ are the resistivity and perpendicular coefficient of viscocity which are assumed uniform. The flow speed, magnetic field and fluid density consist of the equilibrium quantity and the perturbed quantity, $\underline{V}=\underline{V}_0+\underline{V}_1$, $\underline{B}=\underline{B}_0+\underline{B}_1$ and $\rho=\rho_0+\rho_1$, where $\underline{V}_1$, $\underline{B}_1$ and ρ_1 are perturbed quantities.

From the Maxwell equations, we have

$$\underline{j} = \frac{c}{4\pi}\nabla\times\underline{B},$$

so that

$$\frac{1}{c}\nabla\times(\underline{j}\times\underline{B}) = \frac{1}{c}\nabla\times(\frac{c}{4\pi}\nabla\times\underline{B})\times\underline{B} = \frac{1}{4\pi}\nabla\times[(\underline{B}\cdot\nabla)\underline{B}-\frac{1}{2}\nabla B^2]$$

$$= \frac{1}{4\pi}\nabla\times(\underline{B}\cdot\nabla)\underline{B}.$$

The momentum equation may then be written as

$$\nabla\times\rho(\frac{\partial\underline{V}}{\partial t}+\underline{V}\cdot\nabla\underline{V}) = \nabla\times[\frac{1}{4\pi}(\underline{B}\cdot\nabla)\underline{B}+\rho\underline{g}+\mu_\perp\nabla^2\underline{V}]. \qquad (2.5)$$

Linearization, followed by application of the operator $\underline{e}_y\cdot\nabla\times$ to the curled momentum equation (2.5) yields two coupled equations describing the y-components of the first order velocity V_{y1} and magnetic field B_{y1}. Taking all perturbed quantities to vary like $\exp[i(k_x x+k_z z)+\omega t]$ where $\underline{k}=\{k_x, 0, k_z\}$ is the horizontal wave vector and ω is the growth rate, we then find from (2.5)

$$\underline{e}_y\cdot\nabla\times\nabla\times\rho_0(\frac{\partial}{\partial t}\underline{V}_1+\underline{V}_0\cdot\nabla\underline{V}_1+\underline{V}_1\cdot\nabla\underline{V}_0)$$
$$=\underline{e}_y\cdot\{\frac{1}{4\pi}\nabla\times\nabla\times[(\underline{B}_0\cdot\nabla)\underline{B}_1+(\underline{B}_1\cdot\nabla)\underline{B}_0]+\nabla\times\nabla\times(\rho_1\underline{g}+\mu_\perp\nabla^2\underline{V}_1)\}. \qquad (2.6)$$

We now evaluate each term in (2.6) separately as follows. The terms on the left-hand side simplify to

$$\underline{e}_y\cdot\nabla\times\nabla\times\rho_0\frac{\partial}{\partial t}\underline{V}_1=\omega[k^2\rho_0 V_{y1}-(\rho_0 V'_{y1})'], \qquad (2.7)$$

$$\begin{aligned}&\underline{e_y}\cdot\nabla\times\nabla\times\rho_0(\underline{V_0}\cdot\nabla)\,\underline{V_1}\\&=i\,[k^2\rho_0(\underline{k}\cdot\underline{V_0})\,V_{y1}-(\rho_0(\underline{k}\cdot\underline{V_0}))'V_{y1}'-\rho_0(\underline{k}\cdot\underline{V_0})\,V_{y1}''],\end{aligned}\tag{2.8}$$

and

$$\underline{e_y}\cdot\nabla\times\nabla\times\rho_0(\underline{V_1}\cdot\nabla)\,\underline{V_0}=i\,[(\underline{k}\cdot\underline{V_0})''\rho_0V_{y1}+(\underline{k}\cdot\underline{V_0})'(\rho_0V_{y1})'],\tag{2.9}$$

where the prime denotes differentiation with respect to y, while the terms on the right-hand side simplify to

$$\underline{e_y}\cdot\nabla\times\nabla\times(\underline{B_0}\cdot\nabla)\,\underline{B_1}=i\,[k^2(\underline{k}\cdot\underline{B_0})\,B_{y1}-(\underline{k}\cdot\underline{B_0})'B_{y1}'-(\underline{k}\cdot\underline{B_0})\,B_{y1}''],\tag{2.10}$$

$$\underline{e_y}\cdot\nabla\times\nabla\times(\underline{B_1}\cdot\nabla)\,\underline{B_0}=i\,[(\underline{k}\cdot\underline{B_0})''B_{y1}+(\underline{k}\cdot\underline{B_0})'B_{y1}'],\tag{2.11}$$

$$\underline{e_y}\cdot\nabla\times\nabla\times\rho_1\underline{g}=k^2\rho_1g,\tag{2.12}$$

$$\underline{e_y}\cdot\nabla\times\nabla\times\mu_\perp\nabla^2(\underline{V_1})=-\mu_\perp(\nabla^2)^2V_{y1}=-\mu_\perp\left(\frac{\partial^2}{\partial y^2}-k^2\right)^2V_{y1}.\tag{2.13}$$

In the gravitational term (2.12), the density perturbation ρ_1 can be eliminated using the linearized form of (2.3), namely $\rho_1[\omega+i(\underline{k}\cdot\underline{V_0})]+\rho_0'V_{y1}=0$, so that

$$k^2\rho_1g=-k^2g\frac{\rho_0'V_{y1}}{\omega+i(\underline{k}\cdot\underline{V_0})}.\tag{2.14}$$

Following Furth, Killeen and Rosenbluth (1963), we now introduce the standard dimensionless variables

$$\Psi=\frac{B_{y1}}{B},\quad W=-ik\tau_RV_{y1},\quad F=\frac{\underline{k}\cdot\underline{B_0}}{kB},\quad \alpha=ka,$$

$$p=\omega\tau_R,\quad S=\frac{\tau_R}{\tau_H},\quad \rho=\frac{\rho_0}{\langle\rho\rangle},\quad k^2=k_x^2+k_z^2,\quad y=a\mu$$

$$R^* = \tau_R \underline{k}\cdot\underline{V}_0(y) \ , \quad G = -g\frac{\rho_0'}{\rho_0}\tau_H^2 , \quad N^* = 4\pi\frac{\mu_\perp}{\eta} .$$

Here $\tau_R = 4\pi a^2/\eta$ and $\tau_H = a\sqrt{4\pi\rho}/B$ are the resistive and hydrodynamic time scales of the layer, S is the Lundquist (magnetic Reynolds) number, $\langle\rho\rangle$ and B are measures of the density and magnetic field strength and a is the characteristic dimension of the current layer. F denotes the scaling of the magnetic shear and R^* is the scaling of the fluid shear on the resistive diffusion time scale.

The time scales τ_R and τ_H can vary considerably according to the problem under consideration; for example, in the interior of stars $\tau_R \sim 10^9$ years, in Sun spot regions $\tau_R \sim 50$ years while in laboratory thermonuclear fusion plasmas $\tau_R \sim 10$ msec and for typical neutral hydrogen (HI) clouds of 10^4 solar masses, density $10\, m_H$ and magnetic fields of 10^{-6} gauss, $\tau_H \sim 10^7$ years whereas in laboratory thermonuclear fusion plasmas $\tau_H \sim 10^{-6}$ sec. The ratio of the resistive diffusion to hydrodynamic time scales is very large. The values of S for laboratory thermonuclear fusion plasmas are typically in the range $10^3 - 10^7$. In astrophysical applications where the characteristic dimension a is extremely large, S is found similarly to be a large number. The significance of a high magnetic Lundquist number is that resistive diffusion effects are small and flux-freezing may be considered to hold as a good approximation.

In terms of these variables, we have from (2.7)-(2.14) for the left-hand side of (2.6)

$$\underline{e_y}\cdot\nabla\times\nabla\times\rho_0\left[\frac{\partial}{\partial t}\underline{V}_1 + \underline{V}_0\cdot\nabla\underline{V}_1 + \underline{V}_1\cdot\nabla\underline{V}_0\right]$$

$$= \omega\left[k^2\rho_0 V_{y1} - (\rho_0 V_{y1}')'\right] + i\left[k^2\rho_0(\underline{k}\cdot\underline{V}_0)V_{y1} - \rho_0(\underline{k}\cdot\underline{V}_0)V_{y1}'' + \rho_0(\underline{k}\cdot\underline{V}_0)''V_{y1}\right]$$

$$= -\frac{\langle\rho\rangle}{ika^2\tau_R^2}\left\{(p+iR^*)\left[(\rho W')' - \alpha^2\rho W\right] - i\left[\rho(R^*)'\right]'W\right\}, \qquad (2.15)$$

where the prime now denotes differentiation with respect to μ. For the right-hand side of (2.6), we have

$$\underline{e}_x \cdot \{\nabla\times\nabla\times\frac{1}{4\pi}\,[\,(\underline{B}_0\cdot\nabla)\,\underline{B}_1 + (\underline{B}_1\cdot\nabla)\,\underline{B}_0] + \nabla\times\nabla\times(\rho_1\underline{g} + \mu_\perp\nabla^2\underline{V}_1)\,\}$$

$$= \frac{i}{4\pi}\,[k^2(\underline{k}\cdot\underline{B}_0)\,B_{y1} - (\underline{k}\cdot\underline{B}_0)\,B_{y1}'' + (\underline{k}\cdot\underline{B}_0)''B_{y1}] + k^2\rho_1 g - \mu_\perp\nabla^4 V_{y1}$$

$$= i\frac{\langle\rho\rangle}{ka^2\tau_R^2}\,\{\,[\Psi'' - (\alpha^2 + \frac{F''}{F})\,\Psi]\,F\alpha^2S^2 + \frac{\alpha^2S^2GW}{p+iR^*} + N^*(\frac{d^2}{d\mu^2} - \alpha^2)^2 W\}\,. \quad (2.16)$$

Hence, the momentum equation finally becomes

$$(p+iR^*)\,[(\rho W')' - \alpha^2\rho W] - i\,[\rho\,(R^*)']'W + \frac{\alpha^2S^2GW}{p+iR^*}$$

$$= [\Psi'' - (\alpha^2 + \frac{F''}{F})\,\Psi]\,\alpha^2S^2F + N^*(\frac{d^2}{d\mu^2} - \alpha^2)^2 W. \quad (2.17)$$

Likewise, linearization and taking the $y-$ component of the induction equation (2.2) yields

$$\omega B_{y1} = i\,(\underline{k}\cdot\underline{B}_0)\,V_{y1} - i\,(\underline{k}\cdot\underline{V}_0)\,B_{y1} + \frac{\eta}{4\pi}\nabla^2 B_{y1}\,. \quad (2.18)$$

The dimensionless form of the induction equation is therefore

$$(p+iR^*)\,\Psi + FW = \Psi'' - \alpha^2\Psi\,. \quad (2.19)$$

The system of equations describing the resistive tearing and gravitational modes in the presence of an equilibrium shear flow is given by (2.17) and (2.19). The equilibrium diffusion velocity normal to the equilibrium magnetic surfaces has been neglected, as we are looking for incompressible modes in the large S limit with growth rate on time scales significantly shorter than that of ordinary resistive diffusion---that is, growth rates scaling like a fractional power of η as $\eta\to 0$, i.e. $\omega \sim \eta^l$, $0 < l < 1$. .

Bondeson and Persson (1986) observed, however, that the concentration of the dynamics to a thin boundary layer makes the resistive instability sensitive to the perpendicular equilibrium diffusion $v_\perp \sim \eta$. They recognized that the neglect of the resistive diffusion in the FKR paper (1963) is not strictly correct as the perpendicular flow will affect the growth

rate of the resisitive instabilities. The time for a fluid element to diffuse through the resistive boundary layer is $\delta / v_{\perp} \sim \eta^{-3/5}$, which is same as the tearing mode time scale.

2.2 Boundary-layer Problem

In the high conductivity limit, $S = \tau_R / \tau_H \to \infty$, as we are considering small but finite resistivity η, the analysis follows the standard procedure of division of the plasma into two regions:

(a) a narrow boundary-layer centred about the resonant plane $F \equiv (\underline{k} \cdot \underline{B}_0) = 0$, and

(b) an external infinite conductivity region, away from $F \simeq 0$.

The growth rate p is calculated from the condition that the discontinuity in Ψ' in the external infinite conductivity region match to the corresponding quantity in the boundary layer. The equation for Ψ in the ideal region away from $F \simeq 0$, is from (2.17) when G is sufficiently small, given by

$$\Psi'' - (\alpha^2 + \frac{F''}{F})\Psi = 0. \qquad (2.20)$$

The solution Ψ which decays exponentially in the external region as $\mu \to \pm\infty$, or vanishes at conducting boundaries, is discontinuous across the surface $F=0$, which we take without loss of generality to be $\mu = 0$. On the scale of the current layer, the perturbed field component Ψ_1 will appear to have a discontinuity in its first derivative given by

$$\Delta' = \frac{\Psi'(0+) - \Psi'(0-)}{\Psi(0)} = \left[\frac{d}{d\mu} \ln \Psi\right]_{0-}^{0+}. \qquad (2.21)$$

The growth rates of the resistive modes are then determined by requiring that the solution in the resistive layer around $F = 0$ match the discontinuity Δ'_{ext} in the "external" solution. We then need to calculate the change in logarithmic derivative $\Delta'_{int}(p)$ of the "internal" solution across the resistive boundary layer, and the growth rate p found from the eigenvalue equation

$$\Delta'_{int}(p) = \Delta'_{ext}. \qquad (2.22)$$

For example, if $F = \tanh\mu$, then the dimensionless momentum equation (2.20) yields the external solution in the perfectly conducting region away from $F=0$ (see Fig.2.2)

$$\Psi_{ext} = e^{-\alpha|\mu|}\,(\alpha + |\tanh\mu|)\,. \qquad (2.23)$$

The external solution (2.23) holds everywhere in the outer infinite conducting region when the magnetic Lundquist number $S \to \infty$, except in the boundary layer of thickness δ about the resonant surface of $F=0$. The corresponding matching condition in (2.21) in this special case then becomes

$$\Delta'_{ext} = 2\,(\frac{1}{\alpha} - \alpha)\,. \qquad (2.24)$$

The equilibrium flow along the field is considered to be significantly sub-Alfvénic (Paris and Sy, 1983). In terms of the ordering with the resistivity, we choose V_0 to scale

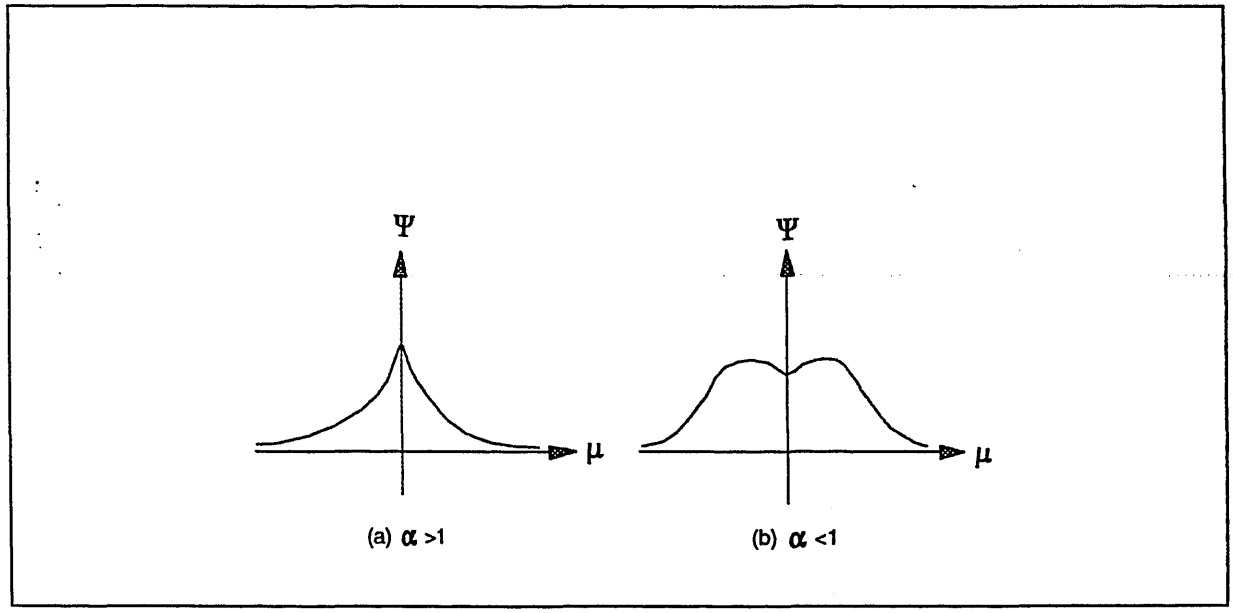

FIGURE 2.2 The external solution Ψ: (a) when α>1 and (b) when α<1.

like $\eta^{1/5}$ (i.e. $V_0 \sim S^{-1/5}V_A$, where V_A is the Alfvén speed). Such an ordering, which corresponds approximately to the range of observed toroidal rotation speeds resulting from neutral beam injection in Tokamak experiments, leads to the following simplifications of the problem:

(i) The effects of flow are thereby confined to the thin resistive boundary layer so that the Kelvin-Helmholtz instability is not excited.

(ii) It is the lowest flow $(V_0 \sim S^{-1/5}V_A)$ which produces a change of the scaling of the FKR flowless growth rate (Paris and Sy, 1983) as the FKR flowless instability condition, $\Delta'_{ext} > 0$, is modified to yield the possibility of instability when $\Delta'_{ext} \leq 0$.

(iii) The solution in the external region is not affected by the flow, thus we need only consider the effect of the flow in the resistive boundary layer. In mathematical terms,

$$\Delta' = [\frac{d}{d\mu} \ln \Psi]_{0^-}^{0^+}$$

in the external region is independent of the flow parameter R^*, and therefore Δ'_{ext} in (2.22) can be taken as an input control parameter determined by the global equilibrium magnetic field structure.

It is clear that the continuity equation (2.3) is valid for both viscid and inviscid fluids, since it is simply a statement of the conservation of mass within an arbitrary volume and is independent of the nature of the fluid. However, the momentum equation (2.1) is modified by the physical effect of viscosity which is to cause a transfer of momentum between adjacent elements of the fluid whenever their relative velocity is non-vanishing, and the consequences of the possibility of inducing instability in the sub-Alfvénic regime has not been investigated in detail.

The inclusion of the collisional part of the viscosity introduces two possible orderings of $\mu_\perp$ with η in the boundary-layer equations: a "weak" viscous ordering $\mu_\perp \sim \eta^{7/5}$, in which viscous terms compete with inertial terms, and a "strong" viscous ordering $\mu_\perp \sim \eta$, which allows for a large effect from $\mu_\perp$ and hence a considerably reduced growth rate. Here we shall be concerned with the "weak" viscous ordering.

In the model of parallel shear flow studied here, the flow parameter R^* will be supposed to vanish like F on the resonant surface $(\underline{k} \cdot \underline{B}_0) = 0$. Hence both R^* and F may be taken to vary linearly with μ in the narrow boundary layer in the neighbourhood

of $F=0$.

For $S\to\infty$ we have from (2.19) the flux-freezing equation

$$(p+iR^*)\Psi + FW = 0 \tag{2.25}$$

which, together with (2.17)

$$\Psi F'' - \Psi'' F + \alpha^2 \Psi F + \frac{GW}{p+iR^*} = 0, \tag{2.26}$$

yields, upon elimination of W in (2.25) and (2.26), the outer infinite conductivity equation for Ψ

$$\Psi'' - \Psi\left(\alpha^2 + \frac{F''}{F} - \frac{G}{F^2}\right) = 0. \tag{2.27}$$

Equation (2.27) holds everywhere in the limit of $S\to\infty$ except in a narrow layer of thickness δ about $F=0$. The thickness of this resistive layer may be estimated from the fact that the neglect of the inertial term in (2.17) breaks down when $p\rho W'' \sim \alpha^2 S^2 \Psi'' F$. Since in the resistive layer we have from (2.19) $p\Psi \sim FW \sim \Psi''$, we find the condition $p\rho W''/\alpha^2 S^2 \sim WF^2$. Putting $F \sim F'\delta$ and $W'' \sim W/\delta^2$ in the layer then yields the estimate for the layer thickness

$$\delta \sim \left(\frac{p\rho}{\alpha^2 S^2 (F')^2}\right)^{1/4}. \tag{2.28}$$

We now order equations (2.15) and (2.17) with respect to the boundary-layer thickness δ (Furth, Killeen and Rosenbluth, 1963):

$$\Psi \sim 1, \quad \frac{d^2}{d\mu^2} \sim \delta^{-2}, \quad R^* \sim \delta^{-1}, \quad G \sim \delta,$$

$$R^{*\prime}, R^{*\prime\prime} \sim \delta^{-2}, \quad S^2 \sim \delta^{-5}, \quad F', F'' \sim 1,$$

$$F \sim \delta, \quad N^* \sim \delta,$$

so that

$$\rho W'' \sim \delta^{-4}, \quad \rho \sim 1, \quad \frac{\alpha^2 S^2 GW}{p+iR^*} \sim \delta^{-5},$$

$$(\rho R^*)' W \sim \delta^{-4}, \quad R^{*\prime\prime} W \sim \delta^{-4}.$$

Substituting (2.19) into (2.17) and then comparing the order, we have for the inertial term

$$(p + iR^*)\ [(\rho_0 W'') - \alpha^2 \rho_0 W] \sim \delta^{-5} + \delta^{-3},$$

$$i(\rho_0 R^{*\prime})' W \sim \delta^{-4};$$

for the field-bending term

$$\alpha^2 S^2 F[(p+iR^*) + FW - \frac{F''}{F}\Psi] \sim \delta^{-4}[\delta^{-1} + \delta\delta^{-2} - \delta^{-1}] = \delta^{-5};$$

and for the viscous term

$$N^*(\frac{d^2}{d\mu^2} - \alpha^2)^2 W \sim \delta\delta^{-4}\delta^{-2} = \delta^{-5}, \quad \alpha^2\Psi \sim 1.$$

From the expansion $\Psi = \Psi_0 + \Psi_1 + \cdots$ and $W = W_0 + W_1 + \cdots$, it follows that the induction equation (2.19) in the resistive layer, to leading order, becomes

$$\begin{aligned} \Psi_0'' &= 0, \\ \Psi_1'' &= (p + iR^*)\,\Psi_0 + FW_0. \end{aligned} \tag{2.29}$$

Thus, we obtain the equations

$$\begin{aligned} \frac{1}{\alpha^2 S^2}[(p+iR^*)W'' - N^* W^{(4)}] - F^2 W + \frac{GW}{p+iR^*} \\ = (p+iR^*)\Psi_0 F - \Psi_0 F'', \end{aligned} \tag{2.30}$$

$$\Psi_1'' = (p + iR^*)\Psi_0 + FW, \tag{2.31}$$

where we observe that the term $R^{*\prime\prime}W$ in (2.17) which drives the Kelvin-Helmholtz instability (Drazin and Reid, 1981) is not present in this ordering of the variables.

Use of the constant- Ψ approximation from (2.29) (*i.e.* $\Psi_0 = 1$) and introduction of the new variable $H = W + iR^{*\prime}/F'$ then leads to the equation

$$\frac{1}{\alpha^2 S^2}\left[(p+iR^{*\prime}\mu)H'' - N^*H^{(4)}\right] - (F')^2\mu^2 H + \frac{G(H-iR^{*\prime}/F')}{p+iR^{*\prime}\mu} \qquad (2.32)$$

$$= pF'\mu - F'',$$

Integration of (2.31) over $(-\infty\ ,\ \infty)$ yields

$$\Delta' = \int_{-\infty}^{\infty} (p + F'\mu H)\, d\mu, \qquad (2.33)$$

where in the boundary layer we set $F \sim F'\mu$ and $R^* \sim R^{*\prime}\mu$, with the gradients $F' \equiv F'(0)$, $F'' \equiv F''(0)$ and $R^{*\prime} \equiv R^{*\prime}(0)$.

Application of the familiar constant- Ψ approximation in the boundary layer in terms of the boundary-layer thickness δ requires the condition $\delta|\Delta'| \ll 1$, as we consider a "weak discontinuity" of the incompressible fluid and magnetic field across the boundary layer. Furth, Killeen and Rosenbluth (1963) show this to be consistent with α in the range

$$2\delta (F')^2 \ll \alpha \ll (2\delta)^{-1}. \qquad (2.34)$$

The long wavelength tearing mode and the short wavelength low G-mode must therefore be restricted to those values of α satisfying (2.34).

We now rescale variables to make all quantities $O(1)$ in the boundary layer by setting the new variable $\theta = \mu/\delta$ and

$$P = p\Delta^{-4/5}(\alpha SF')^{-2/5}, \quad H = F'H\Delta^{-3/5}(\alpha SF')^{-4/5},$$

$$\delta = \Delta^{1/5}(\alpha SF')^{-2/5}, \quad R = R^{*\prime}\Delta^{-3/5}(\alpha SF')^{-4/5},$$

$$N = N^*\Delta^{-6/5}(\alpha SF')^{2/5}, \quad G = G\Delta^{-6/5}(\alpha SF')^{2/5}. \qquad (2.35)$$

Following Bondeson and Persson, we have introduced the new parameter Δ defined from Δ' by

$$\Delta e^{i\chi} = \Delta' - \pi i \frac{F''}{F'}\ ,\ \Delta > 0\ ,\ -\pi < \chi \leq \pi \qquad (2.36)$$

In terms of these scaled variables, the equations in the boundary layer finally reduce to the form

$$(P+iR\theta)\frac{d^2H}{d\theta^2}-\theta^2H+\frac{G}{(F')^2}\frac{H-iR}{(P+iR\theta)}-N\frac{d^4H}{d\theta^4}=P\theta-\frac{F''}{\Delta F'}, \qquad (2.37)$$

$$\Delta'=\Delta\int_{-\infty}^{\infty}(P+\theta H)\,d\theta. \qquad (2.38)$$

It will sometimes be convenient to replace $F''/\Delta F'$ by $-\sin\chi/\pi$: this follows at once from the definition of Δ in (2.36).

Equations (2.37) and (2.38) form the basis of the investigation of the effects of flow along the equilibrium magnetic field (measured by the flow parameter R) and fluid viscosity on resistive instabilities. We emphasise again that, with our ordering of the variables, the dissipative effects and the flow dynamics are concentrated in the narrow resistive boundary layer about $F=0$, with the dynamics in the ideal outer region away from $F=0$ being described by the matching parameter Δ'_{ext}. Below we present the physical significance of each term in (2.37).

TABLE 2.1 The physical significance of each term in the momentum equation (2.37)

Term	Physical significance
$(P+iR\theta)H''$	inertial term
$\theta^2H+P\theta-\frac{F''}{\Delta F'}$	field line bending term
$\frac{G(H-iR)}{(F')^2(P+iR\theta)}$	gravitational term
$N\frac{d^4H}{d\theta^4}$	viscous term

2.3 Transformation of the Boundary-layer Equations

The starting point in this section is the pair of equations in the boundary-layer (in the scaled variables) given by (2.37) and (2.38). In considering the effects of the equilibrium shear flow on the resistive gravitational and tearing modes it is convenient to transform these boundary-layer equations to remove the high derivative resulting from the viscous term by introduction of a Fourier transform. We shall consider two ways of transforming (2.37): (a) to an integro-differential equation and (b) to a third order differential equation. Due to the difficulty of solving an integral-differential equation, we shall base our solution of the boundary-layer equations on method (b).

2.3.1 An integro-differential equation

We introduce the Fourier transform $h(k)$ of $H(\theta)$ defined by

$$h(k) = \int_{-\infty}^{\infty} H(\theta)\, e^{-ik\theta} d\theta .$$

The boundary-layer equation (2.37) with this transformation then takes the form

$$Lh + \frac{G}{(F')^2}\int_{-\infty}^{\infty} (H - iR)\,\frac{e^{-ik\theta}}{P + iR\theta}\, d\theta = 2\pi i P \delta'(k) - 2\pi \frac{F''}{\Delta F'}\delta(k), \qquad (2.39)$$

where L denotes the differential operator of the viscous-tearing mode (Bondeson and Persson, 1986; Paris, Wood and Stewart, 1993)

$$Lh = \frac{d^2h}{dk^2} + R\frac{d(k^2h)}{dk} - (k^2P + k^4N)\,h, \qquad (2.40)$$

and $\delta(k)$ is the Dirac delta function. The above integral can be dealt with by considering the cases $Re(P)$ positive, negative or zero separately. When $Re(P) > 0$, the singularity of the integral $\theta = iP/R$ is in the upper θ half plane; when $Re(P) < 0$, the singularity is in the lower half plane; and when $Re(P) = 0$, the singularity is on the real θ axis [see Figure 2.3 (a), (b) and (c) respectively].

(a) When $Re(P) > 0$:

From the standard result (Table of Integral Transformation, vol.I, p.118)

$$\int_{-\infty}^{\infty} \frac{e^{-ik\theta}}{P+i\theta} d\theta = 0, \quad for\ k>0; \qquad (2.41)$$

$$= 2\pi e^{Pk}, \quad for\ k<0,$$

we find (when $Re(P) > 0$), upon use of the inverse Fourier transform followed by reversal of the order of integration,

$$\int_{-\infty}^{\infty} \frac{He^{-ik\theta}}{P+iR\theta} d\theta = \frac{1}{2\pi} \int_{-\infty}^{\infty} \frac{e^{-ik\theta}}{P+iR\theta} d\theta \int_{-\infty}^{\infty} h(k') e^{ik'\theta} dk'$$

$$= \frac{1}{2\pi} \int_{-\infty}^{\infty} h(k')\, dk' \int_{-\infty}^{\infty} \frac{e^{-i(k-k')\theta}}{P+iR\theta} d\theta = \frac{1}{R} \int_{-\infty}^{\infty} h(k')\, e^{\frac{P}{R}(k-k')} U(k'-k)\, dk'$$

$$= \frac{1}{R} \int_{0}^{\infty} h(x+k)\, e^{-\frac{P}{R}x} dx,$$

where $U(k'-k)$ is the unit step function and we have put $x=k'-k$. Then (2.39) becomes

$$Lh + \frac{G}{R(F')^2} \int_{0}^{\infty} h(x+k)\, e^{-\frac{P}{R}x} dx$$

$$= 2\pi i \frac{G}{(F')^2} e^{\frac{P}{R}k} U(-k) + 2\pi i P\delta'(k) - 2\pi \frac{F''}{\Delta F'} \delta(k). \qquad (2.42)$$

(b) When $Re(P) < 0$:

The integral in (2.39) in this case is, upon using of the standard result (2.41) for $Re(P) < 0$,

$$\int_{-\infty}^{\infty} \frac{H-iR}{P/R+i\theta} e^{-ik\theta} d\theta = -\int_{-\infty}^{\infty} \frac{He^{-ik\theta}}{-P/R-i\theta} d\theta + \int_{-\infty}^{\infty} \frac{iRe^{-ik\theta}}{-P/R-i\theta} d\theta$$

$$= -\int_{-\infty}^{\infty} \frac{e^{-i(k-k')\theta}}{-P/R-i\theta} d\theta \int_{-\infty}^{\infty} h(k')\, dk' + 2\pi i R e^{\frac{P}{R}k} U(k)$$

$$= -\int_{-\infty}^{\infty} e^{\frac{P}{R}(k-k')} h(k')\, U(k-k')\, dk' + 2\pi i R e^{\frac{P}{R}k} U(k)$$

$$= -\int_{-\infty}^{0} h(x+k)\, e^{-\frac{P}{R}x} dx + 2\pi i R e^{\frac{P}{R}k} U(k)\,,$$

where, again, we have put $x=k'-k$, then (2.39) takes the alternative form when $Re(P) < 0$

$$Lh - \frac{G}{R(F')^2}\int_{-\infty}^{0} h(x+k)\, e^{-\frac{P}{R}x} dx \qquad (2.43)$$

$$= -2\pi i \frac{G}{(F')^2} e^{Pk/R} U(k) + 2\pi i P\delta'(k) - 2\pi \frac{F''}{\Delta F'}\delta(k)\,.$$

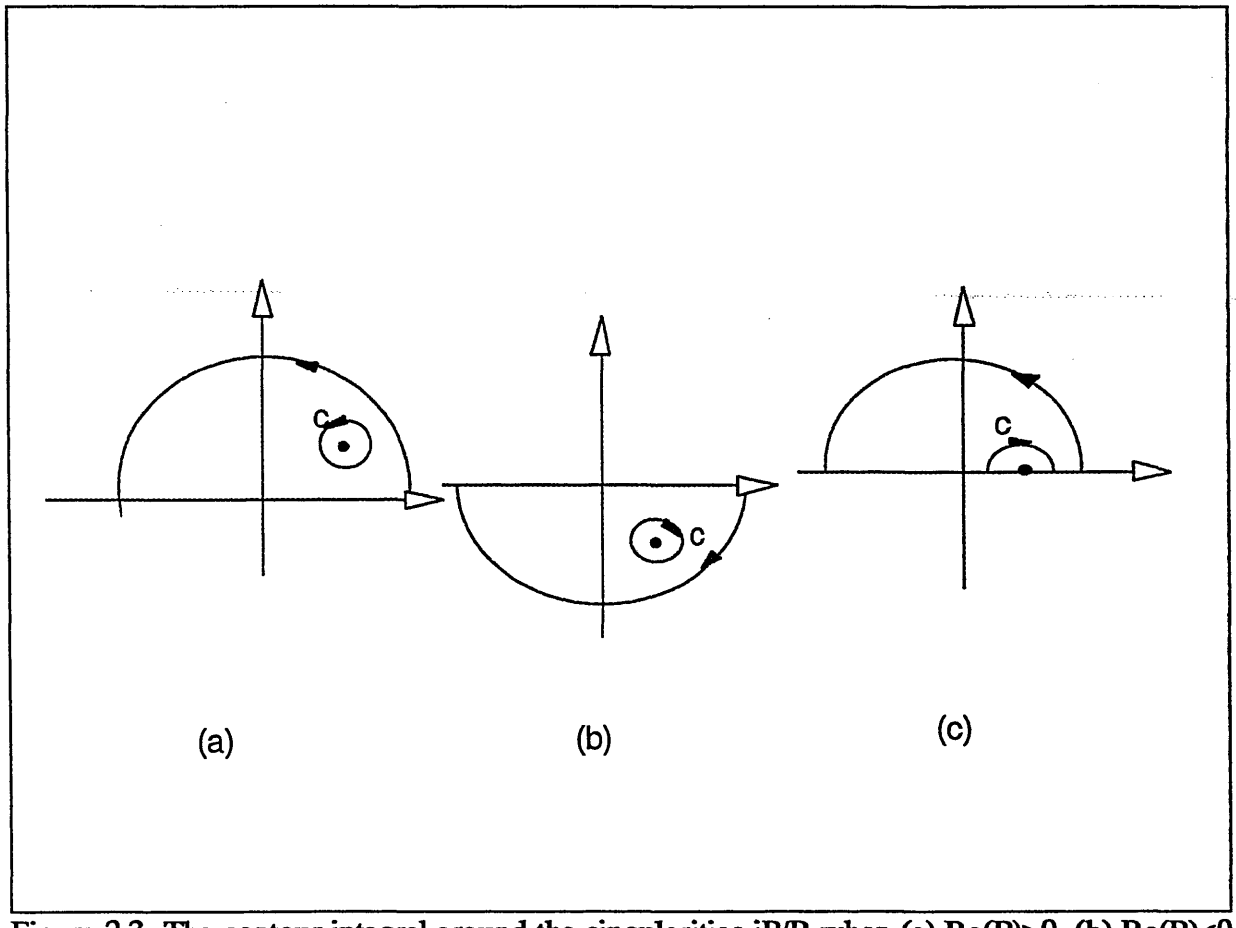

Figure 2.3 The contour integral around the singularities iP/R when (a) Re(P)>0, (b) Re(P)<0 and (c) Re(P)=0.

(c) When $Re(P)=0$:

The integral in (2.39) in this case is obtained by use of the residue calculus around the singularity θ_0 on the real axis

$$\int_{-\infty}^{\infty}\frac{H-iR}{P/R+i\theta}e^{-ik\theta}d\theta=\int_{-\infty}^{\infty}\frac{He^{-ik\theta}}{P/R+i\theta}d\theta-iR\int_{-\infty}^{\infty}\frac{e^{-ik\theta}}{P/R+i\theta}d\theta$$

$$=\int_{-\infty}^{\infty}\frac{He^{-ik\theta}}{P/R+i\theta}d\theta-R\int_{-\infty}^{\infty}\frac{e^{-ik\theta}}{\theta-iP/R}=\int_{-\infty}^{\infty}\frac{He^{-ik\theta}}{P/R+i\theta}d\theta+R\oint_c\frac{e^{-ik\theta}}{\theta-iP/R}d\theta$$

$$=\begin{cases}\int_0^{\infty}h(x+k)\,e^{-P/Rx}dx+i\pi Re^{\frac{P}{R}k}, & k>0;\\ \int_0^{\infty}h(x+k)\,e^{-\frac{P}{R}x}dx-i\pi Re^{\frac{P}{R}k}, & k<0.\end{cases}\qquad(2.44)$$

Thus, when $Re(P)=0$, (2.39) takes the form

$$Lh+\frac{G}{R(F')^2}\int_0^{\infty}h(x+k)\,e^{-\frac{P}{R}x}dx$$

$$=\begin{cases}-\pi i\frac{G}{(F')^2}e^{P/Rk}+2\pi iP\delta'(k)-2\pi\frac{F''}{\Delta F'}\delta(k), & k>0;\\ \pi i\frac{G}{(F')^2}e^{P/Rk}+2\pi iP\delta(k)-2\pi\frac{F''}{\Delta F'}\delta(k), & k<0.\end{cases}\qquad(2.45)$$

The jump conditions for h'', h' and h at the origin may be calculated from (2.42) and (2.45) when $Re(P)\geq 0$, or from (2.43) when $Re(P)<0$. The jump condition for h'' across $k=\pm 0$ is given by

$$[h''(0)]_-^+ = -2\pi i\frac{G}{(F')^2} - \lim_{\epsilon\to 0}\frac{G}{R(F')^2}\int_0^\infty e^{-\frac{P}{R}x}[h(x+\epsilon)-h(x-\epsilon)]\,dx$$

$$=-2\pi i\frac{G}{(F')^2} - \lim_{\epsilon\to 0}\frac{G}{R(F')^2}\left[\int_\epsilon^\infty e^{-\frac{P}{R}(y-\epsilon)}h(y)\,dy - \int_{-\epsilon}^\infty e^{-\frac{P}{R}(y+\epsilon)}h(y)\,dy\right]$$

$$= -2\pi i\frac{G}{(F')^2} - \lim_{\epsilon\to 0}\frac{G}{R(F')^2}\left[\left(e^{\frac{P}{R}\epsilon} - e^{-\frac{P}{R}\epsilon}\right)\int_0^\infty e^{-\frac{P}{R}y}h(y)\,dy\right.$$

$$\left. - \left(e^{\frac{P}{R}\epsilon}\int_0^\epsilon + e^{-\frac{P}{R}\epsilon}\int_{-\epsilon}^0\right)e^{-\frac{P}{R}y}h(y)\,dy\right]$$

$$=-2\pi i\frac{G}{(F')^2}, \qquad Re(P)\geq 0 \qquad (2.46)$$

where $[f(0)]_-^+ = f(0+) - f(0-)$.

For $Re(P)<0$, $[h''(0)]_-^+$ is given by

$$[h''(0)]_-^+ = -2\pi i\frac{G}{(F')^2} + \frac{G}{R(F')^2}\lim_{\epsilon\to 0}\int_{-\infty}^0 e^{-\frac{P}{R}x}[h(x+\epsilon)-h(x-\epsilon)]\,dx$$

$$= -2\pi i\frac{G}{(F')^2}, \qquad Re(P)<0. \qquad (2.47)$$

The calculation in (2.46) and (2.47) yields the same jump condition on h'' when $Re(P)\geq 0$ or $Re(P)<0$.

Similarly, from (2.39), the jump condition for h' and h at the origin are obtained by integrating (2.39) across $k=0\pm$,

$$[h'(0)]_-^+ = \lim_{\epsilon\to 0}\left\{-2\pi i\frac{G}{(F')^2}\int_{-\epsilon}^\epsilon e^{\frac{P}{R}k}dk + 2\pi i P\int_{-\epsilon}^\epsilon \delta'(k)\,dk - 2\pi\frac{F''}{\Delta F'}\int_{-\epsilon}^\epsilon \delta(k)\,dk\right\}$$

$$=-2\pi\frac{F''}{\Delta F'}, \qquad (2.48)$$

and

$$[h(0)]_{-}^{+} = 2\pi i P \lim_{\epsilon \to 0} \int_{-\epsilon}^{\epsilon} \delta(k)\, dk = 2\pi i P \,. \qquad (2.49)$$

Transforming (2.33), we have

$$\Delta' = \Delta \int_{-\infty}^{\infty} \left\{ P + \frac{\theta}{2\pi} \int_{-\infty}^{\infty} h(k)\, e^{ik\theta} dk \right\} d\theta$$

$$= \Delta \int_{-\infty}^{\infty} \left\{ P + \frac{1}{2\pi i} [h e^{ik\theta}]_{-\infty}^{\infty} - \frac{1}{2\pi i} \int_{-\infty}^{\infty} h'(k)\, e^{ik\theta} dk \right\} d\theta \,,$$

where

$$[h e^{ik\theta}]_{-\infty}^{\infty} = \lim_{x \to \infty} h(x)\, e^{i\theta x} - h(0+) - \lim_{x \to -\infty} h(x)\, e^{i\theta x} + h(0-)$$

$$= -h(0+) + h(0-) = -2\pi i P \,.$$

Thus

$$\Delta' = -\frac{\Delta}{2\pi i} \int_{-\infty}^{\infty} \left\{ \int_{-\infty}^{\infty} h'(k)\, e^{ik\theta} dk \right\} d\theta = -\frac{\Delta}{2\pi i} \int_{-\infty}^{\infty} \left\{ \int_{-\infty}^{\infty} e^{ik\theta} d\theta \right\} h'(k)\, dk$$

$$= i\Delta \int_{-\infty}^{\infty} h'(k)\, \delta(k)\, dk = \frac{i}{2} \Delta [h'(0+) + h'(0-)] \,. \qquad (2.50)$$

From the jump condition on h' in (2.48) we have, by substituting in (2.50) and using (2.36),

$$h'(0\pm) = -i e^{\pm i\chi} \,. \qquad (2.51)$$

Substitution of (2.51) into (2.49) then yields the relation for the eigenvalue P in the form

$$2\pi P = \frac{h(0-)}{h'(0-)} e^{-i\chi} - \frac{h(0+)}{h'(0+)} e^{i\chi} \,, \quad -\pi < \chi \leq \pi \,. \qquad (2.52)$$

Note that the only quantity required in the eigenvalue relation (2.52) is the slope of the solution $h(k)$ on either side of the origin $k=0$.

for $Re(P) \geq 0$ or $Re(P) < 0$ as follows:

TABLE 2.2 An integral-differential equation from Fourier transformation of (2.37)

(i) When $Re(P) > 0$	$Lh + \frac{G}{R(F')^2}\int_0^{\infty} h(x+k)\, e^{-\frac{P}{R}x} dx = 0, \quad k>0$ $= 2\pi i \frac{G}{(F')^2} e^{\frac{P}{R}k}, \quad k<0$
(ii) When $Re(P) < 0$	$Lh - \frac{G}{R(F')^2}\int_{-\infty}^{0} h(x+k)\, e^{-\frac{P}{R}x} dx = -2\pi i \frac{G}{(F')^2} e^{\frac{P}{R}k}, \quad k>0$ $= 0, \quad k<0$
(iii) When $Re(P) = 0$	$Lh + \frac{G}{R(F')^2}\int_0^{\infty} h(x+k)\, e^{-\frac{P}{R}x} dx = -\pi i \frac{G}{(F')^2} e^{\frac{P}{R}k}, \quad k>0$ $= \pi i \frac{G}{(F')^2} e^{\frac{P}{R}k}, \quad k<0$

Subject to the jump conditions (3.47)-(3.49) and boundary condition $h(\pm\infty) = 0$. It is obvious from Table 2.2 that the numerical computation on (2.39) is complicated by the presence of integral-differentiation on $h(k)$, so that it is necessary to carry out another approach based on a third-order differential equation from Fourier transformation on (2.37).

2.3.2 A third-order differential equation

The system of equations in (2.37) is complicated by the presence of the denominator $P+iR\theta$ in the gravitational term. As we saw in the last section, Fourier transformation of (2.37) leads to an integro-differential equation for $h(k)$, the Fourier transform of $H(\theta)$. An approach, which avoids this difficulty, is to first multiply (2.37) by $P+iR\theta$ before taking the Fourier transform. In this way, the denominator in the gravitational term has been removed but at the expense of increasing the order of the resulting

differential equation for $h(k)$.

Multiplying (2.37) by $P+iR\theta$ and taking the Fourier transform, we have

$$\int_{-\infty}^{\infty} e^{-ik\theta}\left[(P+iR\theta)^2 H'' - (\theta^2 H + NH^{(iv)})(P+iR\theta) + \frac{G}{(F')^2}(H-iR)\right] d\theta$$

$$= \int_{-\infty}^{\infty} e^{-ik\theta}\left(P\theta - \frac{F''}{\Delta F'}\right)(P+iR\theta)\, d\theta$$

so that

$$P^2\int_{-\infty}^{\infty} e^{-ik\theta}H''d\theta + 2iPR\int_{-\infty}^{\infty}\theta e^{-ik\theta}H''d\theta + (iR)^2\int_{-\infty}^{\infty}\theta^2 e^{-ik\theta}H''d\theta - P\int_{-\infty}^{\infty}\theta^2 He^{-ik\theta}d\theta$$

$$- iR\int_{-\infty}^{\infty}\theta^3 He^{-ik\theta}d\theta - NP\int_{-\infty}^{\infty}H^{(iv)}e^{-ik\theta}d\theta - iNR\int_{-\infty}^{\infty}\theta H^{(iv)}e^{-ik\theta}d\theta$$

$$+ \frac{G}{(F')^2}\int_{-\infty}^{\infty} He^{-ik\theta}d\theta - i\frac{GR}{(F')^2}\int_{-\infty}^{\infty} e^{-ik\theta}d\theta$$

$$= P^2\int_{-\infty}^{\infty}\theta e^{-ik\theta}d\theta + iPR\int_{-\infty}^{\infty}\theta^2 e^{-ik\theta}d\theta - \frac{PF''}{\Delta F'}\int_{-\infty}^{\infty} e^{-ik\theta}d\theta - i\frac{RF''}{\Delta F'}\int_{-\infty}^{\infty}\theta e^{-ik\theta}d\theta .$$

Thus, we obtain the third-order differential equation

$$R\frac{d^3h}{dk^3} + \frac{d^2}{dk^2}\left[(R^2(k^2h) - Ph\right] - \frac{d}{dk}\left[2PRk^2h + NRk^4h\right] + \left(P^2k^2 - \frac{G}{(F')^2} + NPk^4\right)h$$

$$= 2\pi iPR\delta''(k) - 2\pi\left(iP^2 + R\frac{F''}{\Delta F'}\right)\delta'(k)$$

$$+ 2\pi\left[\frac{PF''}{\Delta F'} - iR\frac{G}{(F')^2}\right]\delta(k), \qquad (2.53)$$

with boundary conditions $h(\pm\infty) = 0$.

If we now define the third-order differential operator, which we shall call the viscous tearing-G-mode operator

where Lh is the viscous-tearing mode operator defined in (2.40), then

$$Mh = (R\frac{d}{dk} - P)\, Lh - \frac{G}{(F')^2} h, \tag{2.54}$$

where Lh is the viscous-tearing mode operator defined in (2.40), then

$$Mh = 2\pi i PR\delta''(k) - 2\pi (iP^2 + \frac{RF''}{\Delta F'})\, \delta'(k)$$

$$+2\pi [\frac{PF''}{\Delta F'} - i\frac{RG}{(F')^2}]\, \delta(k)\,. \tag{2.55}$$

This yields the pair of boundary value problems in $(-\infty, 0]$ and $[0, \infty)$ given by

$$Mh = 0, \qquad h(\pm\infty) = 0, \qquad -\infty < k < 0,\ 0 < k < \infty. \tag{2.56}$$

To determine the jump conditions on $h(k)$, $h'(k)$ and $h''(k)$ across the origin $k = 0$, we integrate (2.53) successively over $(-\epsilon, \epsilon)$ and let $\epsilon \to 0$. Making use of the results from integrating (2.53) we obtain

$$\lim_{\epsilon\to 0} \int_{-\epsilon}^{\epsilon} [P^2k^2 - \frac{G}{(F')^2} + NPk^4]\, h(k)\, dk = 0,$$

$$\lim_{\epsilon\to 0} \int_{-\epsilon}^{\epsilon} [2PRk^2 + NRk^4]\, h(k)\, dk = 0,$$

$$\lim_{\epsilon\to 0} \int_{-\epsilon}^{\epsilon} (-R^2k^2 + P)\, h(k)\, dk = 0.$$

This then yields the jump conditions

$$R[h''(0)]_{-}^{+} - P[h'(0)]_{-}^{+} = -2\pi (\frac{PF''}{\Delta F'} - i\frac{RG}{(F')^2}),$$

$$R[h'(0)]_{-}^{+} - P[h(0)]_{-}^{+} = -2\pi\left(iP^2 + \frac{RF''}{\Delta F'}\right),$$

$$[h(0)]_{-}^{+} = 2\pi iP.$$

Thus,

$$[h(0)]_{-}^{+} = 2\pi iP,\ [h'(0)]_{-}^{+} = -2\pi\frac{F''}{\Delta F'},\ [h''(0)]_{-}^{+} = -2\pi i\frac{G}{(F')^2}, \quad (2.57)$$

so that we obtain the same jump conditions as in (2.47)-(2.49).

To summarise, the system of boundary-layer equations we shall investigate in our numerical study of the effects of flow on visco-resistive tearing and gravitational modes is

$$Mh = 0, \qquad h(\pm\infty) = 0, \qquad -\infty < k < 0,\ 0 < k < \infty, \quad (2.58)$$

subject to the jump conditions (2.57), with the eigenvalue relation for the growth rate P given by

$$2\pi P = \frac{h(0-)}{h'(0-)}e^{-ix} + \frac{h(0+)}{h'(0+)}e^{ix}. \quad (2.59)$$

The differential operator M is defined in (2.54) and (2.40). We remark that this eigenvalue problem is not of the usual type, as the eigenvalue parameter P appears nonlinearly in the operator M and in the jump conditions for the solution at the origin. A direct method to calculate the eigenvalue P without applying the Fourier transformation will be given in Chapter 4. This completes the derivation of the boundary-layer equations for visco-resistive tearing and gravitational modes.

2.3.3 Symmetry properties of the eigenvalue relation

From the third-order differential equation $Mh = 0$ and the corresponding eigenvalue relation (2.59), we have the following symmetry properties satisfied by the eigenvalue P:

$$P(-R,G,N,\chi) = P(R,G,N,-\chi) = P^*(R,G,N,\chi)\ , \qquad (2.60)$$

where P^* is the conjugate of P, R is positive and $0 \le \chi \le \pi$.

Proof:

(i) Considering the conjugate of h in $Mh = 0$, we have

$$Mh^* = R\frac{d^3h^*}{dk^3} + \frac{d^2}{dk^2}(R^2k^2-P)\,h^*$$

$$-\frac{d}{dk}(2PRk^2+NRk^4)\,h^* + [P^2k^2-\frac{G}{(F')^2}+NPk^4]\,h^* = 0\ .$$

The corresponding eigenvalue relation is then

$$2\pi P(R,G,N,\chi) = \frac{h^*(0-)}{h^{*'}(0-)}e^{-i\chi} - \frac{h^*(0+)}{h^{*'}(0+)}e^{i\chi}\ , -\pi \le \chi \le \pi\ . \qquad (2.61)$$

On the other hand, taking the conjugate of $Mh=0$ and the eigenvalue relation yields

$$(Mh)^* = R\frac{d^3h^*}{dk^3} + \frac{d^2}{dk^2}(R^2k^2-P^*)\,h^*$$

$$-\frac{d}{dk}(2RP^*k^2+NRk^4)\,h^* + [P^*k^2-\frac{G}{(F')^2}+NP^*k^4]\,h^* = 0\ ,$$

and

$$2\pi P^* = \frac{h^*(0-)}{h^{*'}(0-)}e^{i\chi} - \frac{h^*(0+)}{h^{*'}(0+)}e^{-i\chi}\ , \quad -\pi \le \chi \le \pi\ . \qquad (2.62)$$

Thus, comparing (2.61) and (2.62) we have the symmetry relation

$$P(R,G,N,\chi) = P^*(R,G,N,-\chi)\ , \quad -\pi \le \chi \le \pi\ . \qquad (2.63)$$

(ii) If we now consider $-R$ in $Mh = 0$, then

$$Mh = -R\frac{d^3h}{dk^3} + \frac{d^2}{dk^2}(R^2k^2-P)$$

$$+\frac{d}{dk}(2PRk^2+NRk^4)h + [P^2k^2-\frac{G}{(F')^2}+NPk^4]h$$

$$= R\frac{d^3h}{d(-k)^3} + \frac{d^2}{dk^2}(R^2k^2-P)h$$

$$-\frac{d}{d(-k)}(2PRk^2+NRk^4)h + [P^2k^2-\frac{G}{(F')^2}+NPk^4)h = 0 .$$

Therefore the corresponding eigenvalue relation becomes

$$2\pi P(-R,G,N,\chi) = -\frac{h(0+)}{h'(0+)}e^{-i\chi} + \frac{h(0-)}{h'(0-)}e^{i\chi} = 2\pi P(R,G,N,-\chi) ,$$

where the k-axis has been switched to -k to yield $h'(0\pm) = -h'(0\mp)$. Thus we have

$$P(-R,G,N,\chi) = P(R,G,N,-\chi) , \quad R>0, \quad 0\le\chi\le\pi . \qquad (2.64)$$

Finally, from (2.63) and (2.64) we obtain

$$P(-R,G,N,\chi) = P(R,G,N,-\chi) = P^*(R,G,N,\chi) ,$$

where $R>0$ and $0\le\chi\le\pi$. This symmetry possessed by the eigenvalue enables the investigation in the visco-resistive tearing and gravitational modes to be carried out by only considering positive values of R and χ. This simplification saves a lot of numerical computation.

CHAPTER III
FLOWLESS GRAVITATIONAL AND TEARING MODES

Introduction

In this chapter, a summary of the behaviour of the growth rates of the tearing and gravitational interchange modes (or G-mode) will be given for the flowless case (i.e. R=0). The G-mode is of importance in a variety of laboratory and astrophysical plasmas. The effective destabilizing 'gravitational' force in magnetic confinement devices may be interpreted as resulting from the interaction of an adverse plasma pressure gradient and weak magnetic field line curvature, or from the effects of plasma rotation. The simplest representation of this instability is the ideal, incompressible, magnetized plane plasma slab with a diffuse density profile $\rho_0(y)$ acted upon by a gravitational acceleration g in the positive y-direction. It is then well known that, for adverse density gradients $(\rho_0'>0)$ and for short transverse wavelength perturbations about the equilibrium magnetic field, the linearized growth time of MHD Rayleigh-Taylor modes is characterized by $\tau_g \sim (-g\rho_0'/\rho_0)^{-1/2}$.

The hydrodynamic Rayleigh-Taylor instability is also considered as an illustration of the problem we have to deal with in the resistive G-mode. If fluid lies at rest between two horizontal planes, the lower one being hotter than the upper, then we have lighter fluid below heavy fluid. The buoyancy tends to overturn the fluid. Likewise, two layers of plasma which are unstably stratified in a confining magnetic field will result in an interchange between the two layers. This tendency is countered by the dissipative and diffusive effects of viscosity and resistivity. In the flowless case considered in this chapter, viscosity has only a stabilizing effect. The study will generally require numerical solutions but, as an illustration, we consider special cases which have analytic solutions for the flowless G-mode.

First, an analytic result for the hydrodynamic Rayleigh-Taylor instability is introduced in dealing with discontinuous density across the interface. Then, a discussion on the ideal MHD analogue of this instability is given with a continuous density variation in the direction normal to the magnetic surface. Finally, we consider FKR flowless resistive instabilities in MHD.

3.1 The Rayleigh-Taylor Instability in MHD

An introduction of the Rayleigh-Taylor instability in MHD is given in this section to discuss the cases with two layers of fluid (a) with a discontinuous density profile and (b) with a continuous density profile.

3.1.1 The Rayleigh-Taylor instability with a discontinuous density profile

We first consider an important special case when the equilibrium flow $\underline{V_0} \equiv 0$ in the absence of a magnetic field and any dissipation. If a heavy fluid is layered on top of a light fluid in a gravitational field (or in an accelerating system) then the resulting pure interchange between the two fluids is called the Rayleigh-Taylor instability. The analogue of this instability in a resistive plasma confined by a sheared magnetic field is known as the resistive interchange mode; or resistive G-mode.

To determine the characteristic growth rate of the Rayleigh-Taylor instability, we examine the simplest model in which a heavy fluid of density ρ_1 is set on top of a light fluid of density ρ_2 and separated by a horizontal boundary at $y=0$ (see Figure 3.1). The equation of motion for this case can be obtained from (2.5) [see (2.7) and (2.14)] in the form

$$\omega^2 [(\rho_0 V_{y1}')' - k^2 \rho_0 V_{y1}] = k^2 \rho_0' g V_{y1}, \qquad (3.1)$$

where $k=\sqrt{k_x^2+k_z^2}$ and the prime denotes differentiation with respect to y. For both regions where the density is constant, we have Rayleigh's instability equation (Drazin and Reid, p.130, 1981)

$$V_{y1}'' - k^2 V_{y1} = 0$$

for which the general solution is

$$V_{y1} = Ae^{ky} + Be^{-ky},$$

where A, B are arbitrary constants. Since V_{y1} must vanish when $y \to -\infty$ (in the lower fluid) and $y \to +\infty$ (in the upper fluid), we find

$$V_{y1} = \begin{cases} Ae^{ky}, & y<0, \\ Ae^{-ky}, & y>0, \end{cases} \qquad (3.2)$$

where we have chosen the same constant A in the solutions for $y>0$ and $y<0$ to ensure the continuity of V_{y1} across the interface at $y=0$.

Integration of (3.1) across the interface $y=0$ yields the jump condition

$$\omega^2 [\rho_0 V'_{y1}]^{+}_{-} = k^2 g V_{y1} [\rho_0]^{+}_{-} = k^2 g(\rho_1 - \rho_2) V_{y1}$$

where, as in §2.3, $[f(x)]^{+}_{-} = f(0+) - f(0-)$. Upon observing from (3.2) that $[\rho_0 V'_{y1}]^{+}_{-} = -(\rho_1 + \rho_2) Ak$, we obtain

$$\omega^2 = kg \frac{\rho_2 - \rho_1}{\rho_2 + \rho_1}. \qquad (3.3)$$

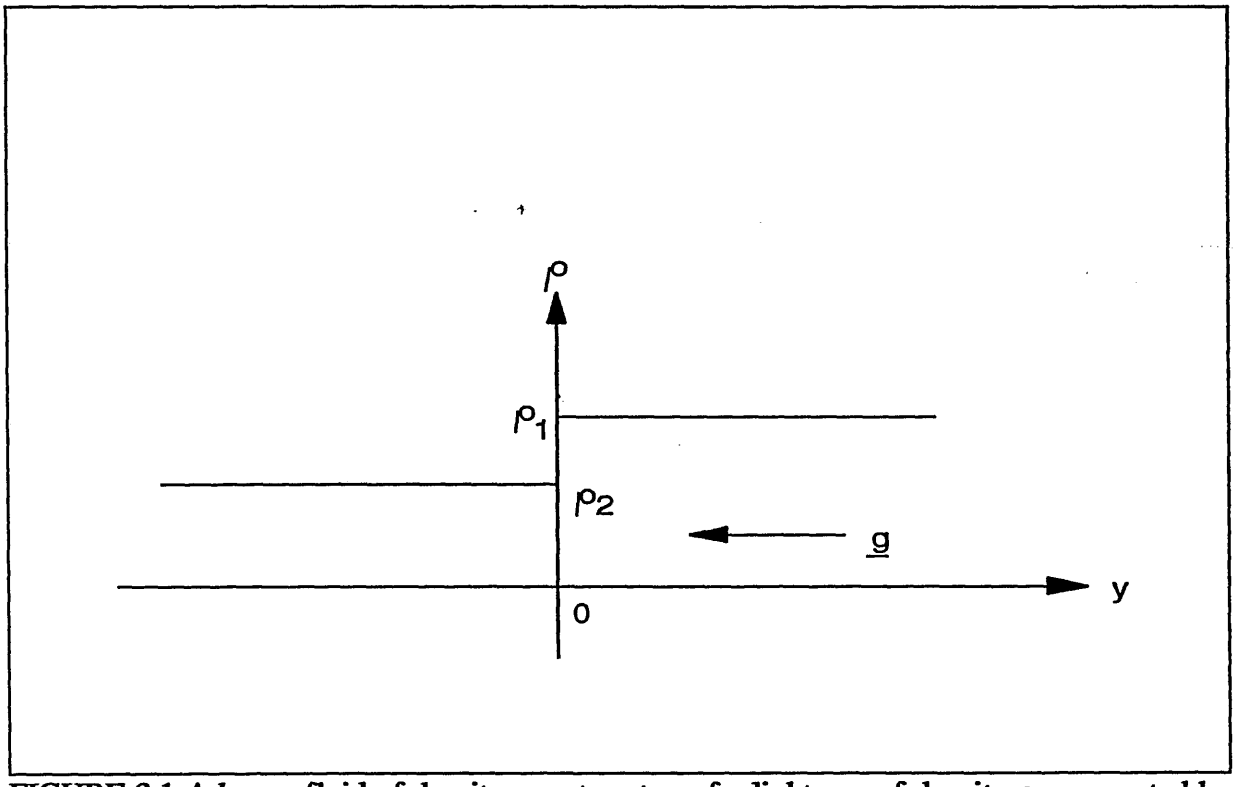

FIGURE 3.1 A heavy fluid of density ρ_1 set on top of a light one of density ρ_2, separated by a horizontal boundary at y=0.

According to (3.3), if $\rho_2 < \rho_1$ the perturbation propagates as a gravity wave along the interface and the arrangement is stable, as ω is a pure imaginary number; while if $\rho_2 > \rho_1$, then ω is a positive real number, so that the arrangement is unstable and the amplitude of the perturbation grows.

3.1.2 The Rayleigh-Taylor instability with a continuous density profile

We now examine the situation of an ideal viscous plasma $(\eta = 0)$ with a weak continuous density profile (see Figure 3.2). The flow parameter R and magnetic shear F are assumed to be zero everywhere i.e. $\underline{k} \perp \underline{B_0}$. From (2.15) and (2.16) the unscaled momentum and continuity equations are

$$\rho_0 \omega (k^2 V_{y1} - V_{y1}'') = k^2 \rho_1 g - \mu_\perp (k^2 - \frac{d^2}{dy^2})^2 V_{y1}, \qquad (3.4)$$

$$\omega \rho_1 = -\rho_0' V_{y1}, \qquad (3.5)$$

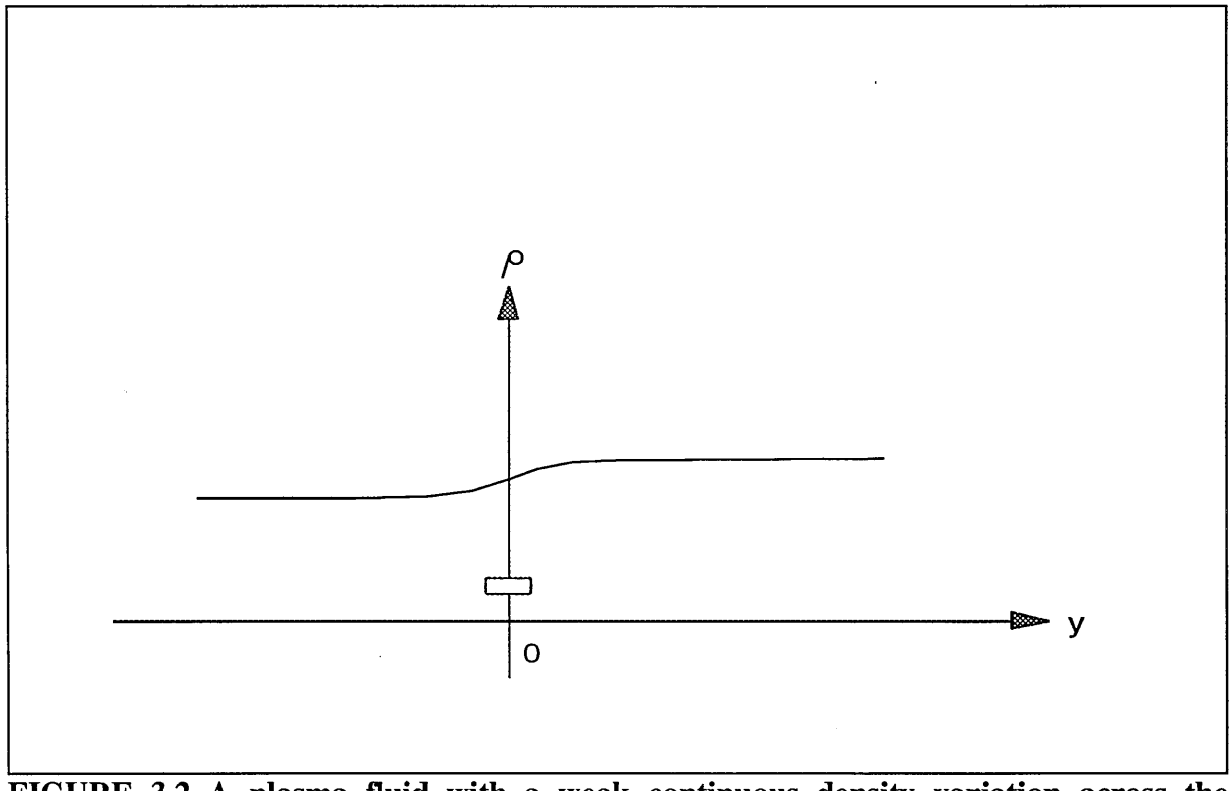

FIGURE 3.2 A plasma fluid with a weak continuous density variation across the interface at y=0.

where two simplifications have been made:

(i) Due to the weak density inhomogeneity, we have made the Boussinesq approximation which consists of neglecting the density gradient in the inertial term while retaining ρ_0' in the gravitational driving term;

(ii) We assume a low- β plasma ($\beta = 8\pi\bar{p}/B^2$ measures the ratio of the plasma pressure $\bar{p}$ to magnetic pressure $B^2/8\pi$) with a strong magnetic field B, so that the magnetic field is approximately uniform in the (x,z) plane.

To obtain the value of the characteristic growth rate of the interchange mode we now simplify the above system of equations by supposing that the vertical scale height l of the equilibrium density variation is long compared to the wavelength of the perturbation in the y-direction i.e. $2\pi/k_y \ll l$. This enables us to make the so-called plane wave approximation:

$$f(y) \sim f_0 \exp(ik_y y),$$

where $f(y)$ denotes a perturbed quantity. This enables the system of differential equations (3.4) and (3.5) to be reduced to an algebraic system.

From (3.4) and (3.5) we find

$$\rho_0 \omega (k^2 - \frac{d^2}{dy^2}) V_{y1} = -\frac{k^2 \rho_0' g}{\omega} V_{y1} - \mu_\perp (k^2 - \frac{d^2}{dy^2})^2 V_{y1}, \qquad (3.6)$$

so that, on putting $V_{y1} \sim V_0 \exp(ik_y y)$, we obtain the quadratic equation

$$\omega^2 = -\frac{k^2}{k^2+k_y^2}\frac{\rho_0' g}{\rho_0} - \mu_\perp \omega \frac{(k^2+k_y^2)}{\rho_0}.$$

In the inviscid limit $\mu_\perp = 0$, we have

$$\omega^2 \approx \frac{k^2}{k^2+k_y^2}\left(-\frac{\rho_0' g}{\rho_0}\right). \qquad (3.7)$$

Perturbations with $\underline{k}\cdot\underline{B}_0 = 0$ are the most dangerous as they do not cause any bending of the field lines and consequently are unaffected by the magnetic field. The growth rate in (3.7) is maximised for short transverse wavelengths, $k \to \infty$ (thin slices) and the characteristic interchange growth rate then becomes $\omega \approx (-\rho_0' g/\rho_0)^{1/2}$, which corresponds to the time

scale τ_g^{-1} . If $\rho_0' g<0$, then $\omega>0$ and the corresponding density gradient is said to be unfavourable to stability; if $\rho_0' g>0$, the corresponding density gradient is favourable to stability as ω is pure imaginary. Hence $\rho_0' g\geq 0$ is the stability criterion in this case.

In a viscous plasma, $\mu_\perp \neq 0$, the quadratic equation (3.6) yields two roots

$$\omega_{1,2} = \frac{1}{2}\left[-\mu_\perp (k^2+k_y^2)^2 \pm \sqrt{\mu_\perp^2 (k^2+k_y^2)^4 - 4\frac{k^2}{k^2+k_y^2}\rho_0' g/\rho_0}\right] . \qquad (3.8)$$

If $\rho_0' g<0$, then $\omega_{1,2}$ are real numbers; if $\rho_0' g>0$, then $\omega_{1,2}$ are complex numbers when $\mu_\perp^2 (k^2+k_y^2)^4 < 4k^2 \rho_0' g/(k^2+k_y^2)\rho_0$. It is obvious that the viscous term reduces the growth rate ω.

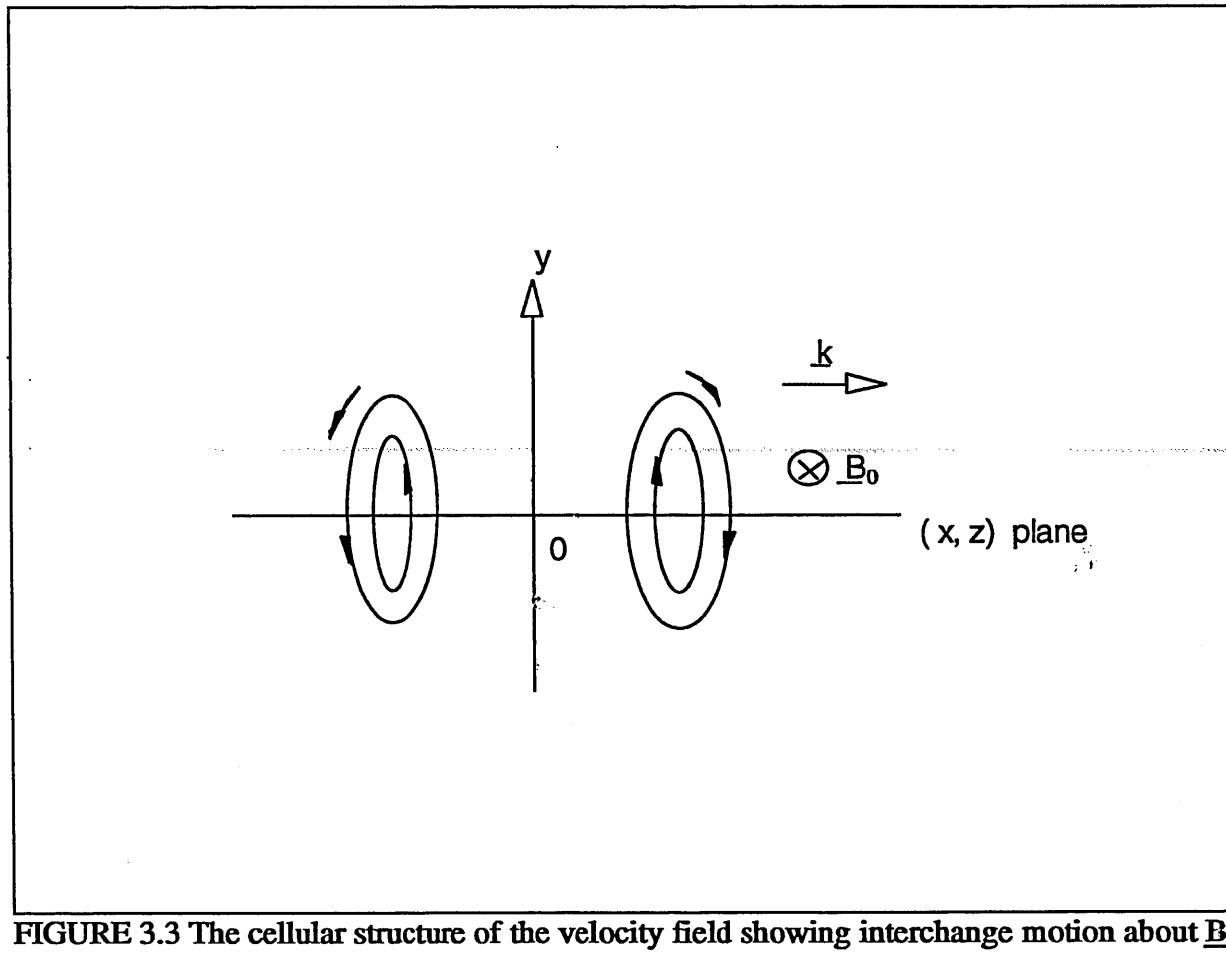

FIGURE 3.3 The cellular structure of the velocity field showing interchange motion about $\underline{B}_0$ on either side of the interface at y=0.

If the ideal plasma is contained in a sheared magnetic field, $\underline{B}_0$ varies in the y-direction across the layer. For perturbations with a given horizontal wave vector $\underline{k}=\{k_x,0,k_z\}$, it is then no longer possible to choose a perturbation of the pure interchange type with $(\underline{k}\cdot\underline{B}_0)\equiv 0$ when $y\neq 0$. The magnetic field lines will necessarily suffer distortion during a perturbation. Since bending of field lines requires energy, we would expect magnetic shear to have a stabilizing effect on the interchange mode, thereby localising the gravitational interchange about the resonant surface $F=0$. In the inviscid case the stability criterion becomes the well-known Suydam criterion $G/(F')^2\leq 1/4$ in an ideal plane plasma slab (FKR, 1963), which corresponds to $\rho_0' g\geq -\rho_0 (F')^2/4\tau_H^2$. This criterion shows a strong stabilizing effect from $F'\neq 0$ to the flowless G-mode.

In the absence of magnetic shear, $F\equiv 0$, the resulting motion of plasma then takes the form of thin slices which roll about the magnetic field lines. The velocity field breaks up and possesses a cellular structure, in which the plasma describes longitudinal rolls in alternate senses about the magnetic field lines (Figure 3.3). The perturbation in this case causes no bending of field lines and thereby is not affected by the magnetic field containment.

3.2 Resistive Modes in the FKR Flowless Case

In this section we consider the resistivity $\eta\neq 0$ in the full boundary-layer equations (2.17) and (2.19) with sheared magnetic field and, again, we assume $\underline{V}_0\equiv 0$.

The solution in the resistive boundary layer in the constant Ψ- approximation may be obtained by using (2.58) when $R=N=0$ for the flowless inviscid case. The G-mode equation then becomes

$$\frac{d^2h}{dk^2}-\left(k^2P-\frac{G}{P(F')^2}\right)h=0, \qquad (3.9)$$

where, by symmetry, it is sufficient to consider only the interval $0\leq k<+\infty$.

With the new variable $x=\sqrt{2}P^{1/4}k$, (3.9) then becomes Weber's equation

$$\frac{d^2h}{dx^2}+\left(\nu+\frac{1}{2}-\frac{x^2}{4}\right)h=0, \qquad \nu=-\frac{1}{2}+\frac{G}{2(F')^2P^{3/2}}. \qquad (3.10)$$

The solution which satisfies $h(0)=1$, and which decays at infinity, is given by

$$h(x) = \frac{D_\nu(x)}{D_\nu(0)}$$

where $D_\nu(x)$ denotes the parabolic cylinder function. By use of the standard values (Abramowitz and Stegun, p.685, 1965)

$$D_\nu(0) = \frac{2^{\nu/2}\sqrt{\pi}}{\Gamma(\frac{1}{2}-\frac{\nu}{2})}, \quad D_\nu'(0) = -\frac{2^{1/2+\nu/2}\sqrt{\pi}}{\Gamma(-\frac{\nu}{2})}$$

we find

$$\frac{d}{dx}h(0) = -\sqrt{2}\frac{\Gamma(\frac{1}{2}-\frac{\nu}{2})}{\Gamma(-\frac{\nu}{2})},$$

which yields

$$\frac{d}{dk}h(0\pm) = \mp 2P^{\frac{1}{4}}\frac{\Gamma(\frac{1}{2}-\frac{\nu}{2})}{\Gamma(-\frac{\nu}{2})}$$

$$= \mp 2P^{\frac{1}{4}}\frac{\Gamma(\frac{3}{4}-\frac{\Lambda}{2})}{\Gamma(\frac{1}{4}-\frac{\Lambda}{2})}, \qquad \Lambda = \frac{G}{2(F')^2P^{3/2}}. \tag{3.11}$$

Substituting (3.11) into the eigenvalue relation (2.59), then gives

$$2\pi P = \frac{h(0-)}{h'(0-)}e^{-i\chi} - \frac{h(0+)}{h'(0+)}e^{i\chi} = \frac{1}{2P^{1/4}}\frac{\Gamma(\frac{1}{4}-\frac{\Lambda}{2})}{\Gamma(\frac{3}{4}-\frac{\Lambda}{2})}(e^{-i\chi}+e^{i\chi})$$

and hence

$$P^{\frac{5}{4}} = \frac{\cos\chi}{2\pi}\frac{\Gamma(\frac{1}{4}-\frac{\Lambda}{2})}{\Gamma(\frac{3}{4}-\frac{\Lambda}{2})}. \tag{3.12}$$

This is the flowless inviscid eigenvalue relation for mixed tearing and resistive G-modes which was obtained by Furth, Killeen and Rosenbluth (1963) by another approach.

We have also solved numerically the differential equation (3.9) on the intervals $-\infty < k < 0$ and $0 < k < \infty$ subject to appropriate boundary conditions by employing the method described in §2.3.2. This enables an independent check to be made on the solution of the eigenvalue relation (3.12). The dependence of P on the parameters χ and G in the flowless case $R=0$ is a necessary and important step for initiation of the numerical investigation on the effects of flow on the resistive instabilities in Chapters 4 and 5.

3.2.1 Discussion of the flowless (R=0) FKR eigenvalue relation (3.12)

We first consider the case $G=0$. This corresponds to the pure tearing mode, for which the classical FKR instability condition is $\Delta' > 0$. In terms of the angle χ this is equivalent to $|\chi| < \pi/2$. In this case, (3.12) yields when $\Lambda=0$ the single eigenvalue P given by

$$P = \{\frac{\cos\chi}{2\pi} \frac{\Gamma(\frac{1}{4})}{\Gamma(\frac{3}{4})}\}^{\frac{4}{5}}$$

which is real and positive when $|\chi| < \pi/2$. When $\pi/2 \le |\chi| \le \pi$, the tearing mode is stable since

$$P = |P| e^{\pm\frac{4}{5}\pi i}$$

lies on the rays $arg P = \pm 4\pi/5$ (see Figure 3.6).

When $G \neq 0$, we see that, unlike the pure tearing mode case above, there is a countably infinite spectrum of G-mode eigenvalues. We shall be interested only in the eigenvalue P with the largest $Re(P)$. If we define the function $f(\Lambda)$ by

$$f(\Lambda) =: \frac{2\pi}{\cos\chi} (\frac{G}{2\Lambda (F')^2})^{\frac{5}{6}},$$

we obtain from (3.12) the equation

$$f(\Lambda) = \frac{\Gamma(\frac{1}{4}-\frac{\Lambda}{2})}{\Gamma(\frac{3}{4}-\frac{\Lambda}{2})}, \qquad (3.13)$$

where we recall that Λ is defined in (3.11). In the subsequent discussion of this equation it will be convenient to consider the eigenvalues corresponding to the situations when G is (a) positive and (b) negative respectively.

(a) When $G>0$, the right-hand side of (3.13) is shown as a function of (real) Λ in Figure 3.4(a), where Λ_0 denotes the lowest eigenvalue (corresponding to the largest growth rate) given by the intersection of $\Gamma(1/4-\Lambda/2)/\Gamma(3/4-\Lambda/2)$ with $f(\Lambda)$. When $|\chi|<\pi/2$ (tearing mode unstable) then Λ_0 satisfies $0<\Lambda_0<1/2$, while when $|\chi|=\pi/2$, $f(\Lambda)$ becomes infinite, so that from (3.13) we must have $\Lambda_0=1/2$; that is $P\sim\{G'\}^{2/3}$, where for brevity we have put $G'=:G/(F')^2$.

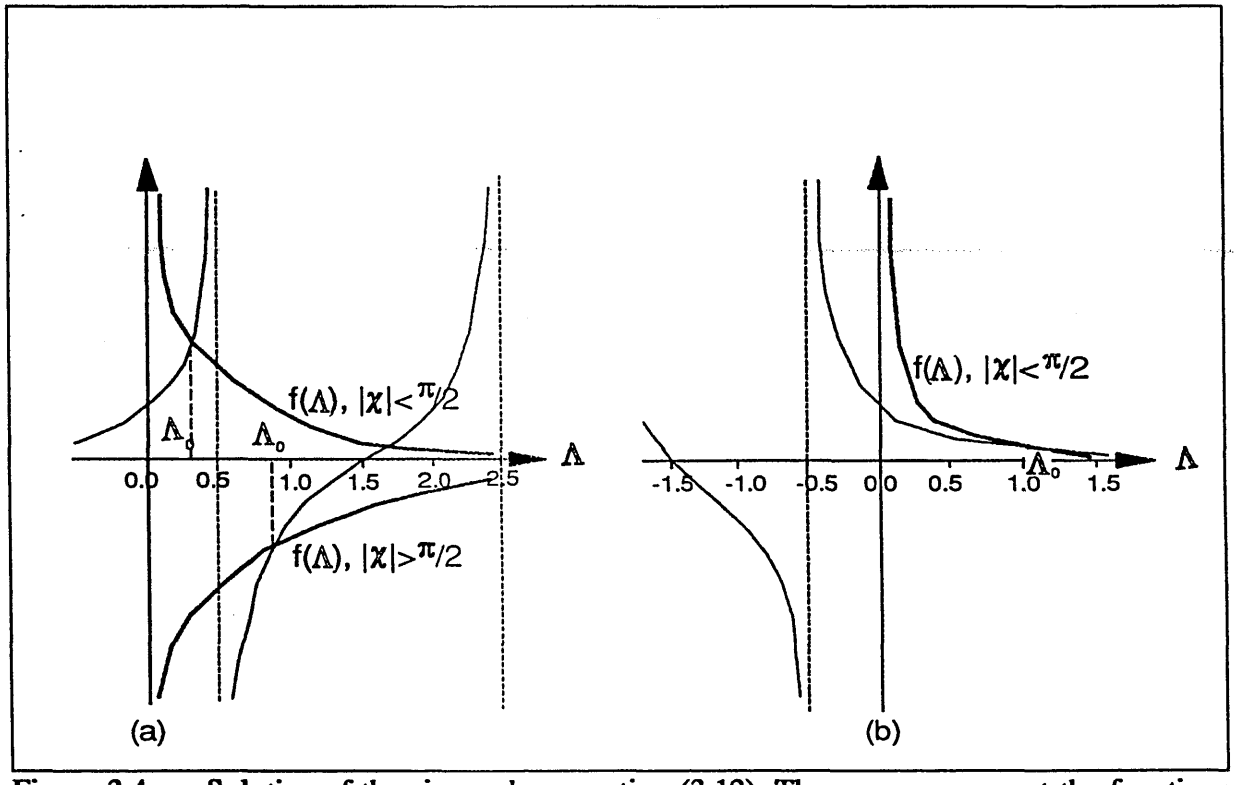

Figure 3.4 Solution of the eigenvalue equation (3.12). The curves represent the functions f(Λ) and Γ(1/4-Λ/2)/Γ(3/4-Λ/2) for the cases (a) G>0 and (b) G<0.

(b) When $G<0$ we have $\Lambda<0$. The right-hand side of (3.12) then decays like $(-\Lambda)^{-1/2}$ for large positive values of $-\Lambda$, so that there is only one point of intersection Λ_0 (since $f(\Lambda)$ is proportional to $(-\Lambda)^{-5/6}$) when $|\chi|<\pi/2$. If $|\chi|\geq\pi/2$ there is no real root; see Figure 3.4(b).

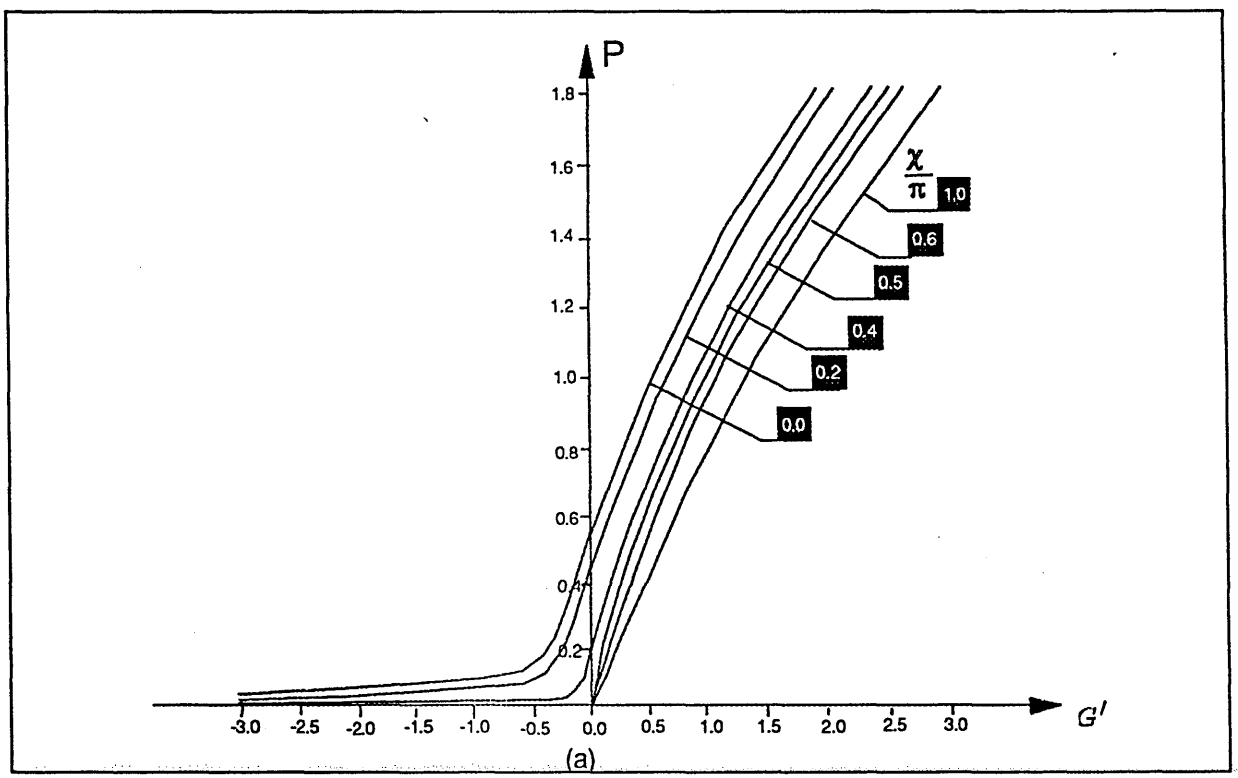

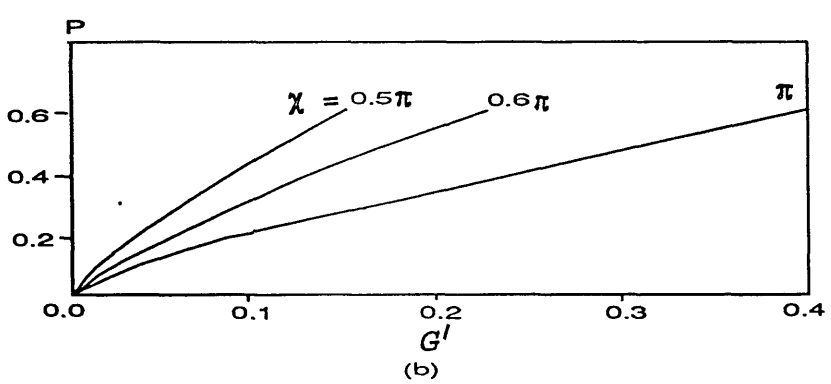

FIGURE 3.5 Real root branch of FKR G-mode (a) the growth rate P increases with G>0 and negative G has a stabilizing effect on the tearing mode; (b) the enlarged loci when the tearing mode is stable ($|\chi|\geq\pi/2$).

Using a Newton-Raphson method, together with a routine for evaluation of the gamma function of complex argument, we have solved (3.12) to obtain the behaviour of the lowest eigenvalue presented in Figures 3.5 and 3.6. These results show a real-root branch and a complex-root branch for modes with the largest growth rate, where the complex-root branch when $G<0$ corresponds to Figure 3.4(b) when $|\chi| \geq \pi/2$.

The principal results in Figures 3.5 and 3.6 may be summarized as follows:

(i) When $|\chi|<\pi/2$ and $G>0$, the growth rate P increases with G; in other words, the mode becomes more unstable. When $G<0$, the growth rate P decreases approaching zero with increasing $|G|$, which means that favourable gravity $G<0$ has a stabilizing effect. Figure 3.5(a) shows that negative G can reduce the growth rate when the tearing mode is unstable, but it never stabilizes the tearing mode completely.

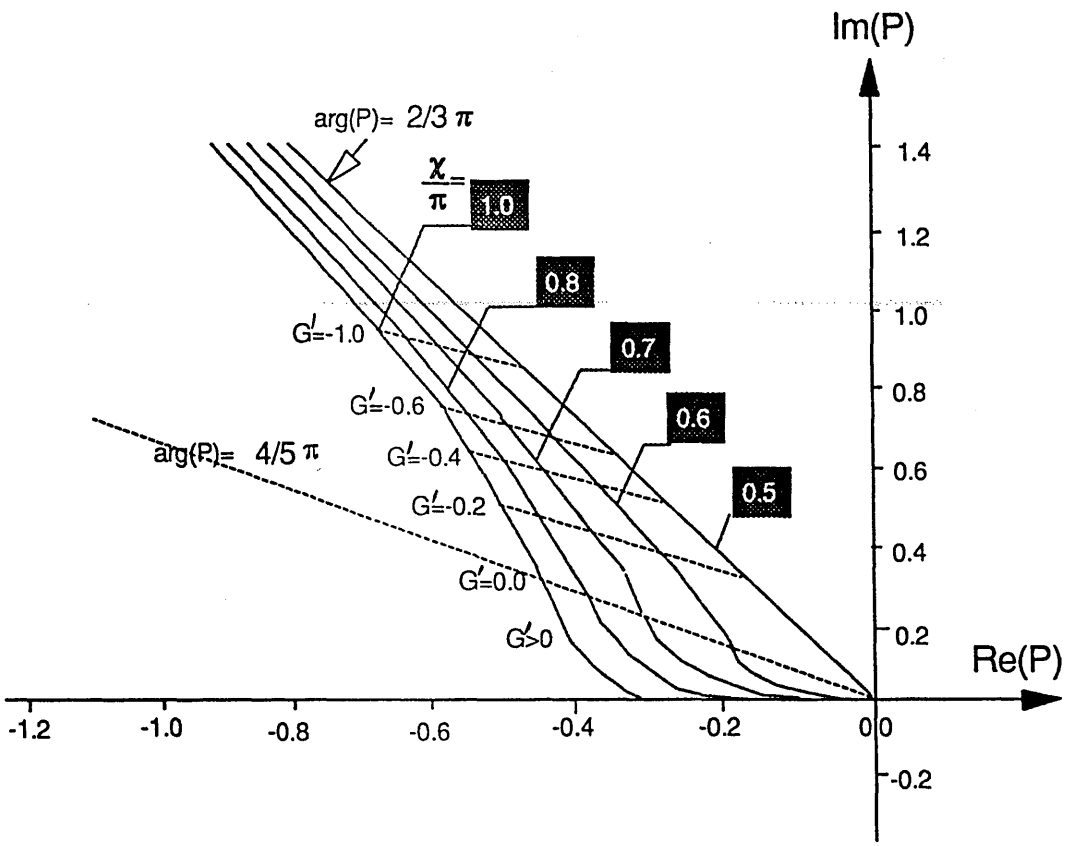

Fugure 3.6 The complex-root loci of the FKR G-mode growth rate as a function of G for different values of χ/π.

(ii) When $|\chi| \geq \pi/2$ and $G \neq 0$, there are two branches of P which appear: one is a real-root branch and the other is a complex-root branch. We found that the real-root branch increases positively with increasing $G > 0$; and the stable complex-root branch situated in the negative half-plane $Re(P) < 0$ approaches the origin as $G \to +\infty$. If G is increased negatively, we cannot find a real-root, but the complex-root branch approaches the ray $arg(P) = \pm 2\pi/3$, as $G \to -\infty$ [see (3.20)].

3.3 Asymptotic Estimates in the FKR Case

The various limits in Figures 3.5 and 3.6 have been estimated by suitable approximation of the quotient of gamma functions in (3.12), as $G \to \pm\infty$.

3.3.1 The estimates for $Re(P)$

When $G \to +\infty$, the real-root branch of P in Figure 3.6 is expected to correspond to large positive values of P. From (3.12), this requires $\Gamma(1/4 - \Lambda/2) \to \infty$ which yields $\Lambda_0 \to 1/2$, i.e. $G' P^{-3/2} \to 1$. Let us assume that $\Lambda_0 = 1/2 - \epsilon$, with $\epsilon \ll 1$. Then we have

$$P^{\frac{5}{4}} = \frac{\cos\chi}{2\pi} \frac{\Gamma(\frac{\epsilon}{2})}{\Gamma(\frac{1}{2} - \epsilon)} \approx \frac{\cos\chi}{2\pi} \frac{\Gamma(\frac{\epsilon}{2})}{\Gamma(\frac{1}{2})}$$

$$= \frac{\cos\chi}{2\pi^{3/2}} \frac{\Gamma(1 + \frac{\epsilon}{2})}{\frac{\epsilon}{2}} \approx \frac{\cos\chi}{\pi^{3/2}\epsilon} = \frac{2\cos\chi}{\pi^{3/2}} (1 - G' P^{-\frac{3}{2}})^{-1}.$$

This then yields the approximation

$$P^{\frac{3}{2}} \approx G' + \frac{2\cos\chi}{\pi^{3/2}} P^{\frac{1}{4}},$$

which may be solved perturbatively. Use of the leading order approximation $P \sim (G')^{2/3}$ in the right-hand side then leads to

$$P^{\frac{3}{2}} \approx G' + \frac{2\cos\chi}{\pi^{3/2}} G'^{\frac{1}{6}} = G'\left(1 + \frac{2\cos\chi}{\pi^{3/2}} G'^{-\frac{5}{6}}\right),$$

whence

$$P \approx (G')^{\frac{2}{3}} \left(1 + \frac{4\cos\chi}{3\pi^{3/2}} G'^{-\frac{5}{6}}\right), \quad G' \to +\infty. \tag{3.14}$$

When $G' \to -\infty$, the real-root branch of P approaches the origin $P=0$, (see §3.2.1 (i) and Figure 3.5) for $|\chi| < \pi/2$; if $|\chi| \geq \pi/2$, then from $\Gamma(1/4 + |G'|P^{-3/2}/4) \to \infty$, when $G' \to -\infty$, we have

$$P \sim |G'|^{\frac{2}{3}} e^{\pm\frac{2\pi i}{3}}, \quad G' \to -\infty \tag{3.15}$$

so that, the complex-root branch approaches the rays $arg(P) = \pm 2\pi/3$ (see Figure 3.6).

Making use of the result for the quotient of gamma functions (Abramowitz and Stegun, p.257, 1965)

$$\frac{\Gamma\left(\frac{1}{4} - \frac{\Lambda}{2}\right)}{\Gamma\left(\frac{3}{4} - \frac{\Lambda}{2}\right)} = \left(-\frac{\Lambda}{2}\right)^{-\frac{1}{2}} \left[1 + O(\Lambda^{-2})\right], \ \Lambda \to \infty \text{ in } |arg(-\Lambda)| < \pi, \tag{3.16}$$

we may obtain immediately from (3.12)

$$P \sim -\frac{\cos^2\chi}{\pi^2 G'}. \quad G' \to \pm\infty. \tag{3.17}$$

This result approximates the real-root branch as $G' \to -\infty$, and also the value of $Re(P)$ for the complex-root branch as $G' \to +\infty$. The expansion in (3.16), however, yields no contribution to the imaginary part of P in this latter case.

3.3.2 An estimate for the imaginary part of the growth rate P

To explore the limit of $Im(P)$ when $|\chi| > \pi/2$ and $G \gg 1$, we use the exponentially-improved asymptotics for the gamma function (Paris and Wood, 1992). A brief summary of these results is given below.

Stirling's asymptotic expansion for the gamma function, which is valid for $|z| \to \infty$ in $|arg(z)| \leq \pi/2 - \epsilon$, for any $\epsilon > 0$, shows that

$$\Gamma(z) \sim \sqrt{2\pi} z^{z-\frac{1}{2}} e^{-z} \left(1 + \frac{1}{12z} + \frac{1}{288z^2} + \cdots\right),$$

as $|z| \to \infty$, in $|arg(z)| \leq \frac{\pi}{2} - \epsilon$.

To obtain the expansion in $|arg(-z)| < \pi/2$, we use the reflection formula

$$\Gamma(z) = -\frac{\pi}{z \sin(\pi z)} \frac{1}{\Gamma(-z)},$$

which yields

$$(1 - e^{\pm 2\pi i z}) \Gamma(z) \sim \sqrt{2\pi} z^{z-\frac{1}{2}} e^{-z} \left(1 + \frac{1}{12z} + \frac{1}{288z^2} + \cdots\right),$$

as $|z| \to \infty$, in $|arg(-z)| \leq \pi/2 - \epsilon$. (3.18)

Comparing the expansions of $\Gamma(z)$ in $|arg(z)| < \pi/2$, $|arg(-z)| < \pi/2$ and on $|arg(z)| = \pi/2$, we find that there is a "switch" multiplier $s(\theta)$ (for fixed $|z|$) multiplying the exponential factors $e^{\pm 2\pi i z}$ (with the upper or lower sign being chosen according to z being in the upper or lower half plane) given by

$$s(\theta) = \begin{cases} 0, & 0 \leq |\theta| < \frac{\pi}{2} \\ \frac{1}{2}, & |\theta| = \frac{\pi}{2} \\ 1, & \frac{\pi}{2} < |\theta| < \pi \end{cases} \qquad (3.19)$$

when $\theta = arg(z)$. In the sector $\pi/2 < |\theta| < \pi$, the terms $e^{\pm 2\pi i z}$ are, of course, exponentially small as $|z| \to \infty$ and so are negligible in the usual Poincaré definition of an asymptotic expansion. As $|\theta| \to \pi$, the terms $e^{\pm 2\pi i z}$ become $O(1)$ and the factor $(1 - e^{\pm 2\pi i z})^{-1}$ is responsible for the poles of $\Gamma(z)$ on the negative real axis.

Hence we can write

$$(1 - s(z)\, e^{\pm 2\pi i z}) \Gamma(z) = \sqrt{2\pi} z^{z-\frac{1}{2}} e^{-z} (1 + O(z^{-1})), \qquad |z| \to \infty$$

in $|arg(z)| < \pi$. We now consider fixed $|z|$ and vary $\theta = arg(z)$. Using the binomial theorem to expand $(1 - s(z)\, e^{\pm 2\pi i z})^{-1}$ and retaining only the first subdominant exponentials $e^{\pm 2\pi i z}$, we obtain

$$\Gamma(z) \sim \sqrt{2\pi} z^{z-\frac{1}{2}} e^{-z} (1 + O(z^{-1}) + s(\theta)\, e^{\pm 2\pi i z}), \quad |z| \to \infty \tag{3.20}$$

where we have introduced the Stokes multiplier $s(\theta)$ and

$$s(\theta) = \begin{cases} 0, & 0 \le |\theta| < \frac{\pi}{2} \\ \frac{1}{2}, & |\theta| = \frac{\pi}{2} \\ 1, & \frac{\pi}{2} < |\theta| < \pi \end{cases} \tag{3.21}$$

By means of detailed analysis, Paris and Wood (1992) showed that, $s(\theta)$ is a continuous function of θ which changes rapidly but smoothly across the Stokes lines $|\theta| = \pi/2$. Following on from earlier treatment of the smoothing of the Stokes phenomenon (Berry, 1989), Paris and Wood showed that in the neighbourhood of $|\theta| = \pi/2$, $s(\theta)$ is described to leading order for large fixed $|z|$ by an error function

$$s(\theta) \approx \frac{1}{2} \pm \frac{1}{2} erf[(\theta \mp \frac{\pi}{2})\sqrt{\pi |z|}], \quad |z| \to \infty. \tag{3.22}$$

where the signs $\pm$ are chosen according as z is in the upper or lower half plane respectively. This representation is in accordance with (3.21) since the extreme values of the error function are ± 1 for large positive and negative arguments respectively and is zero when $\theta = \pm \pi/2$.

Thus, for large $|\Lambda|$, the quotient of gamma functions in (3.21) may be written approximately as

$$\frac{\Gamma(\frac{1}{4} - \frac{\Lambda}{2})}{\Gamma(\frac{3}{4} - \frac{\Lambda}{2})} \sim (-\frac{\Lambda}{2})^{-\frac{1}{2}} \{1 \mp 2is(\theta)\, e^{-\pi i \Lambda}\},$$

where $s(\theta)$ is the Stokes multiplier given by

$$s(\theta) \approx \frac{1}{2} \pm \frac{1}{2} erf[(\theta \mp \frac{\pi}{2})\sqrt{\pi |\Lambda|/2}], \quad \theta = arg(\Lambda), \quad |\Lambda| \to \infty$$

and the upper or lower signs are chosen according as Λ is in the upper or lower half plane. Then from (3.12). we have

$$\frac{2\pi}{\cos\chi}P^{\frac{5}{4}} \sim (-\frac{\Lambda}{2})^{-\frac{1}{2}}[1\mp 2is(\theta)e^{-\pi i\Lambda}], \quad \Lambda=\frac{G'}{2}P^{-\frac{3}{2}}$$

As $arg(P)$ is close to π for the complex branch as $G'\to+\infty$, we may take $arg(P)=\pi-\epsilon$, where $\epsilon=\tan^{-1}|Im(P)/Re(P)|\ll 1$, then

$$\theta = arg(\Lambda) = arg(P^{-\frac{3}{2}}) = \frac{\pi}{2}+\frac{3}{2}\epsilon .$$

Thus

$$s(\theta) \approx \frac{1}{2}\pm\frac{1}{2}erf[\frac{3\epsilon}{4}\sqrt{\pi G'|P|^{-3/2}}], \qquad (3.24)$$

and (3.23) yields

$$P^{\frac{5}{4}} \sim \frac{\cos\chi}{2\pi}(-\frac{G'}{4}P^{-\frac{3}{2}})^{-\frac{1}{2}}[1\mp 2is(\theta)e^{-\frac{\pi}{2}G'iP^{-3/2}}] . \qquad (3.25)$$

Solving perturbatively, we then obtain

$$P \sim -\frac{\cos^2\chi}{\pi^2 G'}(1\mp 4is(\theta)e^{-\frac{\pi^4(G')^{5/2}}{2|\cos\chi|^3}}), \qquad (3.26)$$

whence

$$Re(P) \sim -\frac{\cos^2\chi}{\pi^2 G'},$$

$$Im(P) \sim \pm 4\frac{\cos^2\chi}{\pi^2 G'}s(\theta)e^{-\frac{\pi^4(G')^{5/2}}{2|\cos\chi|^3}} . \qquad (3.27)$$

Thus $Im(P)$ is seen to be exponentially small in the limit $G'\to+\infty$.

From the expansion of $erf(x)$ (Abramowitz and Stegun, 1965)

$$erf(x) = \frac{2}{\sqrt{\pi}}\sum_{n=0}^{\infty}\frac{(-1)^n x^{2n+1}}{n!\,(2n+1)} = O(x), \qquad x\to 0$$

we found the contribution of $erf[3\epsilon\sqrt{\pi G'|P|^{-3/2}}/4]$ in (3.24) to be about $10^{-5}\sim 10^{-6}$ in numerical calculations when $|\Lambda|\gg 1$, so that the error function in (3.22) is ignored when

estimating $s(\theta)$; in this case, we take simply the value on the Stokes lines $|\theta|=\pi/2$ given by $s(\theta)\approx S(\pi/2)=1/2$.

The asymptotic approximation (3.26) consequently yields the result

$$P \sim -\frac{\cos^2\chi}{\pi^2 G'}\left[1 \mp 2ie^{-\frac{\pi^4 (G')^{5/2}}{2|\cos\chi|^3}}\right], \qquad (3.28)$$

which shows good agreement with the result of $Im(P)$ from the Newton-Raphson iterative method (see Table 3.2 and Figure 3.7). It is difficult, however, to obtain high quality numerical results for $Im(P)$ using single-precision arithmetic once G' is greater than 10.

TABLE 3.1 The numerical and asymptotic estimates of the FKR G-mode growth rate for the real-root branch.

		Asymptotic: $P \approx (G')^{\frac{2}{3}}\{1+\frac{4\cos\chi}{3\pi^{3/2}}(G')^{-\frac{5}{6}}\}$,					Numerical: $P^{\frac{5}{4}} = \frac{\cos\chi}{2\pi}\frac{\Gamma(1/4-\Lambda/2)}{\Gamma(3/4-\Lambda/2)}$				
G'	$\frac{\chi}{\pi}$	0.0	0.2	0.5	0.8	1.0	0.0	0.2	0.5	0.8	1.0
2.0		1.80	1.76	1.587	1.41	1.374	1.81	1.769	1.588	1.426	1.39
2.5		2.04	2.01	1.84	1.67	1.63	2.05	2.01	1.84	1.685	1.65
3.0		2.27	2.24	2.08	1.92	1.88	2.288	2.24	2.09	1.926	1.89
3.5		2.49	2.45	2.3	2.14	2.10	2.5	2.47	2.3	2.15	2.12
4.0		2.71	2.67	2.52	2.36	2.33	2.72	2.68	2.52	2.37	2.34
4.5		2.91	2.876	2.725	2.57	2.54	2.92	2.88	2.73	2.58	2.55
5.0		3.10	3.07	2.92	2.77	2.74	3.11	3.07	2.92	2.78	2.75
6.0		3.47	3.44	3.3	3.16	3.12	3.48	3.45	3.3	3.16	3.13
7.0		3.83	3.80	3.66	3.52	3.49	3.84	3.80	3.66	3.52	3.49

The asymptotics of the approximation for the complex branch P yields the results for various limits and shows that when $|\chi|>\pi/2$ (where the tearing mode is stable), from (3.27)

$$Re(P) \sim -\frac{\cos^2\chi}{\pi^2 G'} \to -0, \qquad G' \to +\infty,$$

$$Im(P) \sim \pm 2\frac{\cos^2\chi}{\pi^2 G'} e^{-\frac{\pi^4 (G')^{5/2}}{2|\cos\chi|^3}} \to \pm 0, \qquad G' \to +\infty. \tag{3.29}$$

Here $Re(P)$ decays algebraically and $Im(P)$ decays exponentially in the negative half P-plane when G' is positive. The complex-root branch therefore is well separated from the real-root branch, so that modes of different branches are distinguished. This part of the analysis is vital for the further investigation of the growth rate P when the flow parameter R is non-zero in the following chapters, because we have established the starting point of the growth rate loci in the complex P-plane for R increasing from zero for both the gravitational mode and the tearing mode.

Finally, we summarize the FKR results as follows (Table 3.2):

TABLE 3.2 The asymptotic estimates on the flowless FKR growth rate P

When $\lvert\chi\rvert < \frac{\pi}{2}$	$(G')^{\frac{2}{3}}\left[1+\frac{4\cos\chi}{3\pi^{3/2}}(G')^{-\frac{5}{6}}\right], \quad G' \to +\infty$
	$\frac{\cos^2\chi}{\pi^2\lvert G'\rvert}, \quad G' \to -\infty$
When $\lvert\chi\rvert = \frac{\pi}{2}$	$(G')^{\frac{2}{3}}, \quad G'>0$
	$\lvert G'\rvert^{\frac{2}{3}} e^{\pm\frac{2\pi i}{3}}, \quad G'<0$
When $\frac{\pi}{2} < \lvert\chi\rvert \le \pi$	$Re(P) \sim -\frac{\cos^2\chi}{\pi^2 G'}, \quad G' \to +\infty$
	$Im(P) \sim \frac{2\cos^2\chi}{\pi^2 G'} e^{-\frac{\pi^4 (G')^{5/2}}{2\lvert\cos\chi\rvert^3}}, \quad G' \to +\infty$
	$\sim \lvert G'\rvert^{\frac{2}{3}} e^{\pm\frac{2\pi i}{3}}, \quad G' \to -\infty$

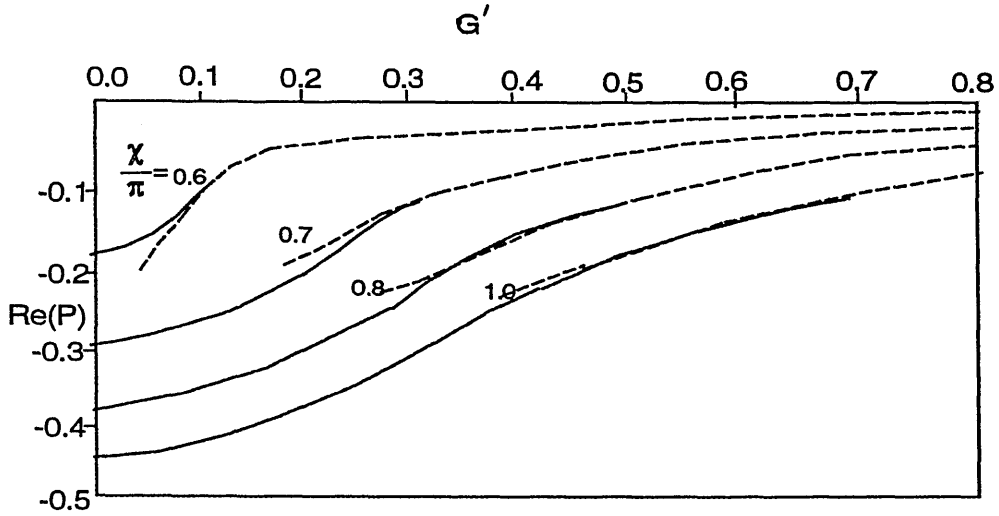

(a)

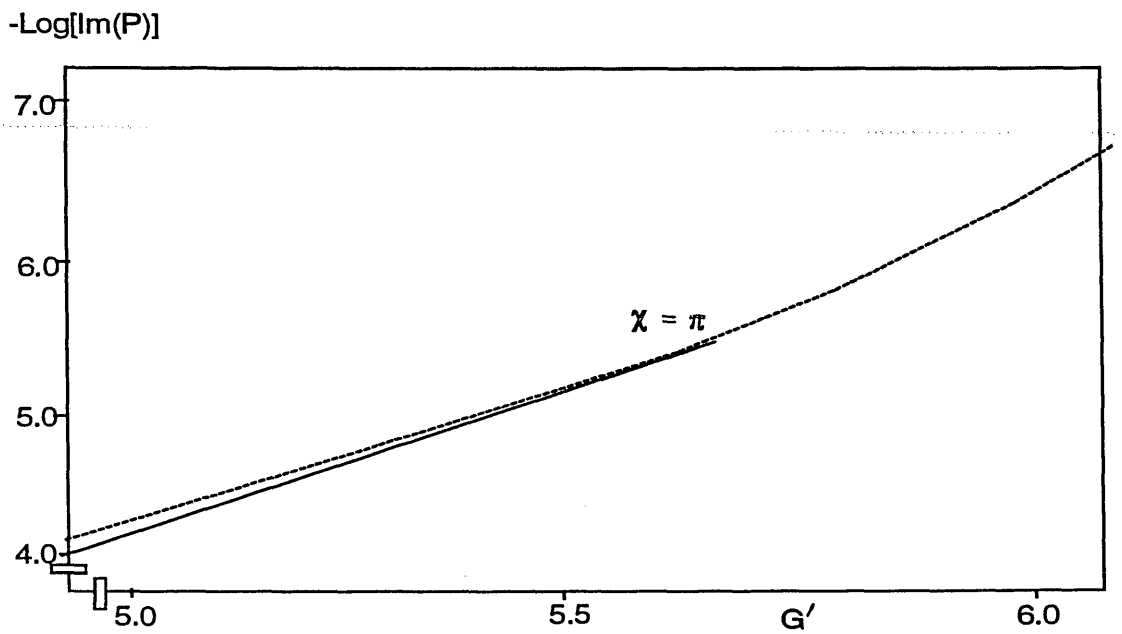

(b)

Figure 3.7 A comparison between the numerical result (solid line) and the asymptotic result (dashed line) for (a) Re(P) and (b) Im(P) respectively.

Each of these limits is found to agree well with the numerically computed values of P. Here we present the results in Table 3.1 for $G>0$ representing the most interesting real root G-mode growing behaviour. In Figure 3.7 (a) and (b), a comparison between the numerical result and the asymptotic result of the complex root branch when $\chi=\pi$ is given for $Re(P)$ and $Im(P)$ respectively.

The numerical results (solid lines in Figure 3.7) show that for the complex-root branch the numerical method is limited in obtaining the exponentially decaying solution. By use of the asymptotic estimate as given in (3.29) we obtain a better approximation of $Re(P)$ and $Im(P)$ (which is denoted by dashed lines in Figure 3.7) when $G\to+\infty$ and $|\chi|>\pi/2$.

CHAPTER IV
THE EFFECTS OF EQUILIBRIUM FLOW ON THE TEARING AND GRAVITATIONAL MODES

Introduction

In Chapter 3 we obtained the behaviour of the growth rate P of the tearing and gravitational interchange modes in the flowless case $R=0$. In this chapter we consider the effects on these modes of an equilibrium flow along the magnetic field, using the results when $R=0$ to initiate our computational procedure for the determination of the loci in the complex P-plane as the flow parameter R increases from zero.

The essential question we ask is: Does the equilibrium flow stabilize or destabilize the tearing and gravitational interchange modes? The complication which arises from the mixing of the hydrodynamic Kelvin-Helmholtz instability due to the relative motion with the resistive instabilities is eliminated in our study. This was achieved by considerating situations where the flow is sufficiently slow on the Alfvén time scale so that its effects are confined to the narrow resistive layer. The problem which remains is, however, still complicated enough when $R\neq0$. Another difficulty is that, although the tearing mode can be studied in isolation (by setting $G=0$), it is not possible to consider the G-mode separately, since when $G\neq0$ a degree of mode mixing is unavoidable. We observe that when $\chi=0$ the tearing mode is most active, while $\chi=\pi$ the effects from the tearing mode are minimised.

The investigation concentrates on the influence of the inviscid flow first. We treat the case when the plasma response is inviscid by setting $N=0$ in (2.37), where the eigenvalue P now corresponds to the growth rate of the inviscid tearing mode and G-mode respectively. Viscous effects will be considered in Chapter 5.

4.1 The Eigenvalue Problem and the Applicable Numerical Methods

The numerical computation of the eigenvalue P in (2.33) is carried out to obtain the complex eigenvalue loci in the complex P-plane for intermediate values of flow

parameter R for the tearing mode (G=0) and the G-mode ($G\neq 0$) cases.

A numerical method for the Fourier transformed equation (2.50) and the associated eigenvalue relation (2.46) has been employed to solve the eigenvalue problem in the complex plane. Another method, called the direct method, has been used to check the eigenvalue P from the Fourier transform method. If the variation of the numerical values of P from these two methods is small then the numerical Fourier transform method can be accepted in our numerical analysis.

To obtain the behaviour of the G-mode, the tearing mode results for different values of R are treated as a standard benchmark when $G=0$. When the parameter G is increased from zero, a smooth transition of the eigenvalue loci from the tearing mode to the G-mode is expected.

4.1.1 The G-mode and tearing mode equations from the Fourier transformation

The G-mode equation has been derived in Chapter 2, by means of Fourier transformation, as

$$Mh = -2\pi\left[\frac{GR}{(F')^2} - \frac{PF''}{\Delta F'}\right]\delta(k) - 2\pi\left[iP^2 + \frac{RF''}{\Delta F'}\right]\delta'(k) + 2\pi iPR\delta''(k),$$

where M denotes the differential operator

$$Mh = R\frac{d^3h}{dk^3} + \frac{d^2}{dk^2}\left[(k^2R^2 - P)h\right]$$

$$-\frac{d}{dk}\left[(2PRk^2 + NRk^4)h\right] + \left[k^2P^2 - \frac{G}{(F')^2} + NPk^4\right]h$$

$$= \left(R\frac{d}{dk} - P\right)Lh - \frac{G}{(F')^2}h,$$

and $Lh = 2\pi iP\delta'(k) + 2\sin\chi\delta(k)$ is the associated viscous tearing mode operator

$$Lh = \frac{d^2h}{dk^2} + R\frac{d}{dk}(k^2h) - (k^2P + k^4N)h.$$

Hence, if $G=0$, then

$$Mh = 2\pi iPR\delta''(k) - 2\pi\left[iP^2 + \frac{RF''}{\Delta F'}\right]\delta'(k) + 2\pi\frac{PF''}{\Delta F'}\delta(k)$$

$$= 2\pi iPR\delta''(k) + 2R\sin\chi\delta'(k) - 2\pi iP^2\delta'(k) - 2P\sin\chi\delta(k)$$

$$= \left(R\frac{d}{dk} - P\right)Lh.$$

Thus the differential operators M and L yield, when $G=0$, equivalently

$$Mh = 0 \quad \Leftrightarrow \quad Lh = 0, \quad -\infty < k < 0, \quad 0 < k < +\infty.$$

The problem of the stabilizing or destabilizing effects of flow R on the eigenvalue P will be investigated for the tearing mode $(G=0)$ first and for G-mode by gradually increasing the gravitational term $G/(F')^2$.

We carry out the numerical investigation when $R>0$, $0\le\chi\le\pi$,

$$Mh = 0, \qquad -\infty < k < 0, \quad 0 < k < +\infty \tag{4.1}$$

with six boundary conditions:

$$\begin{gathered} h'(0\pm) = -ie^{\pm i\chi}, \quad h(\pm\infty) = 0, \quad h(0+) = 1, \\ h''(0-) = h''(0+) + 2\pi i\frac{G}{(F')^2}, \end{gathered} \tag{4.2}$$

and the eigenvalue relation:

$$2\pi P = \frac{h(0-)}{h'(0-)}e^{-i\chi} - \frac{h(0+)}{h'(0+)}e^{i\chi}, \qquad 0\le\chi\le\pi. \tag{4.3}$$

To determine the suitable truncation value k_∞ for $h(k)$ in the numerical computation for the boundary conditions in (4.2), we adopt the following numerical scheme. Fix R, G, N and χ, and choose $k_\infty>1$, we repeat to solve (4.1) (by a standard integration routine) for decaying convergent solutions*, say, $h_1(k)$ and $h_2(k)$ for chosen value $k_1>1$ and for chosen value $k_2>k_1$. Then check $|h_1'(0) - h_2'(0)|$, until the difference is small.

The eigenvalue problem $P =: P(R, G, N, \chi)$ is studied for values of $\chi\in[0,\pi]$, by

considering first the inviscid limit $N=0$. Set $P=P_0$, the first guess of the eigenvalue, for $n=1,2,3,\cdots$, and solve (4.1) with $P=P_n$ and boundary conditions (4.2) until $|P_{n+1}-P_n|<10^{-6}$. To satisfy the eigenvalue relation $Ei(P) = [h(0)]_-^+ - 2\pi iP$, we want to find the growth rate P such that $Ei(P)=0$. An iterative method based on a Newton-Raphson procedure has been used to obtain a new estimate $P=P_{n+1}$. We continue the process until the desired tolerance is achieved. Because of the lack of packages for complex eigenvalues of Sturm-Liouville problems, or for real eigenvalues where the parameter appears in a jump condition at the end point, it was necessary to write our own code in FORTRAN: the viscous G-mode program---MHD.FOR.

In the G-mode program, we made the transformation $k=x/(1-x)$, with a multiplier $C(C=\pm1)$, $Ck=Cx/(1-x)$, enables us to deal with $k\geq0$ or $k<0$. This non-linear transformation facilitates the determination of a decaying solution with the boundary conditions (4.2) now confined to the finite interval [0,1). In this case the derivatives with respect to k become

$$\frac{d}{dk} = (1-x)^2\frac{d}{dx}, \quad \frac{d^2}{dk^2} = (1-x)^4\frac{d^2}{dx^2} - 2(1-x)^3\frac{d}{dx},$$

$$\frac{d^3}{dk^3} = (1-x)^6\frac{d^3}{dx^3} - 6(1-x)^5\frac{d^2}{dx^2} + 6(1-x)^4\frac{d}{dx}.$$

We found that $x_\infty\in[0.8,0.98]$ was generally sufficient for both $x>0$ or $x<0$ cases.

4.1.2 Qualitative discussion of the solution $h(k)$ of (4.1)

To determine suitable values of k_∞ analytically and examine the structure of the eigenfunction $h(k)$ as $k\to\pm\infty$, we use simple dominant balance arguments (Bender and Orszag, 1975) to (4.1).

Let $h(k) \sim e^{-ak^n/n}$, as $k\to\infty$, where a is an unknown parameter and, n is an integer.

---

* **Definition of the decaying convergent numerical solution $h(k)$:** For arbitrary small $\epsilon>0$, there is a large number $N\gg1$. If $k_2>k_1>N$ then any numerical solutions of (4.1), say, $h_1(k)$ and $h_2(k)\in C^2[k]$ satisfy $|h_2(k_2)|<|h_1(k_1)|<\epsilon$ and $|h_1'(0)-h_2'(0)|<\epsilon$.

We find

$$Mh \sim Ra^3k^{3n-3}h - R^2k^2h'' - 4R^2kh' - 2R^2h + Ph'' + 4PRkh + 2PRk^2h'$$

$$+ NRk^4h' + 4NRk^3h - (P^2k^2 - \frac{G}{(F')^2} + NPk^4)\,h. \qquad (4.4)$$

We note that the G term does not enter into the dominant balance equation to leading order, so that the behaviour of the eigen-function is not sensitive to the parameter G.

There are two distinguished limits when $n=1$ and $n=3$, as $k \to \pm\infty$.

(i) When $n=1$, then $h' \sim -ah$ $h'' \sim a^2h$, (4.4) yields

$$Ra^3 - a^2R^2k^2 + 4aR^2k - 2R^2 + a^2P + 4PRk - 2aPRk^2$$

$$-aNRk^4 + 4NRk^3 - P^2k^2 + \frac{G}{(F')^2} - NPk^4 = 0\,.$$

Balancing the leading tems of $O(k^4)$, we have $aNR+NP=0$, or $a=-P/R$. The asymptotic solution satisfying the boundary condition in (4.2) is then

$$h(k) \sim e^{\frac{P}{R}k}, \qquad k \to -\infty;$$

(ii) When $n=3$, we have $h' \sim -ak^2h$ and $h'' \sim -2akh + a^2k^4h$, so that

$$Ra^3k^6 - a^2R^2k^6 + 6aR^2k^3 + a^2Pk^4 - 2aPk^4$$

$$+ 4RPk - 2aRPk^4 - aNRk^6 + 4NRk^3 - P^2k^2 - NPk^4 = 0\,.$$

From the leading terms of $O(k^6)$, we obtain

$$a^3R - a^2R^2 - aNR = 0\,.$$

If $N=0$, then $a=R$ and therefore

We find

$$Mh \sim Ra^3k^{3n-3}h - R^2k^2h'' - 4R^2kh' - 2R^2h + Ph'' + 4PRkh + 2PRk^2h'$$

$$+ NRk^4h' + 4NRk^3h - (P^2k^2 - \frac{G}{(F')^2} + NPk^4)\,h. \qquad \textbf{(4.4)}$$

We note that the G term does not enter into the dominant balance equation to leading order, so that the behaviour of the eigen-function is not sensitive to the parameter G.

There are two distinguished limits when $n=1$ and $n=3$, as $k \to \pm\infty$.

(i) When $n=1$, then $h' \sim -ah$ $h'' \sim a^2h$, (4.4) yields

$$Ra^3 - a^2R^2k^2 + 4aR^2k - 2R^2 + a^2P + 4PRk - 2aPRk^2$$

$$-aNRk^4 + 4NRk^3 - P^2k^2 + \frac{G}{(F')^2} - NPk^4 = 0\,.$$

Balancing the leading tems of $O(k^4)$, we have $aNR+NP=0$, or $a=-P/R$. The asymptotic solution satisfying the boundary condition in (4.2) is then

$$h(k) \sim e^{\frac{P}{R}k}, \qquad k \to -\infty;$$

(ii) When $n=3$, we have $h' \sim -ak^2h$ and $h'' \sim -2akh + a^2k^4h$, so that

$$Ra^3k^6 - a^2R^2k^6 + 6aR^2k^3 + a^2Pk^4 - 2aPk^4$$

$$+ 4RPk - 2aRPk^4 - aNRk^6 + 4NRk^3 - P^2k^2 - NPk^4 = 0\,.$$

From the leading terms of $O(k^6)$, we obtain

$$a^3R - a^2R^2 - aNR = 0\,.$$

If $N=0$, then $a=R$ and therefore

$$h(k) \sim e^{-\frac{R}{3}k^3}, \quad k \to +\infty;$$

If $N \neq 0$, we have $a = [R \pm \sqrt{R^2+4N}]/2$ and

$$h(k) \sim \exp\left[\frac{-(R \pm \sqrt{R^2+4N})\,k^3}{6}\right], \quad k \to \pm\infty.$$

From the above estimates, we see that in the inviscid case ($N=0$) when $k \to +\infty$, both the tearing mode solutions and G-mode solutions $h(k)$ all eventually exhibit the rapid exponential decay like $e^{-Rk^3/3}$.

For $k \to -\infty$, we discuss the cases separately according as $Re(P)$ is positive or negative and R large or small. If we switch on the G-term, it would make little effect on the structure of the eigenfunction as the G-term does not enter into the leading order of $Mh = 0$. When $Re(P) > 0$, $h(k)$ decays exponentially like $e^{Pk/R}$ as $k \to -\infty$. The solution is affected by R, as large R makes $h(k)$ decay more slowly [see Figures 4.3(a) and 4.3(b)]. When $Re(P) < 0$ and R large, the flow term dominates (4.1), so that the solution $h(k)$ satisfies approximately to the equation

$$h'' + R(k^2 h)' = 0.$$

The solution of this equation which satisfies $h(0) = 1$ and decays at infinity, is given by

$$h(k) = ce^{-\frac{R}{3}k^3} \int_{-\infty}^{k} e^{\frac{R}{3}x^3} dx = O(k^{-2}), \quad k \to -\infty$$

where $c = -3^{2/3}R^{1/3}/\Gamma(1/3)$. So that $h(k)$ decays algebraically like $O(k^{-2})$. From Figure 4.2 and Figure 4.5, we can see that the solution decays more slowly than the cases in Figures 4.1 and 4.4 when $Re(P) > 0$.

To explain qualitatively the principal features of Figure 4.3, we proceed to examine the equation for $h(k)$ when $G=0$, namely

$$h'' + R(k^2 h)' - Pk^2 h = 0. \tag{4.5}$$

For $R \ll 1$, and for k satisfying $-k_0 < k \leq 0$, we can ignore the flow term in (4.5) to find approximately Weber's equation

$$h''-Pk^2h = 0\,.$$

This equation has solutions, for k away from the origin, which are characterised by

$$h(k) \sim k^{-\frac{1}{2}} e^{\pm\frac{1}{2}P^{1/2}k^2},$$

showing a parabolic cylinder function type solution. For sufficiently large k, however, the flow term $R(k^2h)'$ will eventually dominate. We may then ignore the P term so that when $k\to-\infty$

$$h''+R(k^2h)' = 0,$$

The transition of the solution from the exponentially oscillatory to the algebraic behaviour will occur when the flow term approximately balances the growth rate term i.e.

$$|Rk^2h'| \approx |Pk^2h|\,.$$

Since $h'\approx kP^{1/2}h$ in the oscillatory region, we find $|Rk_0^3P^{1/2}h| \approx |Pk_0^2h|$, which yields the transition roughly given by

$$k_0 \approx \frac{|P|^{\frac{1}{2}}}{R}.$$

The computed result shows a good agreement with this estimate (see Figure 4.3).

Hence, we are able to classify the eigen-functions into four regimes according to the values of $Re(P)$, R and N.

(i) When N=0, $Re(P)>0$ (see Figure 4.1 and Figure 4.4)

$$h(k) \sim \begin{cases} e^{-\frac{R}{3}k^3}, & k\to+\infty \\ \\ k^{-2}e^{\frac{P}{R}k}, & k\to-\infty. \end{cases}$$

(ii) When N=0, $Re(P)<0$, $R>1$ (see Figure 4.2 and Figure 4.5)

$$h(k) \sim \begin{cases} e^{-\frac{R}{3}k^3}, & k \to +\infty \\ k^{-2}, & k \to -\infty. \end{cases}$$

(iii) When $N=0$, $Re(P)<0$, $R \ll 1$ (see Figure 4.3 and Figure 4.6)

$$h(k) \sim \begin{cases} e^{-\frac{R}{3}k^3}, & k \to +\infty \\ k^{-\frac{1}{2}} e^{\pm\frac{1}{2}P^{1/2}} k^2, & -k_0 < k < 0, \\ k^{-2}, & -\infty < k < -k_0 \end{cases}$$

where $k_0 \approx |P|^{1/2}/R$.

(iv) When $N \neq 0$, (see Figure 4.7)

$$h(k) \sim \begin{cases} \exp\{-[R+\sqrt{R^2+4N}]\, k^3/6\}, & k \to +\infty \\ \exp\{-[R-\sqrt{R^2+4N}]\, k^3/6\}, & k \to -\infty \end{cases}$$

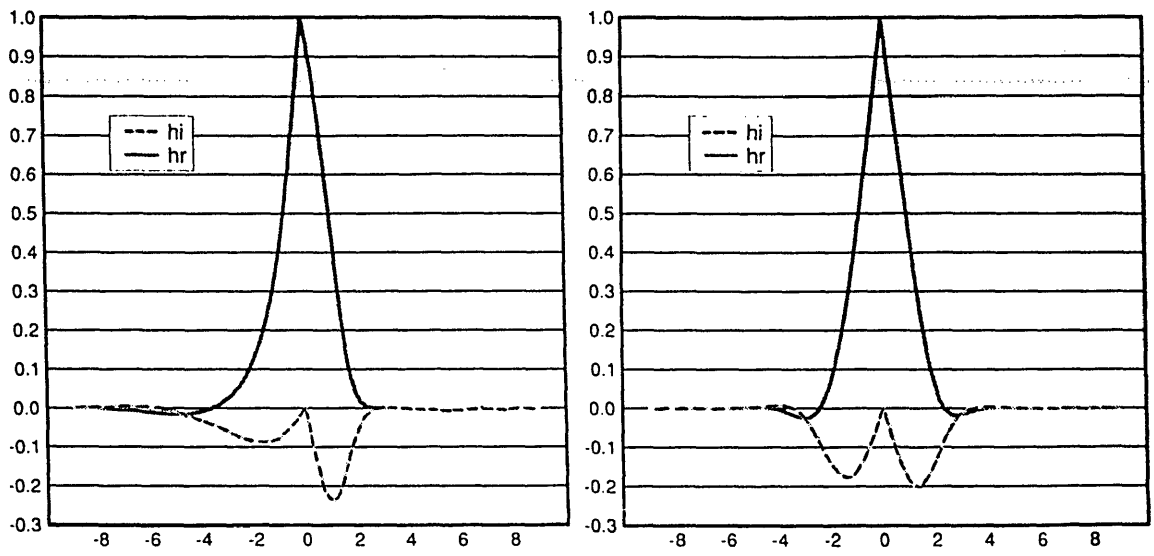

FIGURE 4.1 The tearing mode eigen-function when N=0, Re(P)=0.1 and Im(P)=0.6 (a) R=0.8 (b) R=0.1. Where h_r is the real part of h(k) and h_i is the imaginary part of h(k).

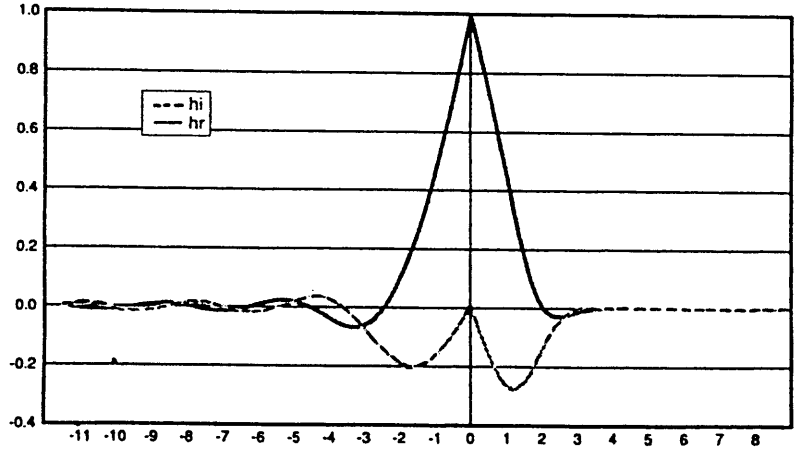

FIGURE 4.2 The tearing mode eigen-function when N=0, Re(P)=-0.1, Im(P)=0.6 and R=1.0.

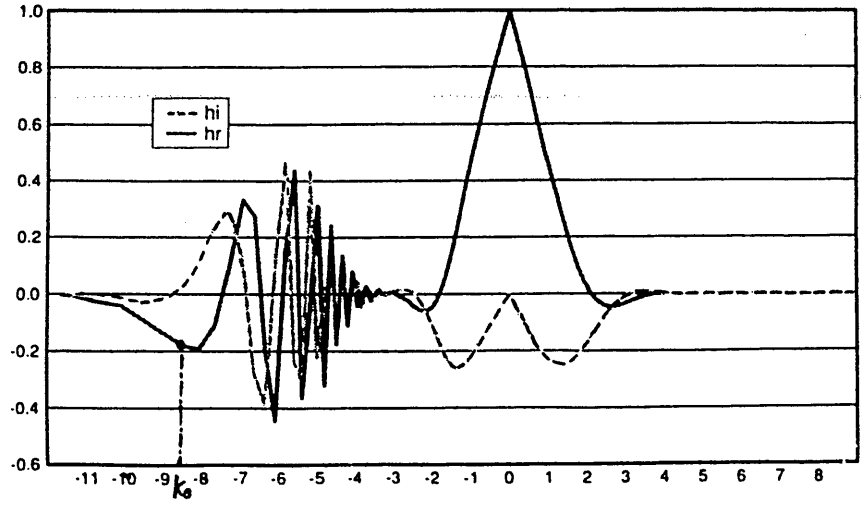

FIGURE 4.3 The tearing mode eigen-function when N=0, Re(P)=-0.1, Im(P)=0.6 and R=0.065.

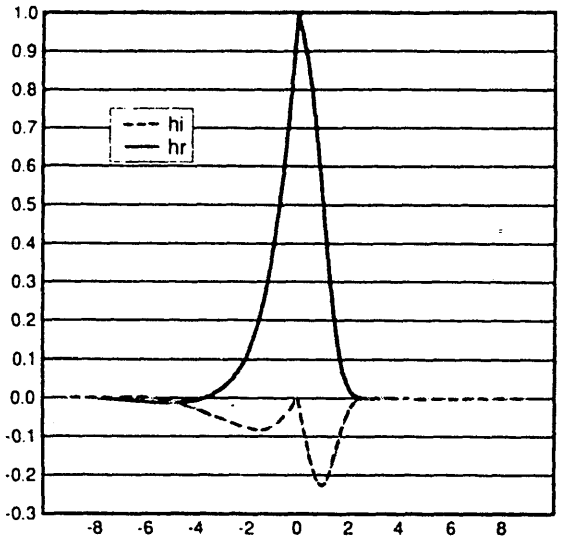

FIGURE 4.4 The G-mode eigen-function when G'=0.1, N=0, Re(P)=0.1 and Im(P)=0.6.

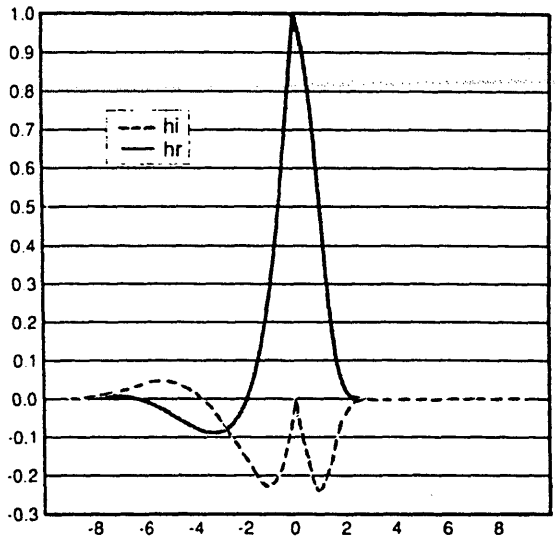

FIGURE 4.5 The G-mode eigen-function when G'=0.1, N=0, Re(P)=-0.1, Im(P)=0.6 and R=1.

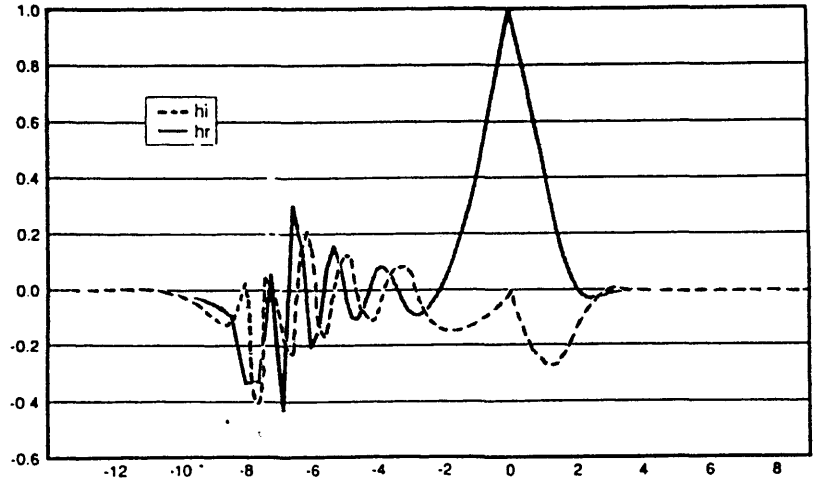

FIGURE 4.6 The G-mode eigen-function when G'=0.1, N=0, Re(P)=-0.1, Im(P)=0.6 and R=0.3.

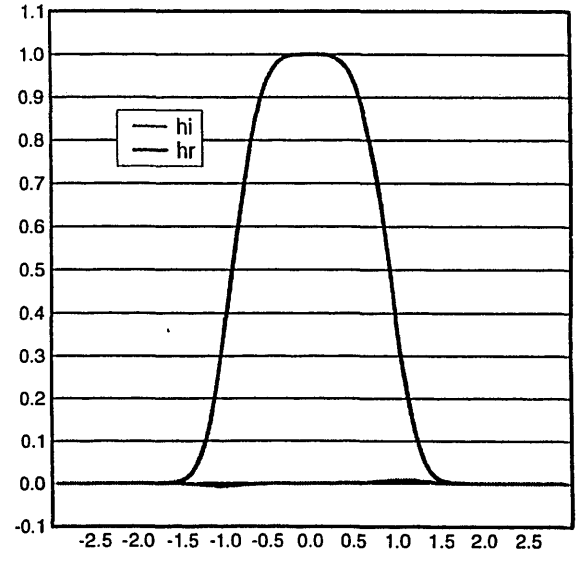

FIGURE 4.7 The visco-tearing mode eigen-function when N=0.1, G'=0, Re(P)=0.1, Im(P)=0.1 and R=1.

In case (iv), as soon as we introduce viscosity effects, the structure of $h(k)$ undergoes another qualitative change. The solution now decays more rapidly when $N\neq 0$ as $k\to+\infty$; when $k\to-\infty$, $h(k)$ is now independent of $Re(P)$ positive or negative and contains an exponentially decaying behaviour rather than the oscillatory algebraic decay in the inviscid case.

4.1.3 The direct method

For very small values of R it was found easier to solve the boundary-layer equations (2.37) and (2.38) by a direct numerical method rather than applying the Fourier transform, although the latter was always more efficient for reasonably large values of R, when good agreement with the asymptotic results (see §6.1) of earlier authors was obtained.

We observe that in the boundary-layer equation (2.38), only the odd part of $H(\theta)$ contributes to the integral for Δ'. We now exploit the fact that the G-mode does not enter into the leading order of (2.37) and the odd part of $H(\theta)$ behaves like $-P/\theta+O(\theta^{-3})$ (Paris and Sy, 1983) for very large positive and negative θ.

We now define

$$h(\theta)=H(\theta)+\frac{P\theta}{1+\theta^2}.$$

Note that $h(\theta)$ is not related to the Fourier transform $h(k)$ in the previous section. Then the odd part of $h(\theta)$ behaves like

$$-\frac{P}{\theta}+\frac{P\theta}{1+\theta^2}+O(\theta^{-3})=O(\theta^{-3}),\quad \theta\to\infty.$$

Then, from (2.36) and (2.38), we have

$$\cos\chi=:\frac{\Delta'}{\Delta}=\int_{-\infty}^{\infty}(P+\theta H)\,d\theta=\int_{-\infty}^{\infty}\left(\frac{P}{1+\theta^2}+\theta h\right)d\theta=\pi P+\int_{-\infty}^{\infty}\theta h\,d\theta.$$

Hence

$$P=\frac{1}{\pi}\cos\chi-\frac{1}{\pi}\int_{-\infty}^{\infty}\theta h\,d\theta. \qquad (4.6)$$

The integrand in (4.6) behaves like θ^{-2} as $\theta\to\pm\infty$. Convergence of this integral is rather slow for numerical methods, but we obtain a more rapidly convergent integral as follows.

Let $\theta_0 = iP/R$. Then (2.37) may be written in the form, when $N=0$

$$iRH'' = \frac{\theta(P+\theta H)}{\theta-\theta_0} + \frac{\sin\chi}{\pi(\theta-\theta_0)} - \frac{G(H-iR)}{iR(\theta-\theta_0)^2}. \qquad (4.7)$$

Integrating over $(-\infty,\infty)$ by using the fact that $H(\theta) = O(\theta^{-1})$ as $\theta\to\pm\infty$, we have

$$0 = \int_{-\infty}^{\infty} iRH''d\theta = \int_{-\infty}^{\infty}\left\{\frac{\theta(P+\theta H)}{\theta-\theta_0} + \frac{\sin\chi}{\pi(\theta-\theta_0)} + \frac{G}{(\theta-\theta_0)^2} - \frac{GH}{iR(\theta-\theta_0)^2}\right\}d\theta$$

$$= \int_{-\infty}^{\infty}(P+\theta H)\,d\theta + \theta_0\int_{-\infty}^{\infty}\frac{(P+\theta H)}{\theta-\theta_0}d\theta + \frac{1}{\pi}\int_{-\infty}^{\infty}\frac{\sin\chi}{\theta-\theta_0}d\theta + \int_{-\infty}^{\infty}\frac{G}{(\theta-\theta_0)^2}\left\{1-\frac{H}{iR}\right\}d\theta.$$

If $Re(P)>0$, the pole θ_0 lies in the upper half plane and computing its residue yields

$$i\sin\chi + \int_{-\infty}^{\infty}\frac{\theta(P+\theta H)}{\theta-\theta_0}d\theta + G\int_{-\infty}^{\infty}\frac{1-H/iR}{(\theta-\theta_0)^2}d\theta,$$

which, on noting that

$$\int_{-\infty}^{\infty}(P+\theta H)\,d\theta = \cos\chi,$$

we may rearrange in terms of the new variable $h(\theta)$ as

$$e^{i\chi} - \frac{\pi P^2}{P+R} + i\frac{P}{R}\int_{-\infty}^{\infty}\frac{\theta h}{\theta-\theta_0}d\theta + \frac{G}{iR}\int_{-\infty}^{\infty}\frac{1}{(\theta-\theta_0)^2}\left\{iR-h+\frac{P\theta}{1+\theta^2}\right\}d\theta = 0.$$

Observe that the last integrand has poles in the upper half plane at θ_0 and i. Integrating round a large semicircular arc in the upper half plane and calculation of residues shows that the last integral contributes $\pi GPR/(P+R)^2$. We finally obtain

$$\frac{\pi P^2}{P+R} = e^{i\chi} + i\frac{P}{R}\int_{-\infty}^{\infty}\frac{\theta h}{\theta-\theta_0}d\theta + \frac{\pi GPR}{(P+R)^2} + i\frac{P}{R}\int_{-\infty}^{\infty}\frac{h}{(\theta-\theta_0)^2}d\theta. \qquad (4.8)$$

Although the integrand still behaves like θ^{-2} for large values of θ, it has been found numerically to converge more rapidly than (4.6).

When $Re(P)<0$, a similar argument shows that (4.6) is replaced by

$$\frac{\pi P^2}{P-R} = e^{-i\chi} + i\frac{P}{R}\int_{-\infty}^{\infty} \frac{\theta h}{\theta-\theta_0} d\theta - \frac{\pi PRG}{(P-R)^2} + i\frac{P}{R}\int_{-\infty}^{\infty} \frac{h}{(\theta-\theta_0)^2} d\theta . \qquad (4.9)$$

When $Re(P)=0$, then we obtain

$$\frac{\pi P^2}{P^2-R^2} = e^{i\chi} + i\frac{P}{R}\oint_{-\infty}^{\infty} \frac{\theta h}{\theta-\theta_0} d\theta - \frac{2\pi GP^2R^2}{(P^2-R^2)^2} + i\frac{G}{R}\oint_{-\infty}^{\infty} \frac{h}{(\theta-\theta_0)^2} d\theta . \qquad (4.10)$$

This approach does not work well when θ_0 is close to the real axis, that is when P/R is small, but elsewhere shows good agreement with the Fourier transform method. In terms of the new variable $h(\theta)$, with

$$h' = H' + P\frac{1-\theta^2}{(1+\theta^2)^2}, \quad h'' = H'' - 2P\theta\frac{3-\theta^2}{(1+\theta^2)^3},$$

(2.37) becomes

$$h'' + \left\{\frac{G}{(P+iR\theta)^2} - \frac{\theta^2}{P+iR\theta}\right\} h(\theta) = f(\theta), \qquad (4.11)$$

where

$$f(\theta) = \left\{\frac{P\theta}{1+\theta^2} + \frac{\sin\chi}{\pi}\right\}\cdot[P+iR\theta]^{-1} - \frac{2P\theta(3-\theta^2)}{(1+\theta^2)^3} + \frac{G}{(P+iR\theta)^2}\left\{\frac{P\theta}{1+\theta^2} + iR\right\}$$

with boundary conditions $h(\theta)\to 0$ as $\theta\to\pm\infty$. Equations (4.8)-(4.10) enable the growth rate P to be estimated by using a Newton-Raphson iterative method, while the integrals are evaluated by a NAG routine.

Further, we introduce the transformation: $\theta = x/(1-x^2)$, to facilitate the determination of $h(\theta)$, with $h\to 0$ as $x\to\pm 1$. Thus (4.11) becomes

$$\frac{(1-x^2)^4}{(1+x^2)^2}\frac{d^2h}{dx^2} - 2x(3+x^2)\left[\frac{1-x^2}{1+x^2}\right]^3\frac{dh}{dx} + \frac{G(1-x^2)^2 - Px^2 - iRx^3/(1-x^2)}{[P(1-x^2)+iRx]^2}h$$

$$= f(x), \qquad (4.12)$$

where

$$f(x) = \frac{Px(1-x^2)^2/(1-x^2+x^4)+\sin\chi(1-x^2)/\pi}{P(1-x^2)+iRx} - \frac{2Px(1-x^2)^3[3(1-x^2)^2-x^2]}{(1-x^2+x^4)^3}$$

$$+ \frac{G(1-x^2)^2}{[P(1-x^2)+iRx]^2}\left\{\frac{Px(1-x^2)}{(1-x^2+x^4)}+iR\right\}.$$

Note that $f(x)\to 0$, as $x\to\pm 1$, and $f(0) = \frac{\sin\chi}{\pi P} + i\frac{GR}{P^2}$.

4.2 Dependence of the Eigenvalue P in the Equilibrium Flow Case

From the definition of Δ in (2.31), we know that the value of χ is decided by the global field structure which depends on both the external matching parameter Δ' and the internal field shear gradient $F''(0)$:

$$\cos\chi = \frac{\Delta'}{\Delta}, \quad \sin\chi = -\frac{\pi F''(0)}{\Delta F'(0)}, \quad \Delta>0, \quad -\pi<\chi\le\pi. \qquad (4.13)$$

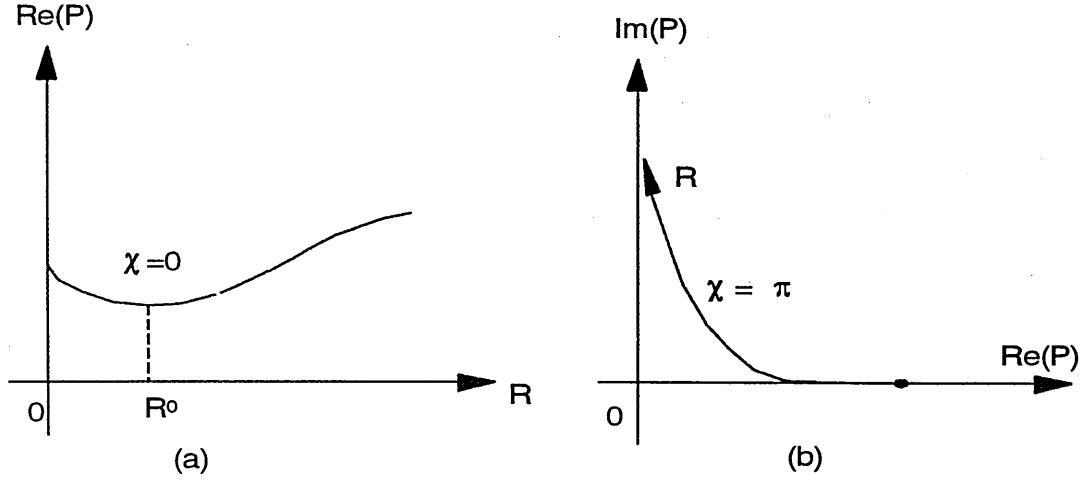

FIGURE 4.8 The general behaviour of the eigenvalue loci for (a) χ=0; (b) χ=π

when $\Delta'=\Delta$, then $\chi=0$ implies that $F''(0)=0$; When $\Delta'=-\Delta<0$, then $\chi=\pi$ corresponds to the field structure without tearing instability.

If we consider the effects of flow R on mixed tearing and G-modes when $G>0$, the flowless modes are modified to yield stabilizing or destabilizing effect of flow for various different values of χ, thereby modifying the classical instability condition $\Delta'>0$. For a sufficiently large $G>0$, however, the flow parameter R surprisingly stabilizes the flowless modes for any value of χ. If $\chi=0$, the instability is dominated by the tearing driving mechanism. Increasing R can reduce $Re(P)$ consistently before reaching the destabilizing turning point R_0 [see Figure 4.8(a)]. If $\chi=\pi$, the only instability driving mechanism is the gravitational interchange. Flow R will reduce $Re(P)$ to approach the marginal stable state with $Re(P)\to 0$ [see Figure 4.8(b)]. The high value of $Im(P)$ implies a high frequency of oscillation in the large flow case.

4.2.1 Tearing mode loci of the eigenvalue P

When $G=0$, we present the numerical results obtained from the tearing mode program (Paris, Wood and Stewart, 1993) which is confirmed by the G-mode program and also by the direct method for small values of R. The agreement is shown in Table 4.1 for a range of values of P.

Using the Fourier transform or direct method according to the region of R large or small, we present the eigenvalue loci in the complex P-plane as the flow parameter R increases from zero for (a) the unstable branch and (b) the stable branch. The level curves of R are indicated by dashed lines at the values 0.2, 0.4, 0.6, 0.8, 1.0, 2.0 and 3.0 [see Figure 4.9 (a)] for the unstable branch; and at the values 0.1, 0.2, 0.3, 0.4 and 0.5 [see Figure 4.9 (b)] for the stable branch $(0.5\pi<\chi<1.0\pi)$.

TABLE 4.1 The comparison between the tearing mode result and the G-mode programme (when G=0).

$\chi=0.8\pi$		Tearing Mode Result	
R	P	$h'(0+)$	$h'(0-)$
3.0	(0.101735, 0.650859)	(-0.069236, -0.196783)	(1.125453, 0.028209)
2.0	(0.047401, 0.526264)	(-0.083055, -0.233219)	(0.983358, 0.034229)
1.0	(-0.03423, 0.354565)	(-0.109232, -0.309653)	(0.776612, 0.047038)
0.5	(-0.10630, 0.196043)	(-0.121026, -0.434686)	(0.595484, 0.058722)
0.25	(-0.06364, 0.047774)	(0.0758342, -0.477859)	(0.454645, 0.032239)
0.1	(-0.01777, 0.011748)	(0.1111246, -0.323777)	(0.335795, 0.019622)

$\chi=0.8\pi$		Gravitational Interchange Program (G=0)	
R	P	$h'(0+)$	$h'(0-)$
3.0	(0.101735, 0.650859)	(-0.0692414, -0.196788)	(1.1254701, 0.0282156)
2.0	(0.047401, 0.526243)	(-0.0830619, -0.233211)	(0.983356, 0.034226)
1.0	(-0.03423, 0.354565)	(-0.1092291, -0.309654)	(0.776605, 0.047037)
0.5	(-0.10629, 0.196043)	(-0.1210376, -0.434706)	(0.595497, 0.058740)
0.25	(-0.63641, 0.047774)	(0.07586391, -0.477867)	(0.454611, 0.032238)
0.1	(-0.01777, 0.011748)	(0.11112039, -0.323758)	(0.335811, 0.019607)

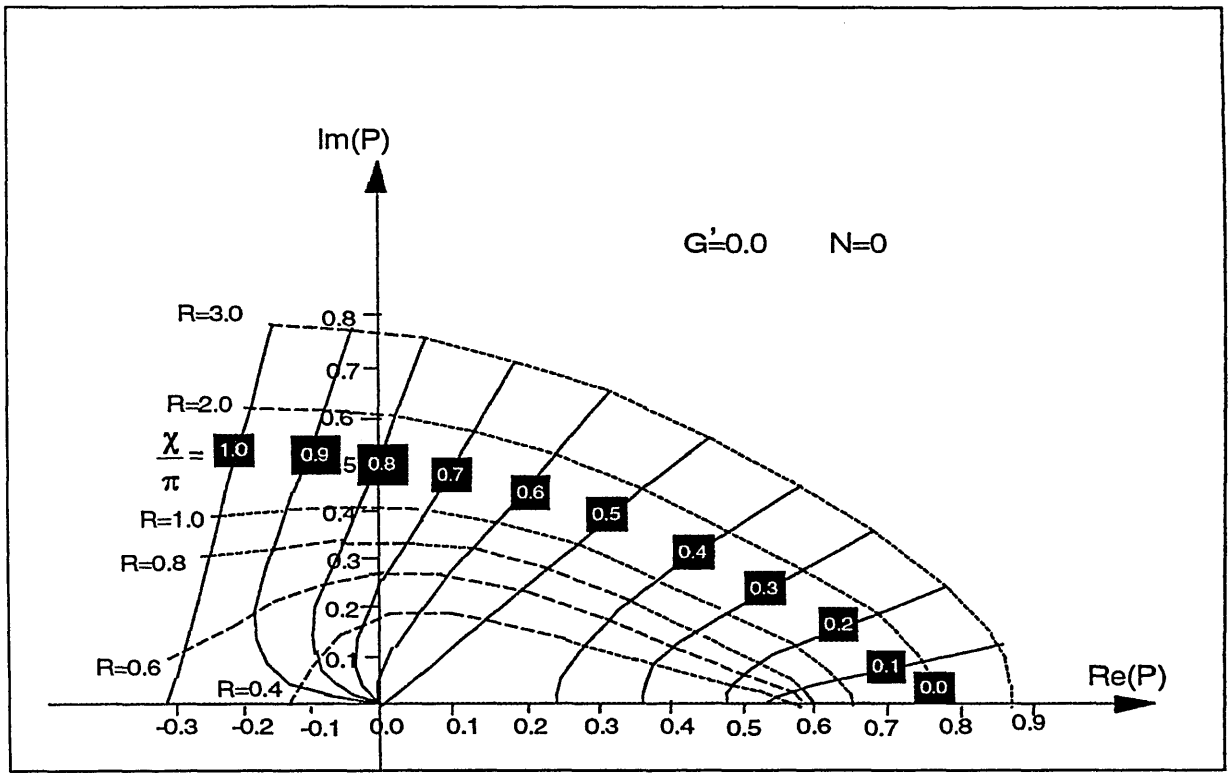

FIGURE 4.9(a) The unstable branch of the inviscid tearing mode loci.

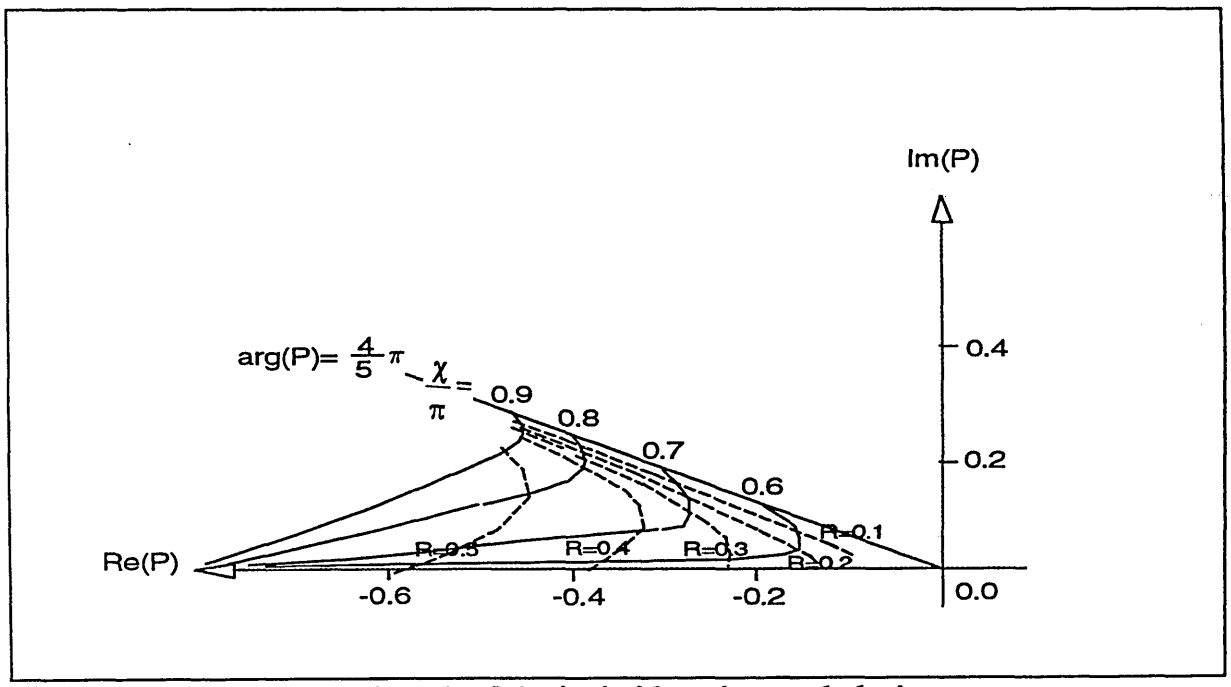

FIGURE 4.9(b) The stable branch of the inviscid tearing mode loci.

Recall the unperturbed spectrum (R=0) in Chapter 3, we have the eigenvalue loci when $G=0$ for various values of χ in $[0,\pi]$. When $0\le\chi/\pi\le0.5$, the growth rate $Re(P)$ increases with flow R, which indicates that the equilibrium flow destabilizes the tearing mode. It is found to agree with the asymptotic estimate (Paris and Sy, 1983 and Bondeson and Persson, 1986) in the limit as R tends to infinity,

$$P \sim \left\{\frac{R}{2\pi}e^{i\chi}\right\}^{\frac{1}{2}} + \frac{\cos\chi\Gamma(\frac{1}{3})}{3^{2/3}2\pi R^{1/3}}. \qquad (4.14)$$

The eigenvalue loci which eventually form part of the unstable spectrum when $0.5<\chi/\pi<1.0$ are seen not to originate from the corresponding unperturbed eigenvalue situated on the Ray $arg(P)=4\pi/5$ (except when $\chi=\pi$), but to emerge from the origin $P=0$. The new eigenvalue loci initially have $Re(P)<0$ when $R\ll1$ but eventually move over into $Re(P)>0$ for sufficiently large R. The stable eigenvalues located originally on $arg(P)=4\pi/5$ when $R=0$ move towards and out along the negative real axis with increasing flow R. A similar behaviour of the eigenvalue loci in the negative $Im(P)$ half plane for these eigenvalues originally on the ray $arg(P)=-4\pi/5$ is not presented as from the symmetry properties of the eigenvalue (see §2.3.3)

$$P(-R,G,N,\chi) = P(R,G,N,-\chi) = P^*(R,G,N,\chi), \qquad (4.15)$$

where P^* denotes the complex conjugate; it is sufficient to consider $R\ge0$ and $0\le\chi\le\pi$ only.

We remark that this discontinuous behaviour of the spectrum when R is turned on is not unexpected. Regarding R as the perturbation parameter, the differential equation (4.1) may be seen to be singularly perturbed.

4.2.2 Location of the G-mode eigenvalue and the nature of the spectrum

As in the preceding sections, we shall employ a numerical method which depends on making an initial guess for the eigenvalue $P(R,G,N,\chi)$ and solving the differential equations (4.1) with this value of P, thus obtaining the values of the solutions $h(k)$ and their derivatives on either side of the origin. These we substitute in the eigenvalue relation (4.3) to obtain an improved estimate of P, repeating this process until the desired degree

of accuracy is obtained. Where possible, we shall confirm our numerical results by asymptotic estimates of P and $h(k)$ for the certain values and limits. In order to make a good initial guess for the eigenvalue when $R \neq 0$, we require information on the unperturbed (FKR) case $R = N = 0$ from Chapter 3. The program used in the G-mode case is MHD.FOR which is given in Appendix A. Good agreement with the tearing mode results in §4.2.1 were found when $G=0$.

The results of the numerical analysis are presented in a set of Figures 4.10 (a), (b), (c), (d) and (e) below. This set of figures gives the eigenvalue loci with increasing flow parameter R in the inviscid case for $G=0.05, 0.1, 0.5, 1.0$ and 2.0 respectively. The level curves of R are shown by dashed lines at the values of $R=0.2, 0.4, 0.6, 0.8, 1.0, 2.0$ and 3.0, as in the corresponding figures for the tearing mode. The values of χ/π are indicated on each curve labled at intervals of 0.1 from 0 to 1.

These figures show the G-mode loci moving away from the tearing mode loci [Figure 4.9(a)]. The unstable branch is most interesting in the instability analysis in the $Re(P)>0$ region, when G is increased gradually. For $\chi/\pi>0.5$, the loci emanate from the accumulation point on the real axis which was the origin $P=0$ in the $G=0$ case and move towards to the point with $Re(P)>0$ when $G>0$. The loci pattern moves to the right without topological change, we may entitle this set of moving figures as the "Butterfly's Wing" (referred to as BW thereafter). We see that while for low G (i.e. $G=0.1$) the mode is still destabilized by increasing flow parameter R, as for the tearing mode, for higher values of G the flow has a stabilizing effect for an increasing range of values of χ/π. The loci when $\chi=0$ in Figure 4.10(d) was illustrated in Figure 4.8(a) where the locus, which lies on the real axis, at first moves towards the origin from the point with $Re(P)>1.2$, and then moves backwards again for R greater than the value R_0 of approximately 1.6. This curve indicates that increasing the flow shear may have a stabilizing effect on the G-mode before R exceeds a critical value. This corresponds to the turning point of the growth rate P whereby the eigenvalue P will bend over with $Re(P)$ increasing positively and the system will become more unstable. The other loci with a different value of χ show a similar behaviour of the stabilizing then destabilizing effects of R; these are interesting and important properties.

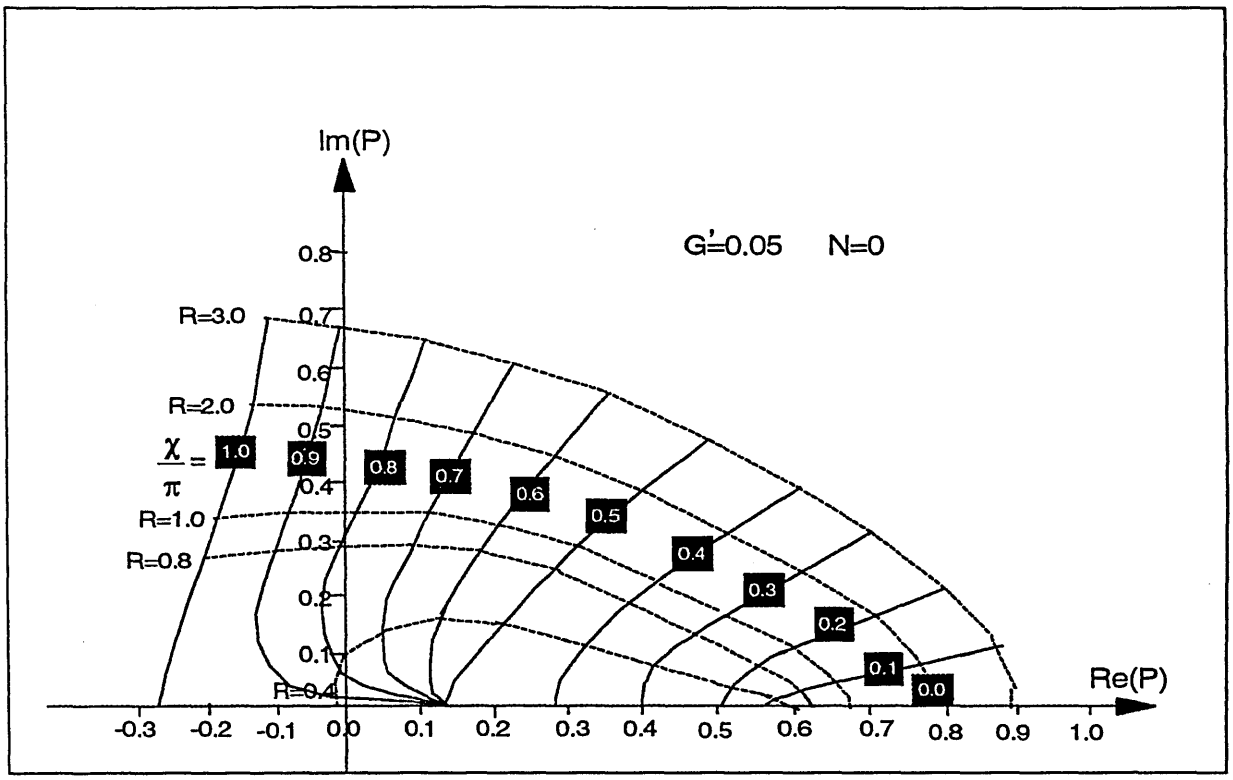

FIGURE 4.10 (a) The G-mode loci when G'=0.05 and N=0.

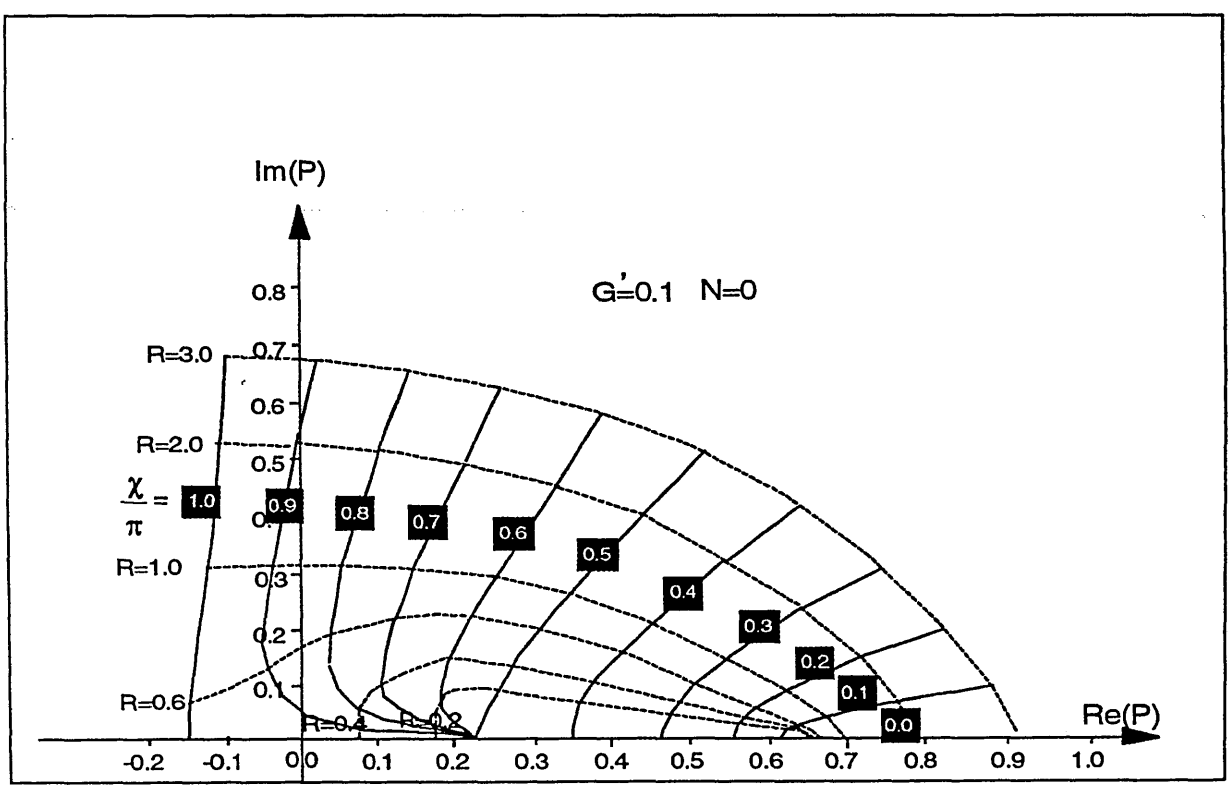

FIGURE 4.10 (b) The G-mode loci when G'=0.1 and N=0.

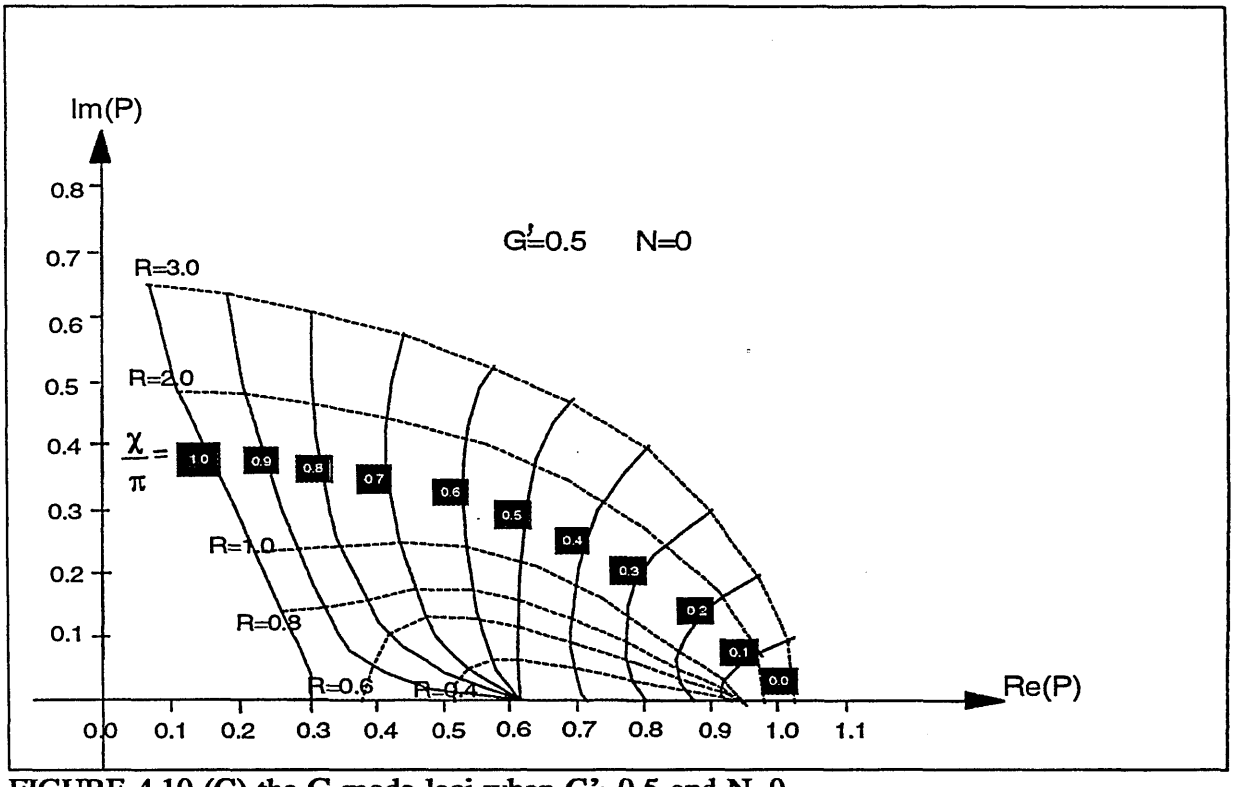

FIGURE 4.10 (C) the G-mode loci when G'=0.5 and N=0.

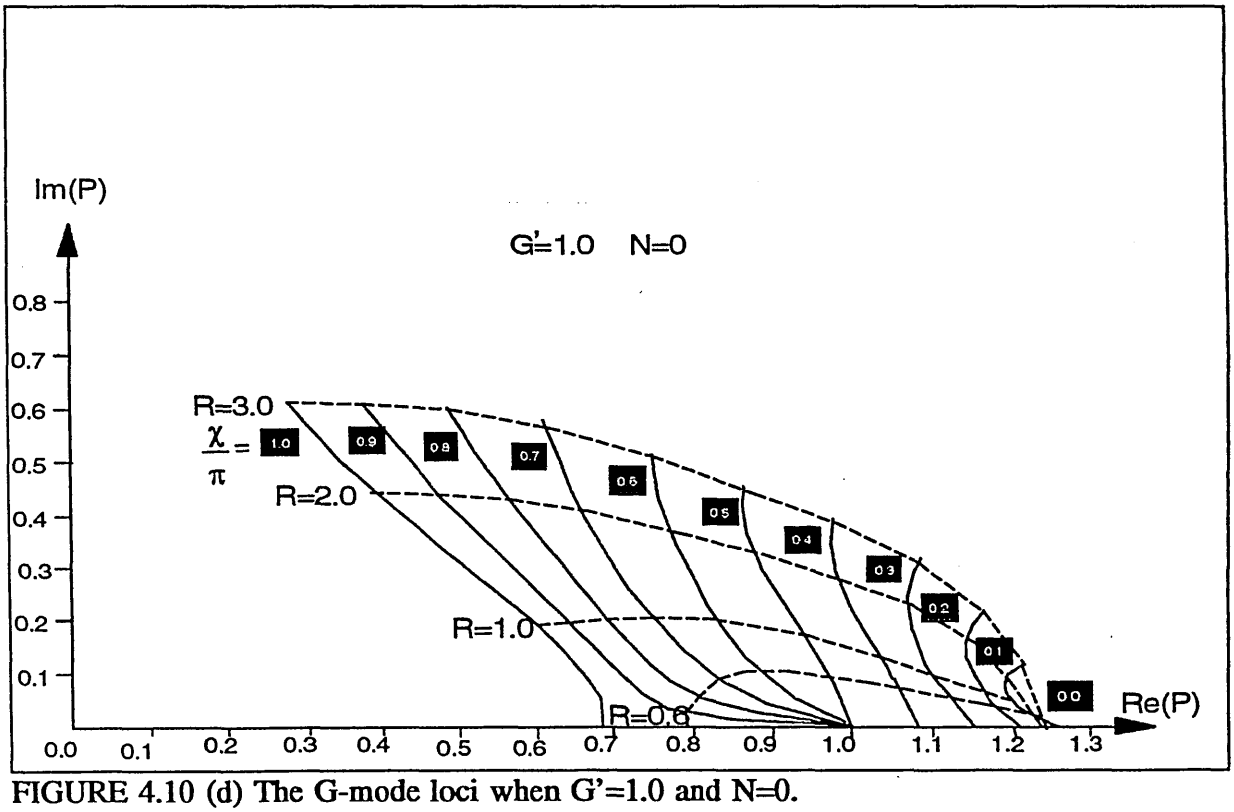

FIGURE 4.10 (d) The G-mode loci when G'=1.0 and N=0.

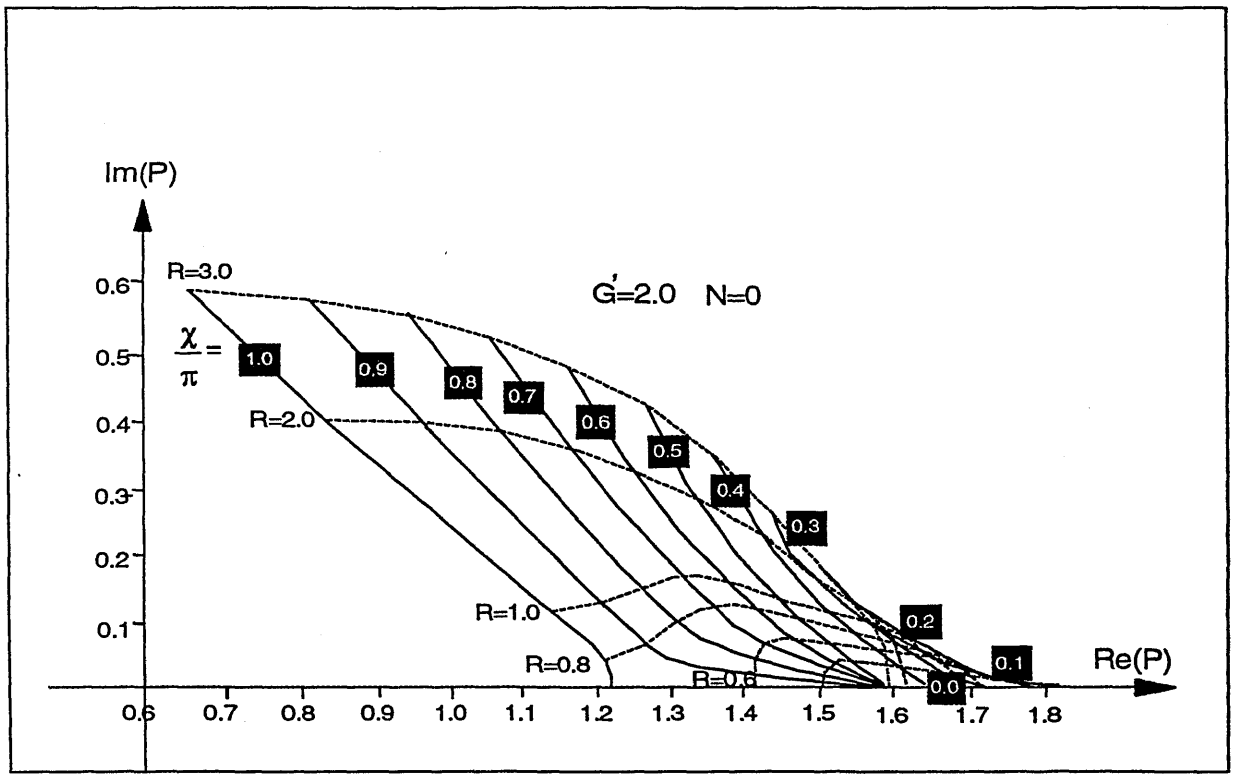

FIGURE 4.10 (e) The G-mode loci when G'=2.0 and N=0.

Physically we would like to discuss this phenomenon in the mixed tearing and gravitational interchange instabilities. The effects of flow show that a shear flow can reduce the growth rate of gravitational interchange or MHD Rayleigh-Taylor instability significantly, before Kelvin-Helmholtz instability sets in, no matter if the tearing mode is stable $(\chi \geq \pi/2)$ or unstable $(\chi < \pi/2)$.

If $F'' = 0$ and $\Delta' > 0$ $(i.e.\ \chi = 0)$ then mixed flowless tearing and G-modes are completely unstable. Increasing shear flow can only stabilize the gravitational interchange mode therefore reduce the growth rate $Re(P)$. Sufficiently large shear flow however will stimulate the tearing mode to become more and more active and eventually dominate the instability.

If $F''=0$ with $\Delta' < 0$ $(i.e.\ \chi = \pi)$ then the tearing mode is effectively removed. From the eigenvalue locus for increasing R, we observe that the flow will stabilize the

gravitational interchange growth rate when $\chi=\pi$ and approach the marginal stable state with $Re(P)=0$. This is a special case when we switch off the tearing mode, otherwise ($i.e.\ \chi/\pi<1$) the tearing mode will always dominate the instability once R becomes sufficiently large. Large flow will also increase the existing oscillatory behaviour with a higher $Im(P)$.

When $G<0$, we found that the eigenvalue loci move towards the $Re(P)<0$ region and the system becomes more stable. For brevity the effects of negative G are discussed only in the marginal stability curves (Figure 4.11).

4.2.3 Marginal stability and plasma oscillation

If the growth rate of instability is purely an imaginary number with $Re(P)=0$ then the system is in a marginal stable state with oscillation of frequency $|Im(P)|>0$.

In the tearing mode case ($G=0$), modes with $\chi>0.5\pi$ remain stable when the value R is small. The loci will, however, cross over into the $Re(P)>0$ region when R exceeds the marginal value R_m (i.e. in Figure 4.9(a) $R_m\approx 0.6$ for $\chi=0.7\pi$).

In the G-mode case when G is positive, the marginal stable region for corresponding values of χ is reduced in comparison with the tearing mode. For example, when $G'=0.05$ and $\chi=0.8\pi$ then increasing the flow: $0.4\le R\le 0.8$ can secure the system in a stable state. The stable (upper) region shrinks when $G'>0.27$, so that there is no stable region for any value of χ when G' is very large. If we reduce the value of G' then the stable region is increased significantly for $\chi\ge 0.5\pi$. These results are summarized in Figure 4.11.

Considering the effects of negative G we obtain the marginal curve showing an obvious stabilizing $G'<0$. If we increase $-G'$ substantially, the flow driven instability may be eliminated in a larger region of R.

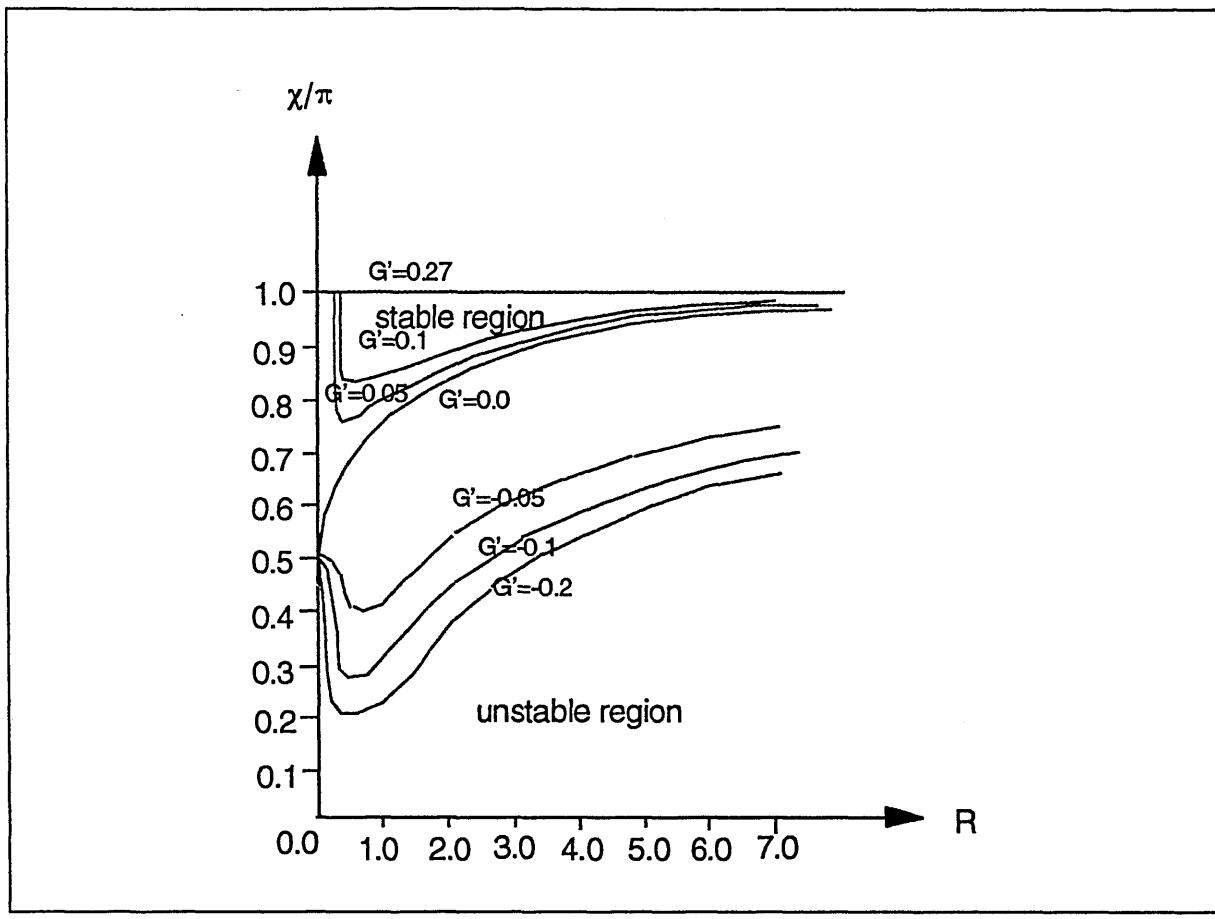

FIGURE 4.11 The marginal stability curves show that for each value of G' the region is divided into (a) the stable (upper) region; and (b) the unstable (lower) region.

CHAPTER V
THE EFFECTS OF VISCOSITY

Introduction

In an ordinary fluid with viscosity, the collisions between particles transfer momentum to the adjacent fluid elements. This tends to equalize the velocity of fluid elements at different points, resulting in resistance to shear flow is what we intuitively think of as viscosity. The longer the mean free path, the farther momentum is carried, and the larger is the viscosity. In a plasma there is a similar effect which occurs even in the absence of collisions. The Larmor gyration of particles (particularly ions) brings them into different parts of the plasma and tends to equalize the velocity of the fluid. If there is a neutral gas, the charged fluid will exchange momentum with it through collisions.

The equation of motion including the gravitational interchange is given in (2.1). An analogous system, except for the absence of electromagnetic forces, illustrating an ordinary fluid obeys the Navier-Stokes-type equation

$$\rho \left[\frac{\partial \underline{V}}{\partial t} + (\underline{V}\cdot\nabla)\,\underline{V} \right] = -\nabla p + \rho \underline{g} + \mu_{\perp} \nabla^2 \underline{V} \,.$$

We found that the theory of ordinary viscous fluid supplies useful information in the study of MHD viscous flow.

In Chapter 3, we have obtained results for an unstably stratified viscous fluid in a gravitational field. Viscosity only presents a stabilizing effect on the growth rate of tearing-G modes in the flowless case. We discuss two possible effects of viscosity in this chapter. In hydrodynamic stability theory, there are two hypotheses concerning the dual role played by viscosity. These are:

(i) The inviscid fluid may be unstable and the viscous fluid stable. The effect of viscosity is then purely stabilizing.

(ii) The inviscid fluid may be stable and the viscous fluid unstable. In this case viscosity would be the cause of the instability.

Although Reynolds (1883) was unable to suggest a physical mechanism by which viscosity could cause instability he refused to exclude such possibility.

The visco tearing-G modes in MHD instability is introduced in this chapter. This study shows that viscosity can introduce instability exchange on gravitational modes while it stabilizes the unstable mode. As the detailed examination of viscous effects may be found in any text on fluid dynamics, we shall now only use simple physical arguments to indicate how the viscous stress in a sheared flow affects the growth rate of resistive instabilities.

To explain the complicated visco-resistive mode behaviour, we analyse the loci bifurcation and instability exchange behaviour thereby distinguish the dominant effects of various parameters in the instability growth rate. For example, as we found in Chapter 4, the flow R destabilize the tearing mode and stabilize the G-mode. When G is large, then flow R is found to stabilize the G-mode until the G-term contribution is suuficiently small. The tearing mode always dominates when flow R becomes large.

In the viscous tearing mode loci (Paris, Wood and Stewart, 1993) viscosity determines the stability when the flow R is small. Increasing the flow R then the loci move to the right with increasing $Re(P)$. In the viscous tearing-G mode loci, the loci structure shows bifurcation and instability exchange behaviour. Increasing the flow R, the loci move to the left first and then move to the right. So it is necessary to illustrate the complicated viscous loci structure in some detail by considering separately the cases when the flow R is small, moderate and large (see §5.1).

We note that the nonlinear term containing the Reynolds stress in (2.5) has been neglected in the linearization; therefore the transition from the unstably stratified flow to the turbulent flow is not considered in this study.

5.1 The Exchange Between the Stable Branch and the Unstable Branch of Viscous Eigen-loci

The numerical method for the viscous tearing mode proceeds along exactly the same lines as the non-viscous case, except that we retain the term k^4Nh in the differential equation (2.56). The boundary conditions and the jump conditions (2.47)-(2.49) across the origin remain unchanged. The program MHD.FOR (see Appendix B) yields the same results as the tearing mode results from the previous investigation (Paris, Wood and Stewart, 1993) when

$N \neq 0$ and $G=0$ (see Table 5.1).

TABLE 5.1 The comparison of the results from the tearing-mode and G-mode (G=0) programs

			Tearing mode		G-mode	
N	R	χ	$Re(P)$	$Im(P)$	$Re(P)$	$Im(P)$
0.05	3.0	0.4	0.5835912	0.4047520	0.5835829	0.4047484
0.05	0.5	0.9	-0.273999	0.2751073	-0.273992	0.2751001
0.1	2.0	0.1	0.6887209	8.2912E-2	0.6887225	8.2911E-2
0.1	3.0	0.5	0.4477947	0.4901944	0.4478289	0.4902009
0.5	3.0	0.5	0.3071095	0.4772715	0.3071077	0.4772697
0.5	0.5	0.8	-0.499066	0.2366306	-0.499069	0.2365472
1.0	3.0	0.2	0.5451976	0.1761418	0.5451971	0.1761423
1.0	0.3	0.9	-0.519152	0.0243913	-0.515368	0.0214583

The tearing mode spectrum undergoes a qualitative change from the inviscid case as soon as the viscous parameter is increased from zero as shown in the set of Figures 5.1 (a)-(d). The viscous modes grow, instead from the accumulation point of the eigenvalue modes (referred to as AP thereafter) in the inviscid case, from the classical FKR no flow (refered to as NF) values when $|\chi| > 0.5\pi$. These show the eigenvalue loci in the complex P -plane as R increases from 0 to 1 in steps of 0.2 and then for $R=2,3$ with values of the viscosity parameter $N=0.05, 0.1, 0.5$ and 1.0 . The level curves of R are indicated by dashed lines. The flow R is found to destabilize the visco-tearing mode as it does in the inviscid case. In the inviscid case when $G \leq 0$, the eigenvalues for $\chi \geq 0.5\pi$ are complex numbers while the modes become real positive numbers when $G > 0$. When we switch on the viscosity in the $G=0$ case, the accumulation point $P=0$ splits up and modes are

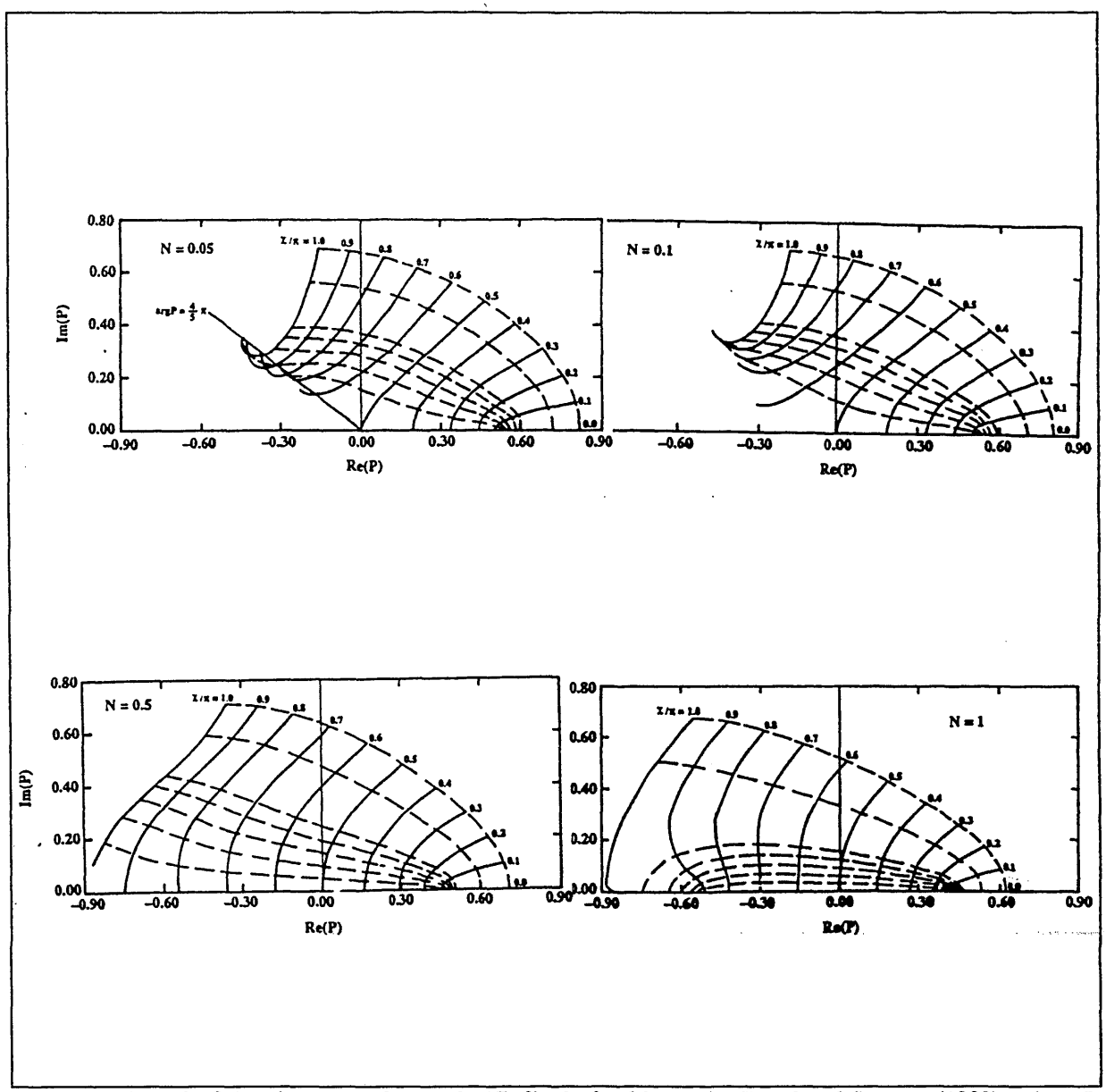

FIGURE 5.1 Loci of the viscous tearing mode (G=0) obtained by Paris, Wood and Stewart (1993), where R increases from 0 to 3 for the viscosity parameter N=0.05, 0.1, 0.5, 1.0 with $0 < \chi/\pi < 1$.

distributed on a ray with $arg(P) > 4\pi/5$ when $R=0$. These stable eigenvalues eventually become unstable with $Re(P) > 0$ when R large. These originate instead from the eigenvalues which lie on the ray $arg(P) = 4\pi/5$ when $R=N=0$, although this ray itself is distorted as N increases, being pulled down gradually on to the negative real axis. Moreover, the $\Delta' > 0$ instability condition, which is removed in the inviscid case, is restored when viscosity becomes large.

The effects of viscosity on the G-mode are significant. The detailed investigation shows

that there are two branches developing from two different origins with $Re(P)>0$ when $G>0$. One branch eventually goes to the stable region with $Re(P)<0$, while the other branch grows consistently in the $Re(P)>0$ region as R increases. If we increase N, then we observe that there are instability exchanges which occur when N exceeds a critical bifurcation point where the stable branch meets the unstable branch at the same R value, which is called the bifurcation point, and results in a change of the loci topology. The exchange behaviour is illustrated in figures 5.2 and 5.3. One example when $G=0.1, \chi=0.6\pi$ is introduced in Figure 5.2. The first exchange has taken place when $N=0.016$ in Figure 5.2(c); the AP locus switches off into the stable region while the NF locus becomes an unstable one. The locus from NF has developed a loop and grows in $Re(P)>0$ when $N\geq 0.2$. It approaches the critical bifurcation point when $N=0.236$. We then see that a second instability exchange has taken place when $N=0.238$ in Figure 5.2(f). The locus from AP now switches back to the region $Re(P)>0$ forming an unstable branch, while the NF locus eventually enters the region $Re(P)<0$. This configuration persists in Figures 5.2(g) and 5.2(h) for $N=0.3$ and $N=0.4$ respectively.

Another example is given in Figure 5.3. In Figure 5.3(a) when $G=0.5, \chi=0.8\pi$ and $N=0$, one locus emanates from the AP at $Re(P)\approx 0.64$, while another emanates from the classical NF modes at $Re(P)\approx 0.45$, which is the value found when solving (3.12) with $R=0$ and G, N non-zero. When $N<0.15$, we see that the effect of viscosity is to reduce $Re(P)$ which, therefore stabilizes the modes. When $N=0.15$, in Figure5.3(b), the locus from AP possesses negative $Im(P)$ for small R before eventually turning off into $Im(P)>0$. The locus from NF develops a sharp bend. The flow R shows a surprisingly destabilizing then stabilizing effect on the NF locus. In Figure 5.3(c), for $N=0.17$, the first exchange between the loci has taken place and the stable (NF) branch has been destabilized while the unstable (AP) branch has been completely stabilized. The locus from AP now goes off into $Re(P)<0$, while the locus from NF has developed a loop and remains in $Re(P)>0$. When $N=0.42$, [see Figure 5.3(d)] the loop developed in the NF locus has expanded and approaches the maximum of $Im(P)$ on the AP locus; therefore the level-crossing from the stable branch to the unstable branch has been taken place to obtain the largest growth rate.

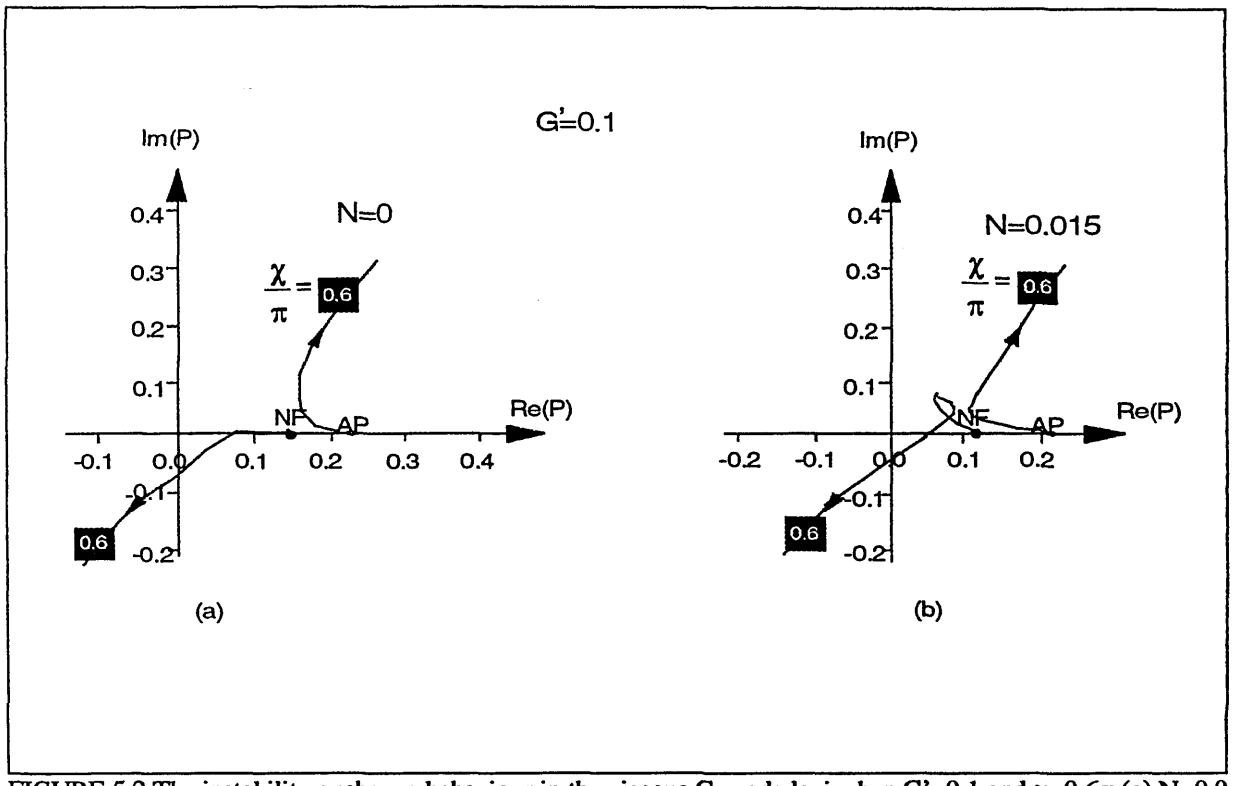

FIGURE 5.2 The instability exchange behaviour in the viscous G-mode loci when G'=0.1 and $\chi=0.6\pi$ (a) N=0.0 (b) N=0.015.

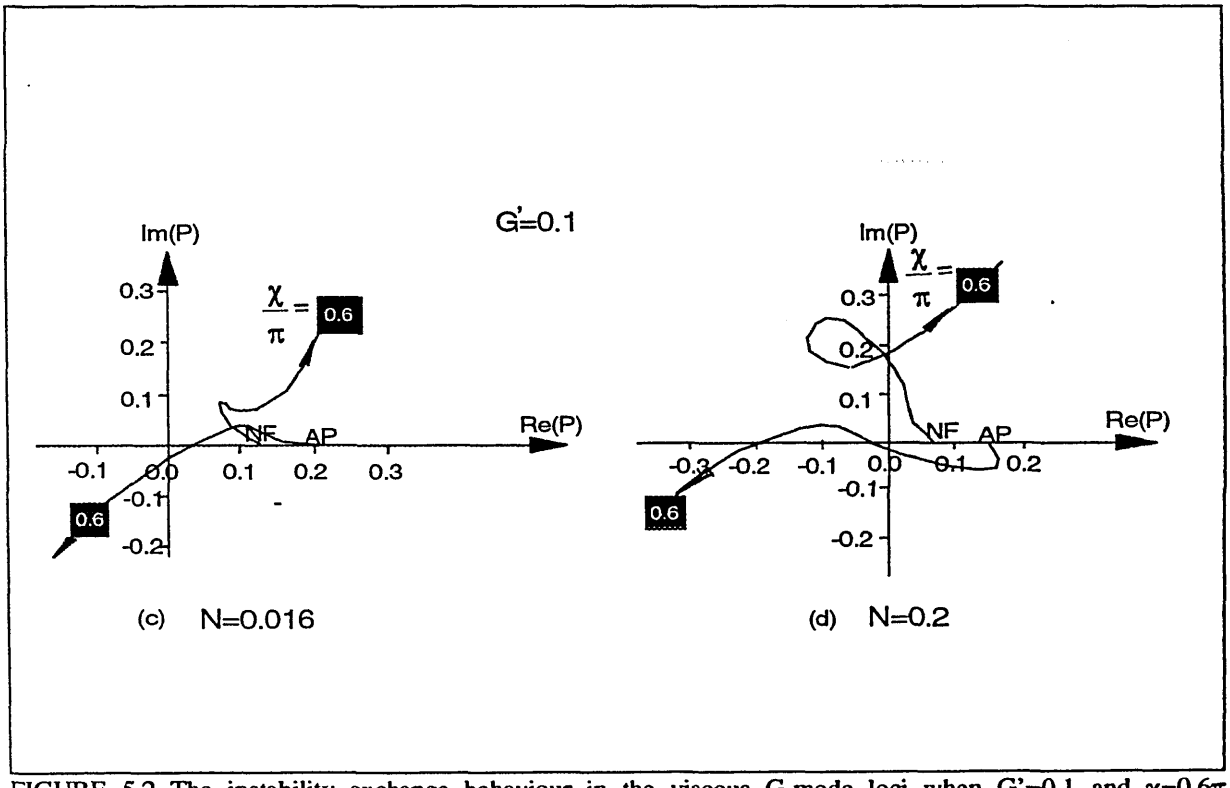

FIGURE 5.2 The instability exchange behaviour in the viscous G-mode loci when G'=0.1 and $\chi=0.6\pi$ (c)N=0.016 (b) N=0.2.

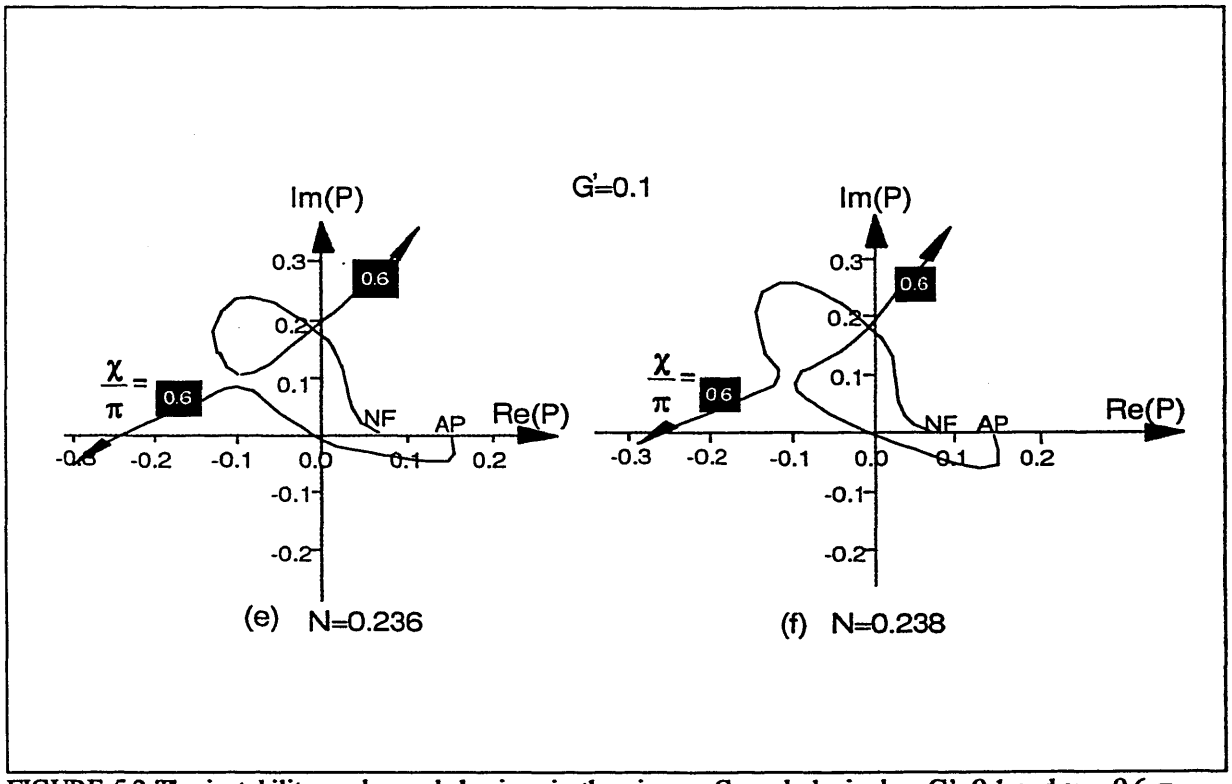

FIGURE 5.2 The instability exchange behaviour in the viscous G-mode loci when G'=0.1 and $\chi = 0.6\ \pi$ (c) N=0.016 (d) N=0.2 (e) N=0.236 (f) N=0.238.

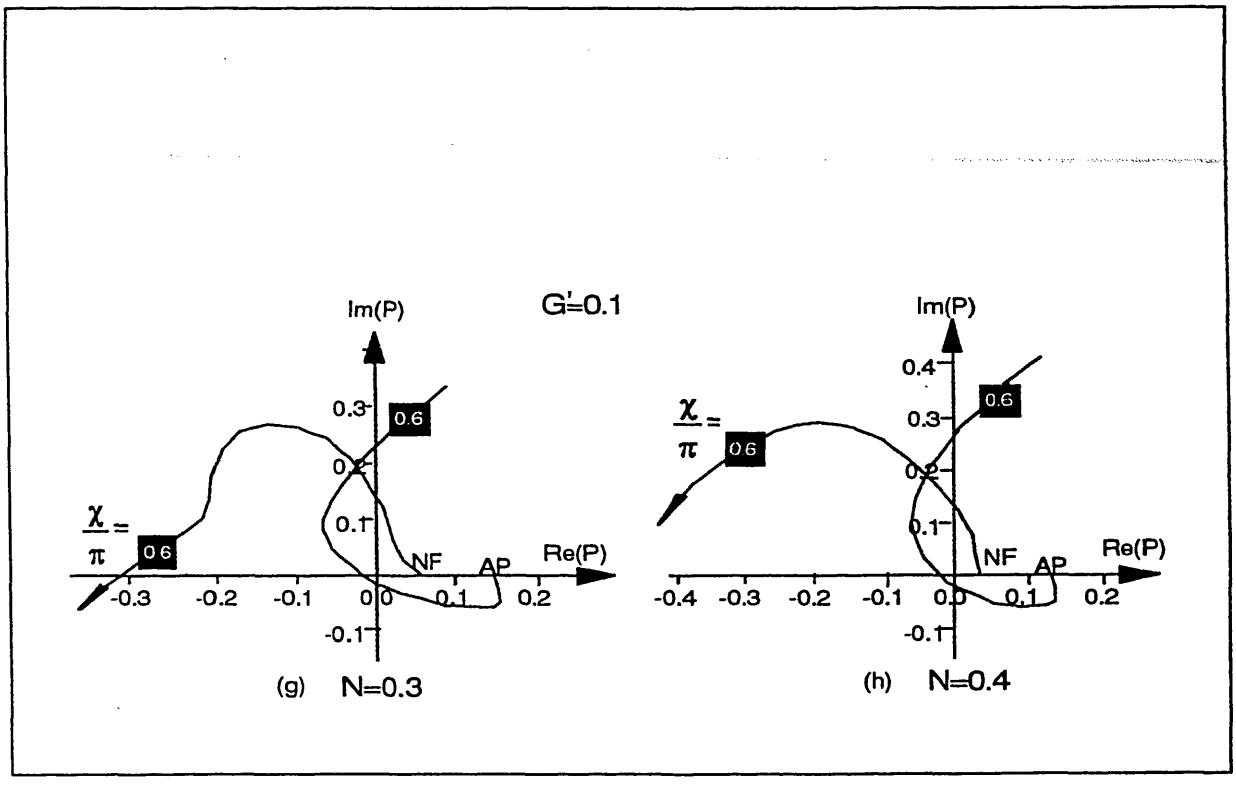

FIGURE 5.2 The instability exchange behaviour in the viscous G-mode loci when G'=0.1 and $\chi = 0.6\ \pi$ (g) N=0.3 (h) N=0.4.

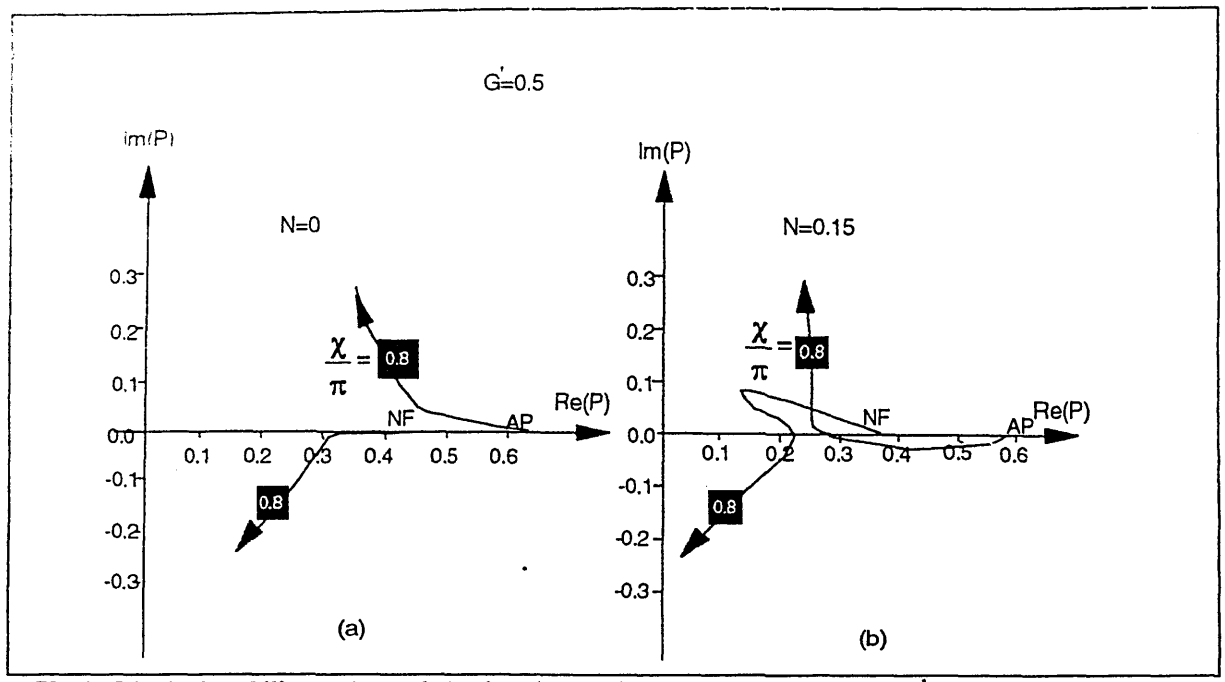

FIGURE 5.3 The instability exchange behaviour in the viscous G-mode loci when G'=0.5 and $\chi=0.8\pi$ (a) N=0.0 (b) N=0.15.

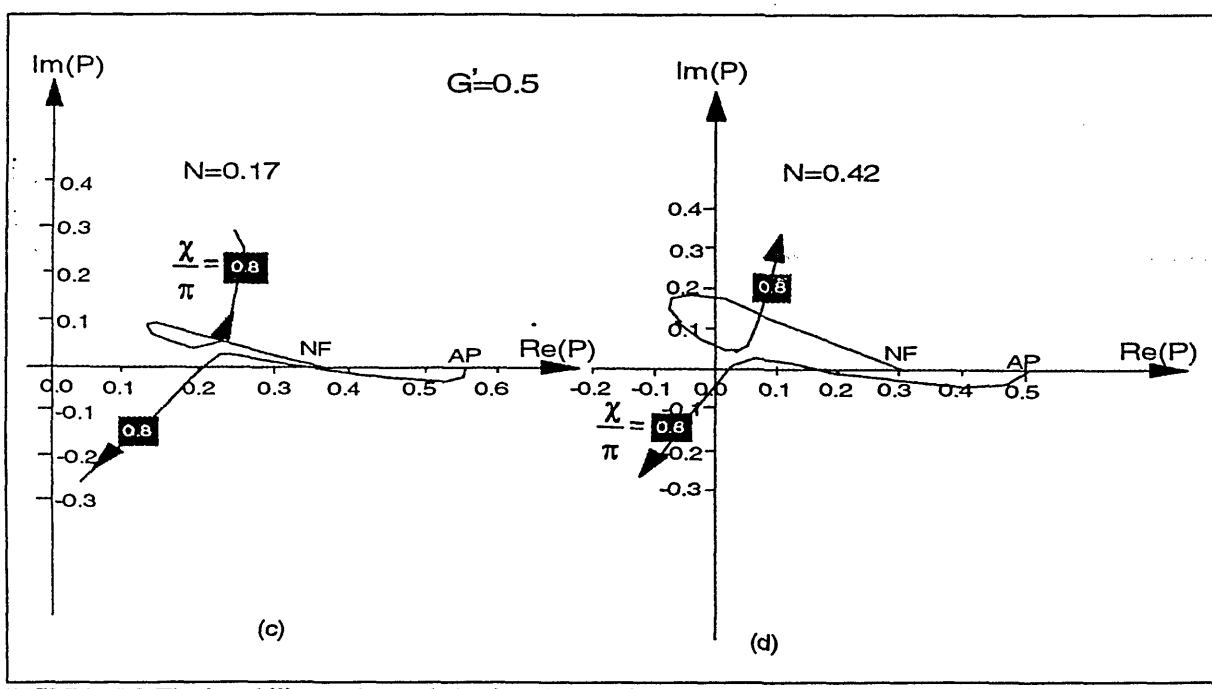

FIGURE 5.3 The instability exchange behaviour in the viscous G-mode loci when G'=0.5, $\chi=0.8\pi$ (c) N=0.17 (d) N=0.42.

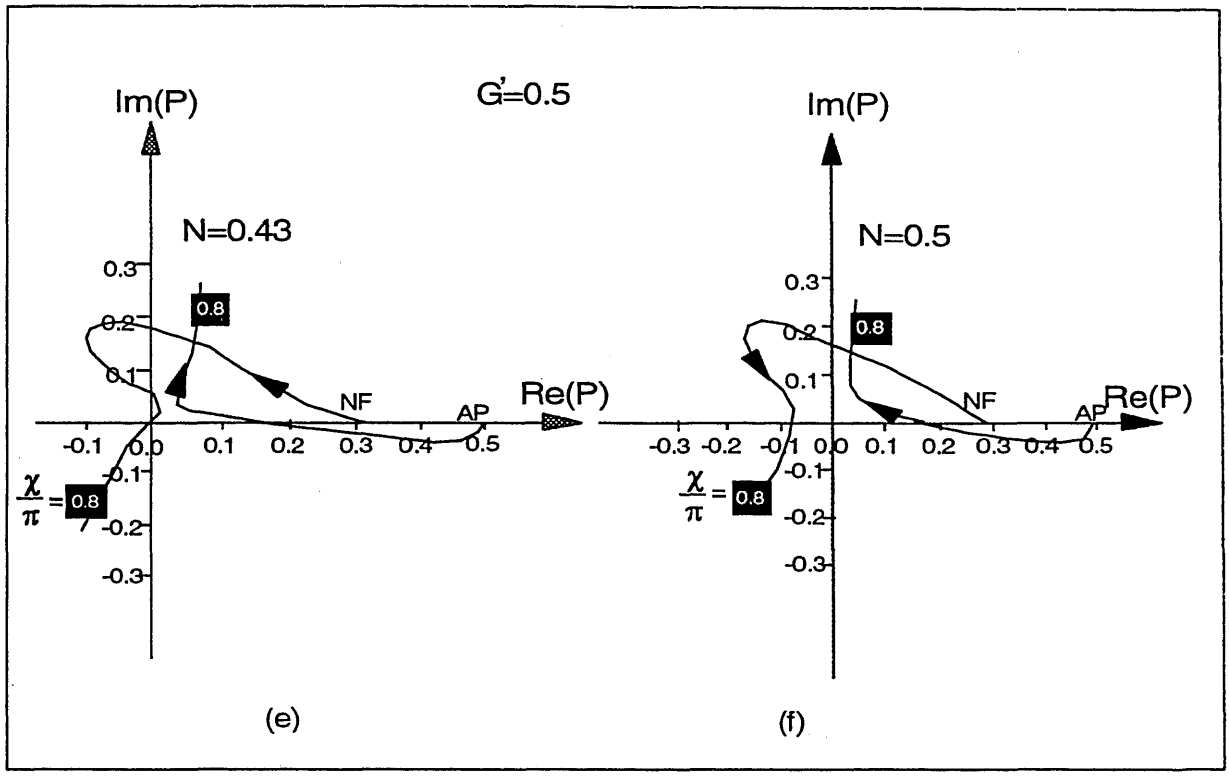

FIGURE 5.3 The instability exchange behaviour in the viscous G-mode loci when G'=0.5, $\chi = 0.8\,\pi$ (e) N=0.43 (f) N=0.5.

As we are primarily interested in the most unstable modes, the loci presented here should be only that with the largest $Re(P)$. The figures of inviscid eigen-loci in Chapter 4 shown the destabilizing effects of the flow on the tearing mode when the flow parameter R increases. The viscous loci presented in this chapter show the level crossing, or discontinuity, during the transition from the G-mode branch to the tearing mode branch because of the bifurcation and the instability exchange which are illustrated in Figures 5.2 and 5.3. The coexistence of both the stabilizing and destabilizing effects of the flow on the visco-resistive instability are interesting and therefore a further analysis is necessary. The dashed lines in figures 5.4, 5.5 and 5.6 denote the level-crossing occuring at the jump points between the NF and AP loci. The physical correspondences of transition from the stabilizing effect to the destabilizing effect of the flow at this stage is complicated as the viscosity plays the instability exchange and makes the behaviour of the plasma flow most difficult to predict. We shall pay more attention to the problem explored in the visco-resistive modes analysis.

In analogy with the fluid dynamic theory of the stability of parallel shear flow, the phenomenon illustrated above could be the unstable flow resulting from the viscous stress.

The increase of viscosity in the G-mode loci can induce the changing of the loci topology and, therefore changing the rate of stabilizing or destabilizing effects of the flow. It is obvious that the viscosity reduces the growth rate of the instability in the flowless case (see §3.2) by dissipating the fluid density gradient, no matter whether the plasma is tearing stable or unstable. However, the instability exchange behaviour presented in the equilibrium flow case posed the following question: Does the viscosity introduce instability in the MHD model as can arise in fluid dynamic systems?

5.2 The Topology of the Viscous G-mode Loci

The behaviour of coupled stable and unstable branches presents amazing evidence of instability exchange in the visco-gravitational modes. It supplies a good understanding of the eigenvalue spectrum with discontinuous behaviour. The viscous tearing mode loci in §5.1 shown that viscosity stabilise the tearing mode; the inviscid G-mode loci in §4.2.2 shown the contrasting results that $G>0$ destabilise the tearing mode. All of the results we have obtained, nevertherless, indicate that the tearing mode eventually takes over and shows an overwhelming destabilizing effect when the flow R becomes large. The results in this section for the visco-tearing-G mode loci show that when $R<1$ then the viscous effect and the G-mode effects compete, thereby forming the level crossings from the stable branch to the unstable branch. The tearing mode dominates the instability when $R>1$ which remains unchanged in the visco-resistive instability. The loci patterns are now presented in Figures 5.4(a)-(c) for $G'=0.1$, Figures 5.5(a)-(c) for $G'=0.5$ and Figures 5.6(a)-(c) for $G'=1.0$. The letters (a), (b) and (c) now refer to the N values of $0.05, 0.1$ and 0.5 respectively. These should be compared with the corresponding tearing mode loci in Figure 5.1.

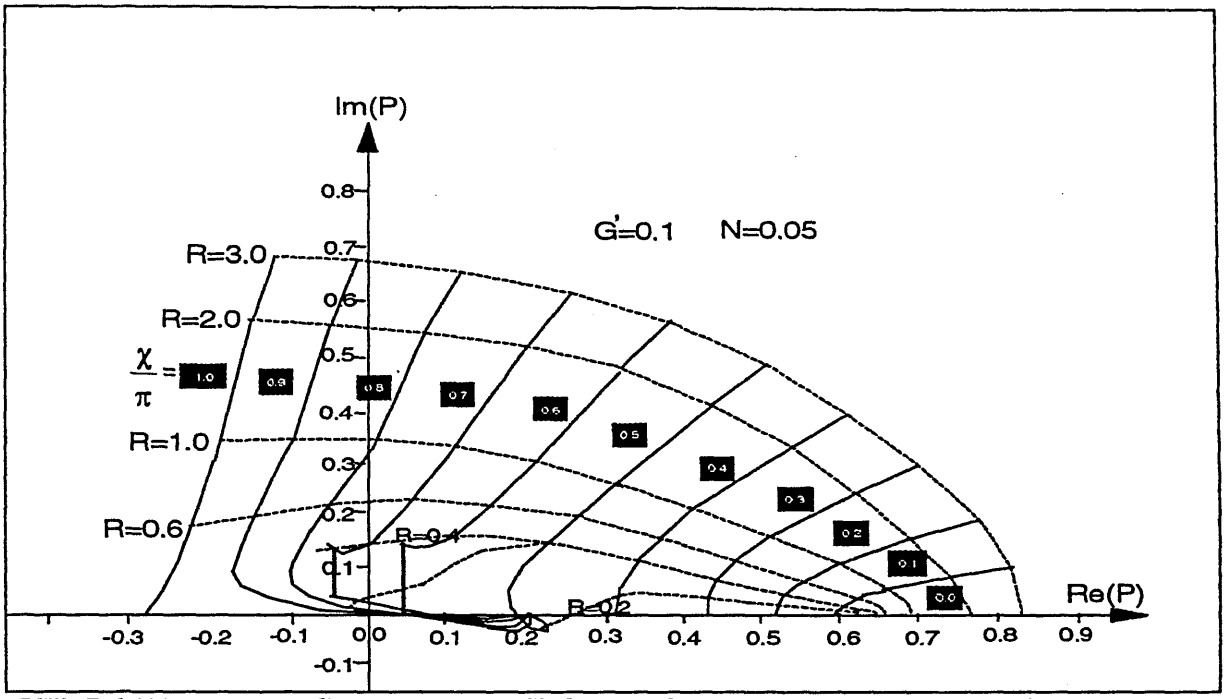

FIGURE 5.4(a) The viscous G-mode loci when G'=0.1, N=0.05 for different values of R and χ/π. There are level crossings when $0.5\pi < \chi < 0.8\pi$ which denote the bifurcations between the stable branches and the unstable branches.

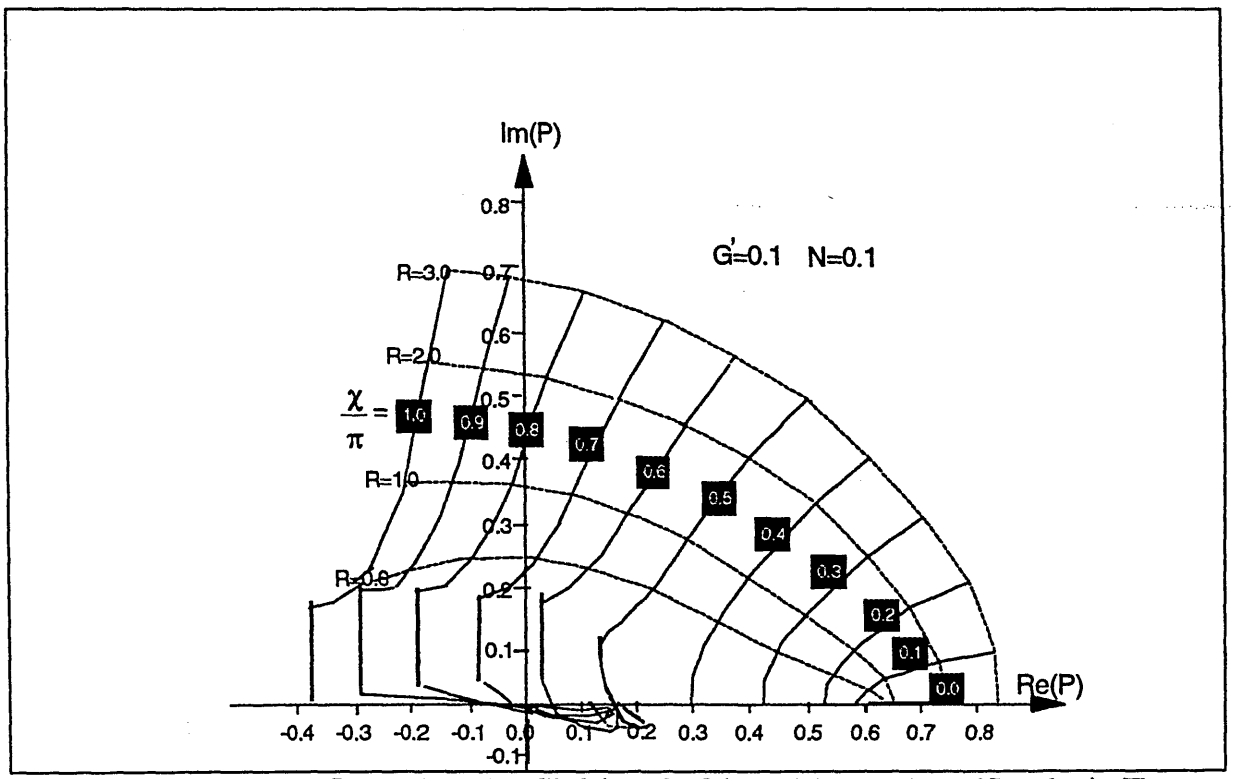

FIGURE 5.4(b) The viscous G-mode loci when G'=0.1 and N=0.1 for different values of R and χ/π. There are level crossings when $0.5\pi < \chi < \pi$.

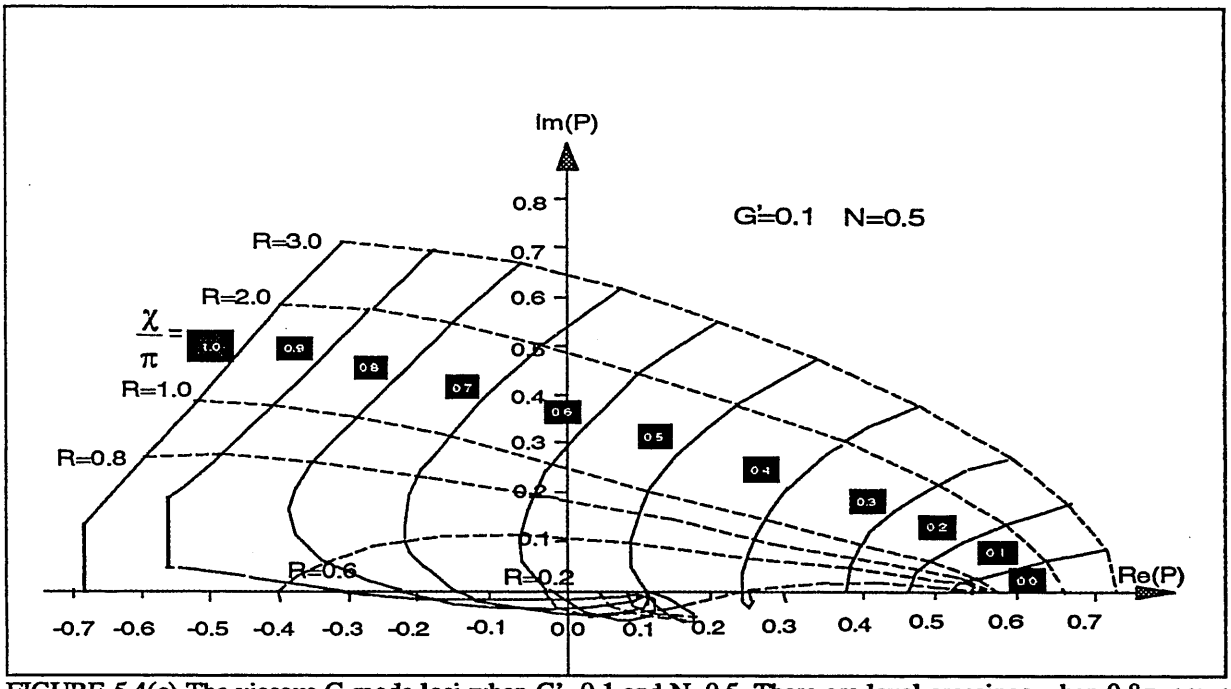

FIGURE 5.4(c) The viscous G-mode loci when G'=0.1 and N=0.5. There are level crossings when $0.8\pi < \chi < \pi$. The level crossings in (b) for $0.5\pi < \chi < 0.8\pi$ have been smoothed out after the second instability exchange.

5.2.1 Order in the loci topology

Figures 5.4, 5.5 and 5.6 show an interesting jump in the loci for certain values of χ/π. The vertical dashed lines result from the instability exchange. The explanation of this phenomenon is as follows.

Recall that we are primarily interested in the mode with the largest $Re(P)$, which is the eigenvalue plotted in Figures 5.4-5.6. Consider the case $N=0.17$ in Figure 5.2(c) and remember that R is increasing along the paths shown. Then there is a critical value R_0 such that for $0<R<R_0$ the eigenvalue with the largest $Re(P)$ lies on the AP branch of the eigenvalue locus, but for $R>R_0$ the eigenvalue with largest real part is found on the branch emanating from NF. Thus a vertical jump occurs from the part of the AP locus in $Im(P)>0$ to the lower part of the loop in the NF locus. The loci topology is changed.

The scaling of the growth rate is very difficult at this disordered stage. This accounts for the jumps in Figures 5.4-5.6. For example, the discontinuous loci in Figure 5.4 ($G'=0.1$) are the combination of the AP and NF branches as we are only looking for the modes with

the largest growth rate $Re(P)$. If we increase the viscosity (i.e. $N \geq 0.016$) then the first level-crossing from the AP branch to the NF branch occurs. When N is increased further (i.e. $N \geq 0.5$) then after the second bifurcation point we observe that the discontinuities on the loci corresponding to $\chi/\pi = 0.6, 0.7$ and 0.8 have been smoothed out. The unstable branch emanating from AP now grows continuously as R increases. The growth rate $Re(P)$ has been reduced substantially from the inviscid case [i.e. compare $Re(P)$ in Figure 5.4(c) with $Re(P)$ in Figure 4.10(b)] for the same parameters R, G and χ. The loci topology has been restored into order after the second instability exchange has taken place. Viscosity yields a purely stabilising effect at this stage.

In Figure 5.4(a), the loci for $\chi \geq 0.5\pi$ present various behaviours: when $\chi = 0.5\pi$ the smooth locus is obtained after the second bifurcation; when $\chi = 0.6\pi$ and 0.7π, the vertical jumps occur after the first bifurcation; and when $\chi \geq 0.8\pi$ the loci are continuous without level-crossing.

As we discussed previously, the fact that the plasma tearing mode is stable or unstable has a significant effect on the growth rate, c.f. Figure 5.4, when R increases. When $\chi = 0.5\pi$ the instability exchange is found to be limited by a marginally stable tearing mode; if $\chi = 0.6\pi$ then the stable tearing mode is excited by an unfavourable gravity but depressed by viscosity. Therefore the instability exchange happens; and if $\chi = \pi$, so that the tearing mode has effectively been removed, then viscosity only shows a stabilizing effect on the G-mode.

We must point out that we have reached a difficult point: the isolation of the stable branch and the unstable branch is no longer straightforward, as was the case in the tearing and inviscid G-modes. In the previous cases, the stable and the unstable eigen-modes were located in different regions of the P-plane for the same parameters R and χ. Now, for the viscous G-mode, the stable modes are very close to the unstable modes so that very delicate computation is vital to obtain the disordered loci pattern. These unstable features are not unexpected in the study of the effects of viscous flow where the coexistence of the stabilizing and destabilizing effects plays an important role.

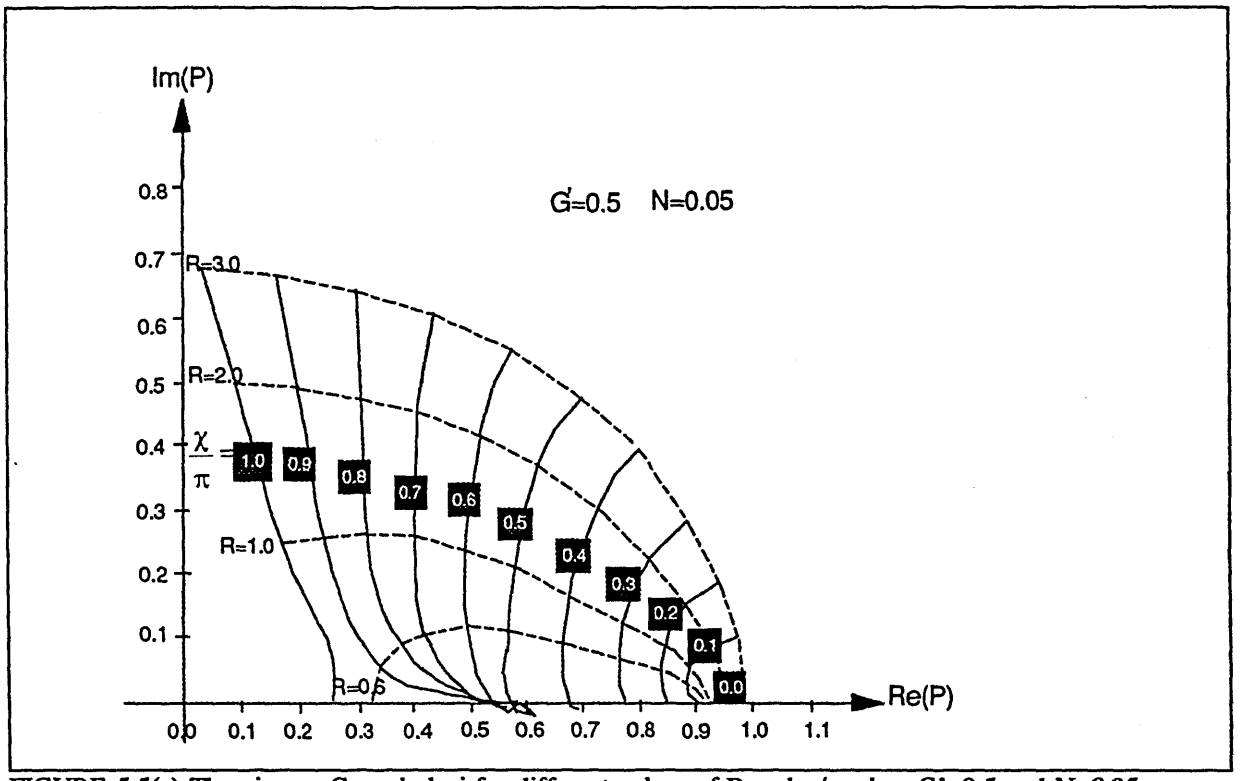

FIGURE 5.5(a) The viscous G-mode loci for different values of R and χ/π when G'=0.5 and N=0.05.

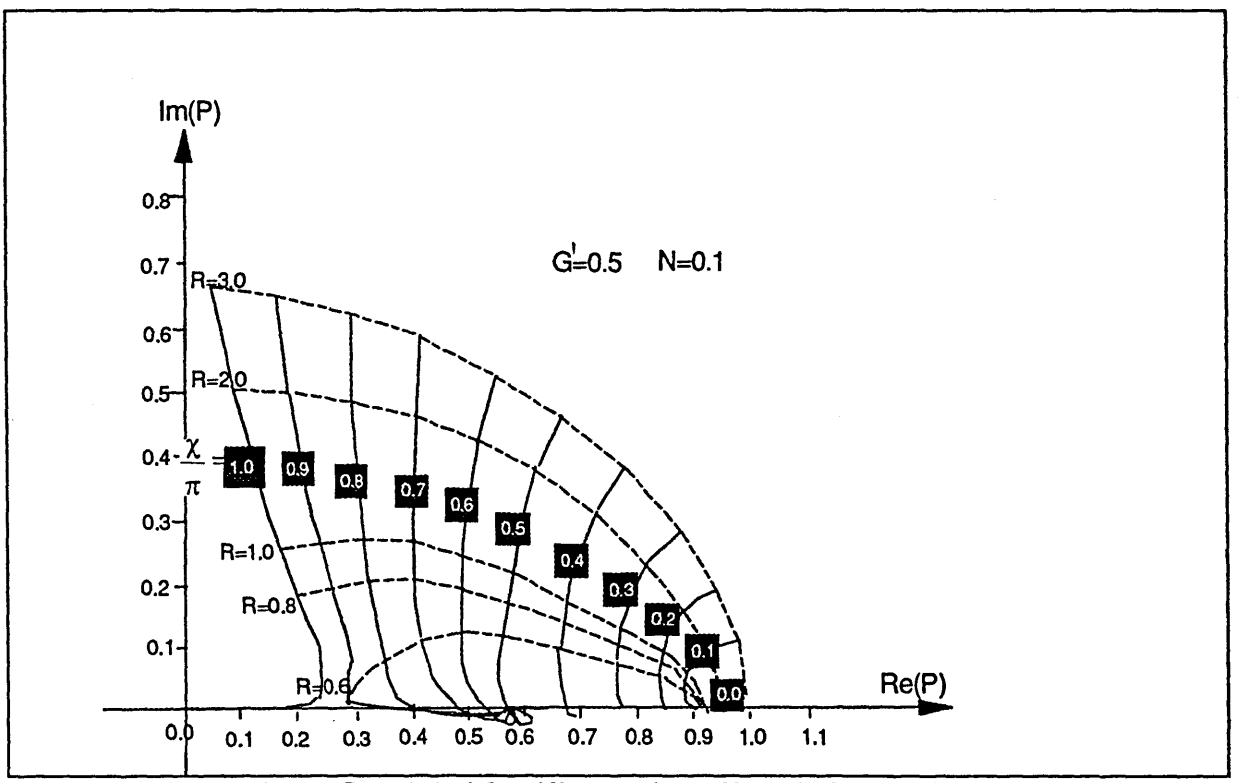

FIGURE 5.5 (b) The viscous G-mode loci for different values of R and χ/π when G'=0.5 and N=0.1.

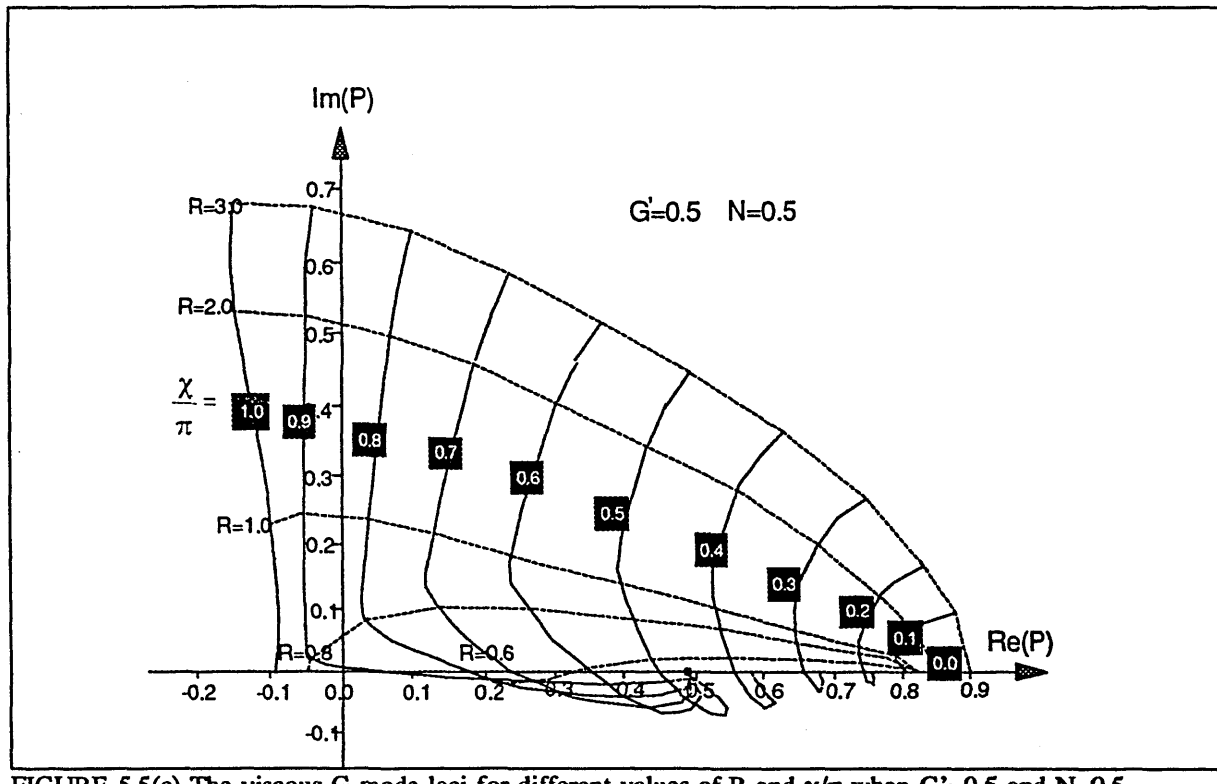

FIGURE 5.5(c) The viscous G-mode loci for different values of R and χ/π when G'=0.5 and N=0.5.

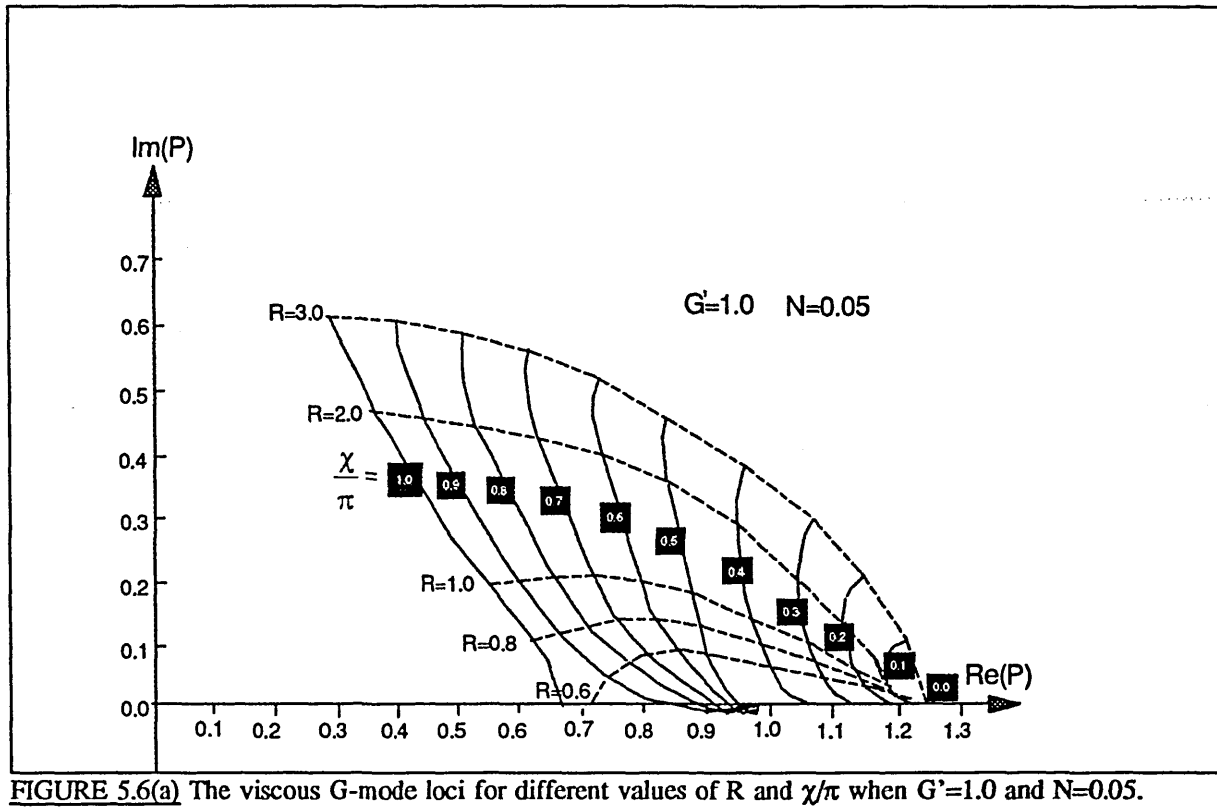

FIGURE 5.6(a) The viscous G-mode loci for different values of R and χ/π when G'=1.0 and N=0.05.

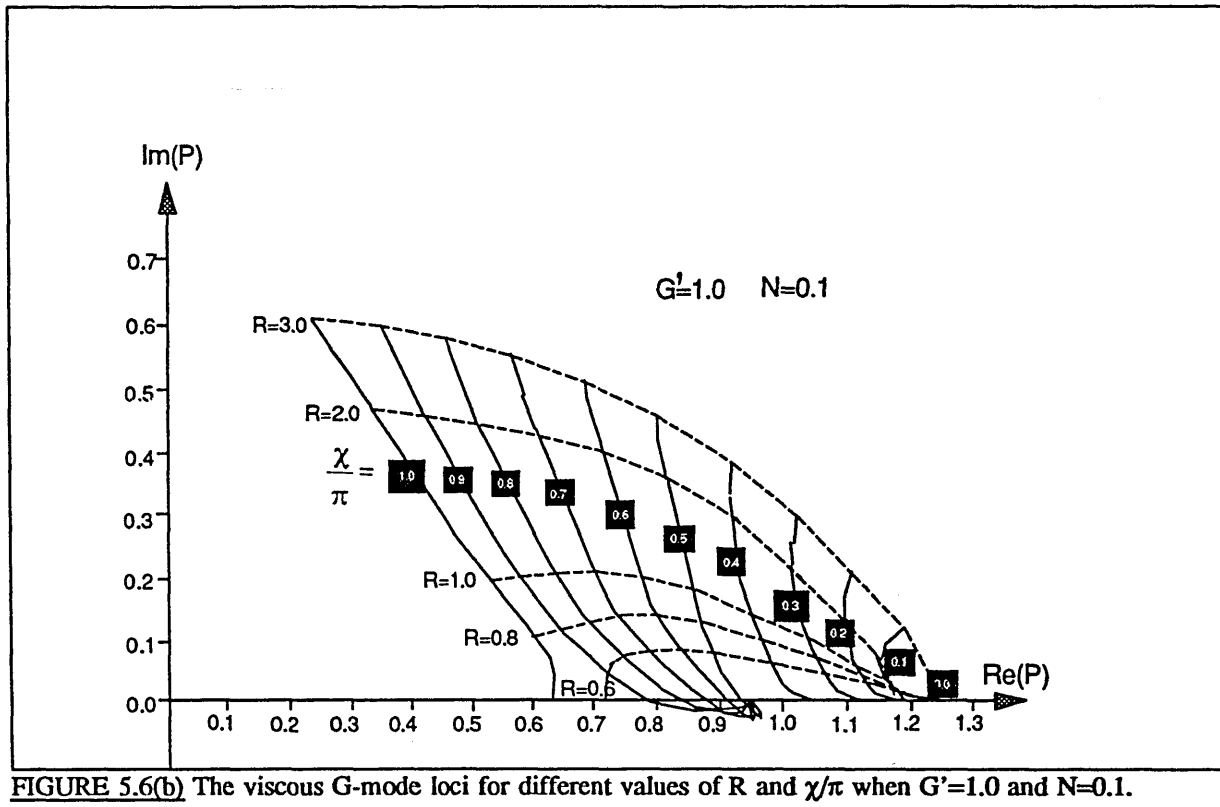

FIGURE 5.6(b) The viscous G-mode loci for different values of R and χ/π when G'=1.0 and N=0.1.

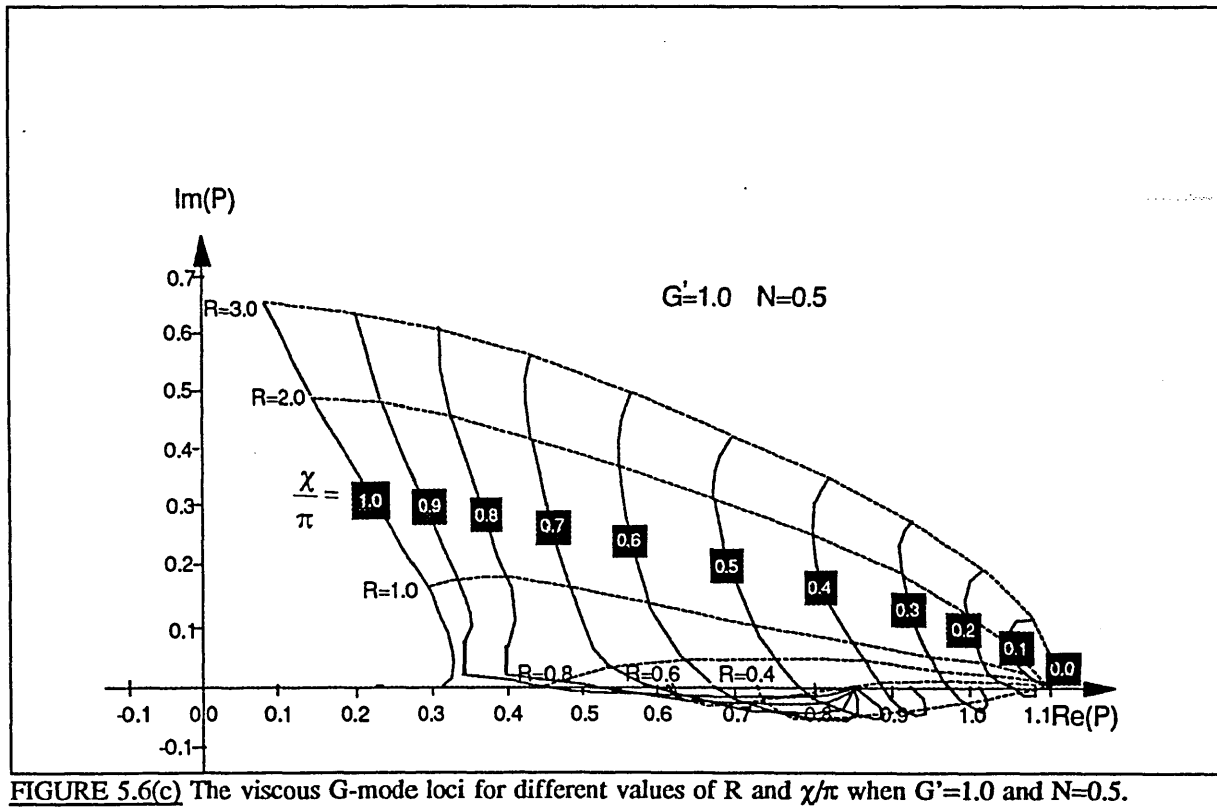

FIGURE 5.6(c) The viscous G-mode loci for different values of R and χ/π when G'=1.0 and N=0.5.

5.2.2 Features of the visco-resistive instability

The loci when $|\chi| \geq \pi/2$ in the inviscid tearing mode case $(G=0)$ develop from the AP as we introduced in Chapter 4. The AP origin splits up in the presence of viscosity to preduce the unstable spectrum for $\chi > \pi/2$ growing from the stable region. However in the gravitational mode with viscosity, loci develop from either NF as we obtained in §3.2 or AP from the small R limit. Both origins of the G-mode are unstable with $Re(P) > 0$. The AP loci do not disappear even for large viscosity. As with the inviscid loci pattern we observed in Chapter 4, the viscous loci pattern will have a BW shape (see §4.2.2), but with various details according to various values of G and N. The visco-tearing-G mode-mixing behaviour which is illustrated in §5.2.1 plays an important part in driving the BW loci pattern to move in the complex P-plane. The BW moves to the left with reduced $Re(P)$ under the influence of viscosity; or it moves to the right with increased $Re(P)$ when G is increased.

Increasing viscosity when $G'=0.1$, we have obtained the loci pattern in the stable region when $|\chi| \geq 0.5\pi$ and N is large or in the unstable region when N is small (see Figure 5.4). For example, when $N \geq 0.5$, the BW pattern in Figure 5.4(c) approaches the position of the classical instability criterion of $\chi \approx 0.5\pi$; therefore the viscosity shows a stabilizing effect on the G-mode.

When $G'=0.5$, the stabilizing effect of viscosity is still sufficient to pull back the loci pattern into the stable region when the tearing mode is stable and $N > 0.5$. Shear flow now shows a strong stabilizing effect as in the inviscid case (see Figure 5.5).

If $G \geq 1.0$, the BW viscous loci is far away from the stable region (see Figure 5.6). The instability exchanges have been smoothed out and the shear flow presents stabilizing effect on the G-mode then a destabilizing effect on the tearing mode when R is sufficiently large.

The shear flow would slow down the gravitational interchange while speed up the reconnection of the magnetic field. Observing the limits when the shear flow is small or large, we may conclude that there is a transition from the stabilizing effect on the G-mode to the destabilizing effect on the tearing mode. The viscosity can induce the bifurcation and level-crossing during the instability transition.

CHAPTER VI

AN ANALYTIC ESTIMATE FOR THE GROWTH RATE OF THE G-MODE INSTABILITY IN THE LARGE FLOW LIMIT

Introduction

To account for the behaviour of the growth rate P when the flow R becomes large, we carry out an asymptotic study which enables us to estimate P in the large R limit analytically. From Chapter 2, the viscous G-mode equation takes the form

$$(R\frac{d}{dk}-P)\,Lh-\frac{G}{(F')^2}h=0,\quad -\infty<k<0,\ 0<k<\infty \tag{6.1}$$

where

$$Lh=\frac{d^2h}{dk^2}+R\frac{d}{dk}(k^2h)-(k^2P+k^4N)\,h \tag{6.2}$$

is the viscous tearing mode operator. The associated boundary and jump conditions at the origin $k=0$ are

$$h(\pm\infty)=0,\ h(0+)=1,\ h'(0\pm)=-ie^{\pm i\chi}, \tag{6.3}$$

$$h''(0+)-h''(0-)=2\pi i\frac{G}{(F')^2}, \tag{6.4}$$

together with the eigenvalue relation

$$2\pi P=\frac{h(0-)}{h'(0-)}e^{-i\chi}-\frac{h(0+)}{h'(0+)}e^{i\chi},\quad -\pi<\chi\le\pi. \tag{6.5}$$

The values of h and h' at both sides of the origin are required to obtain the asymptotic estimate of P.

In this chapter we perform an asymptotic analysis to determine the eigen-solution h first,

In this chapter we perform an asymptotic analysis to determine the eigen-solution h first, and then predict the eigenvalue P for large values of the flow parameter R to support the numerical analysis in Chapters 4 and 5. The asymptotic approximation to determine the growth rate for the tearing mode in (6.2), given by $Lh=0$, was introduced by Paris and Sy (1983) and formulated by Bondeson and Persson (1986). They found that the growth rate P for the tearing mode, when R becomes large, behaves like

$$P \sim \left(\frac{R}{2\pi} e^{i\chi}\right)^{1/2} + \frac{\cos\chi\,\Gamma(1/3)}{2\pi R^{1/3} 3^{2/3}}, \quad R \gg 1 \tag{6.6}$$

in the inviscid limit $N=0$. It follows from this formula that the growth rate $Re(P)$ increases as the flow R increases, with the physical interpretation that shear flow along $\underline{B_0}$ destabilizes the tearing mode, with obvious consequences for neutral beam injection in Tokamaks. It was observed by these authers that large flows $(R \gg 1)$ could exist with $Re(P)>0$ for $|\chi|<\pi$, so that the tearing mode corresponding to $\Delta'<0$ $(i.e.\ \pi/2<|\chi|<\pi)$ can be driven unstable.

By the transformation $Y \equiv h'/h$, introduced by Bondeson and Persson (1986) to deal with the tearing mode equation, (6.2) becomes a nonlinear Ricatti equation

$$F(Y', Y^2, Y, k) = 0. \tag{6.7}$$

With a perturbation expansion $Y = Y_0 + Y_1 + Y_2 + \cdots$, we may obtain the asymptotic form of the eigenvalue P in (6.5). However, in considering the gravitational mode equation (6.1) with the same method, we found that it is difficult to deal with a second-order nonlinear equation

$$F(Y'', Y', Y^2, Y, k) = 0, \tag{6.8}$$

to obtain the asymptotic form of P in (6.5).

Our attempt in this chapter is to present an alternative asymptotic method to estimate the growth rate of the gravitational mode. To illustrate the method, we estimate the tearing mode first, including the viscous term, by using a singular perturbation method to solve the differential equation order-by-order.

6.1 Asymptotic Estimate of P for the Viscous Tearing Mode in the Large Flow Limit

An asymptotic approach to the problem of estimating the eigenvalue P for the viscous tearing equation (6.2) can be expressed in terms of a singular perturbation expansion

$$h=h_0+h_1+h_2+h_3+\cdots, \qquad R\gg 1 \tag{6.9}$$

where h_n, $n=1,2,3,\cdots$ are nth order perturbation solutions with $h_n \to 0$, for $R\gg 1$. The asymptotic recurrence relations of the nth order solution h_n and (n-1)th order solution h_{n-1} are

$$\begin{aligned} h_0''+R(k^2h_0)' &= 0, \\ h_n''+R(k^2h_n)' &= (k^2P+k^4N)\,h_{n-1}, \quad n=1,2,3,\cdots. \end{aligned} \tag{6.10}$$

For sufficiently large values of the flow parameter R, the solution h_n and its derivatives $h_n^{(m)}$, $m=0,1,2$, are assumed to decay as we know from the qualitative discussion of the eigen-function $h(k)$ in §4.3. The leading-order solution $h_0(k)$ and the nth order solutions $h_n(k)$ satisfy the boundary conditions

$$h_0(\pm\infty)=h_0'(\pm\infty)=0, \quad h_n(\pm\infty)=h_n'(\pm\infty)=0, \tag{6.11}$$

so that we may solve (6.10) for k positive and k negative respectively.

6.1.1 Asymptotics of the leading-order solution $h_0(k)$

A straightforward general form of leading-order solution from the homogeneous equation in (6.10) is obtained as

$$h_0(k)=c_0e^{-\xi}+c_1e^{-\xi}\int_0^k e^{\xi}dk, \quad \xi=\frac{R}{3}k^3 \tag{6.12}$$

where c_0 and c_1 are arbitrary constants.

The asymptotic behaviour of the solution suggests that $h(k)$, which satisfies the required boundary conditions, should be considered separately for k positive and negative. Bondeson and Persson (1986) showed that by considering the validity of the leading-order solutions, one must consider the next order solution to decide on the values of the constants c_0 and c_1.

The first-order equation is, from (6.10) with $n=1$

$$(h_1' + Rk^2 h_1)' = (k^2 P + k^4 N) h_0 . \tag{6.13}$$

Integration of (6.13) over $[k, +\infty)$ for $k>0$ or, over $(-\infty, k]$ for $k<0$, then yields

$$\begin{aligned} h_1' + Rk^2 h_1 &= P\int_{\infty}^{k} k^2 h_0 dk + N\int_{\infty}^{k} k^4 h_0 dk, \quad k>0 \\ h_1' + Rk^2 h_1 &= P\int_{-\infty}^{k} k^2 h_0 dk + N\int_{-\infty}^{k} k^4 h_0 dk, \quad k<0 . \end{aligned} \tag{6.14}$$

The approximation of h_0 when $k \to \pm\infty$ is based on the following lemma.

Lemma 6.1

If (i) $a(x)$ and $b(x)$ are continuous functions; (ii) $a(x) \to \infty$ and $b(x) \to \infty$ as $x \to \infty$ then

$$\lim_{x\to\infty} \frac{b(x)}{a(x)} = \lim_{x\to\infty} \frac{b'(x)}{a'(x)} .$$

Proof:

From the Stolz theorem*, we have the extension for continuous functions $a(x)$ and $b(x)$

$$\begin{aligned} \lim_{x\to\infty} \frac{b(x)}{a(x)} &= \lim_{x\to\infty} \lim_{\Delta x\to 0} \frac{b(x+\Delta x) - b(x)}{a(x+\Delta x) - a(x)} \\ &= \lim_{x\to\infty} \lim_{\Delta x\to 0} \frac{(b(x+\Delta x) - b(x))/\Delta x}{(a(x+\Delta x) - a(x))/\Delta x} = \lim_{x\to\infty} \frac{b'(x)}{a'(x)} . \end{aligned}$$

---

* **Stolz Limit Theorem (Stolz, O., 1842-1905):**

To calculate the limit of the sequence $\{\frac{x_n}{y_n}\}$, where x_n, y_n are both monotonic increasing and satisfy (i) $\lim_{n\to\infty} y_n = +\infty$, (ii) $\lim_{n\to\infty} \frac{x_{n+1} - x_n}{y_{n+1} - y_n} = A$, then we have

$$\lim_{n\to\infty} \frac{x_n}{y_n} = \lim_{n\to\infty} \frac{x_{n+1} - x_n}{y_{n+1} - y_n} = A.$$

From Lemma 6.1, we can then estimate $h_0(k)$ as $k\to\infty$

$$\lim_{k\to+\infty} h_0(k) = c_0 \lim_{k\to\infty} e^{-\xi} + c_1 \lim_{k\to\infty} \frac{\int_0^k e^{\xi} dk}{e^{\xi}}$$

$$= c_1 \lim_{k\to\infty} \frac{e^{\xi}}{Rk^2 e^{\xi}} \tag{6.15}$$

From (6.14) and (6.15), we note that $h_1(k) = O[h_0(k)] \to 0$ as $k\to\infty$, so that

$$h_1'(k) \sim P\int_{\infty}^{k} dk + N\int_{\infty}^{k} k^2 dk, \qquad k\to+\infty \tag{6.16}$$

which is not acceptable as $h_1'(k)$ is assumed decaying when k becomes large. Thus, the coefficient c_1 must be set to zero; that is

$$h_0(k) = c_0 e^{-\xi}, \qquad k>0. \tag{6.17}$$

Likewise, for $k<0$, we have from (6.12)

$$h_0(k) = e^{-\xi}[c_0 + c_1\int_0^k e^{\xi} dk] = e^{-\xi}[c_0 + c_1(\int_0^{-\infty} + \int_{-\infty}^{k}) e^{\xi} dk]$$

$$\sim e^{-\xi}[c_0 + c_1\int_0^{-\infty} e^{\xi} dk] = e^{-\xi}[c_0 - \frac{c_1}{3^{2/3}R^{1/3}}\Gamma(\frac{1}{3})] \to \infty, \quad k\to-\infty. \tag{6.18}$$

where $\Gamma(a) = \int_0^{\infty} u^{a-1}e^{-u}du$ $(a>0)$ is the Gamma function. The growing solution must be eliminated by choosing

$$c_0 + c_1\int_0^{-\infty} e^{\xi} dk = 0,$$

and therefore, by use of Lemma 6.1

$$h_0(k) = c_1 e^{-\xi}\int_{-\infty}^{k} e^{\xi} dk = O(k^{-2}), \qquad k\to-\infty. \tag{6.19}$$

It follows from (6.17) and (6.19) that the values of the solution $h_0(k)$ at the origin $k=\pm 0$ are

From Lemma 6.1, we can then estimate $h_0(k)$ as $k\to\infty$

$$\lim_{k\to+\infty} h_0(k) = c_0 \lim_{k\to\infty} e^{-\xi} + c_1 \lim_{k\to\infty} \frac{\int_0^k e^{\xi} dk}{e^{\xi}}$$

$$= c_1 \lim_{k\to\infty} \frac{e^{\xi}}{Rk^2 e^{\xi}} \tag{6.15}$$

From (6.14) and (6.15), we note that $h_1(k) = O[h_0(k)] \to 0$ as $k\to\infty$, so that

$$h_1'(k) \sim P\int_{\infty}^{k} dk + N\int_{\infty}^{k} k^2 dk, \qquad k\to+\infty \tag{6.16}$$

which is not acceptable as $h_1'(k)$ is assumed to decay when k becomes large. Thus, the coefficient c_1 must be set to zero; that is

$$h_0(k) = c_0 e^{-\xi}, \qquad k>0. \tag{6.17}$$

Likewise, for $k<0$, we have from (6.12)

$$\begin{aligned} h_0(k) &= e^{-\xi}[c_0 + c_1\int_0^k e^{\xi} dk] = e^{-\xi}[c_0 + c_1(\int_0^{-\infty} + \int_{-\infty}^{k}) e^{\xi} dk] \\ &\sim e^{-\xi}[c_0 + c_1\int_0^{-\infty} e^{\xi} dk] = e^{-\xi}[c_0 - \frac{c_1}{3^{2/3}R^{1/3}}\Gamma(\frac{1}{3})] \to \infty, \quad k\to-\infty. \end{aligned} \tag{6.18}$$

where $\Gamma(a) = \int_0^{\infty} u^{a-1}e^{-u}du$ $(a>0)$ is the Gamma function. The growing solution must be eliminated by choosing

$$c_0 + c_1\int_0^{-\infty} e^{\xi} dk = 0,$$

and therefore, by use of Lemma 6.1

$$h_0(k) = c_1 e^{-\xi}\int_{-\infty}^{k} e^{\xi} dk = O(k^{-2}), \qquad k\to-\infty. \tag{6.19}$$

It follows from (6.17) and (6.19) that the values of the solution $h_0(k)$ at the origin $k=\pm 0$ are

$$h_0(0+) = c_0, \quad h_0'(0+) = 0, \tag{6.20}$$

and

$$h_0(0-) = \frac{c_1\Gamma(\frac{1}{3})}{R^{1/3}3^{2/3}}, \quad h_0'(0-) = c_1. \tag{6.21}$$

6.1.2 Asymptotics of the first-order solution

Upon use of the leading-order solution $h_0(k)$, we may now estimate the derivatives of the first-order solution $h_1'(k)$ at the both sides of the origin. From (6.10), we obtain

$$h_1'(0+) = P\int_{\infty}^{0} k^2 h_0 dk + N\int_{\infty}^{0} k^4 h_0 dk = Pc_0\int_{\infty}^{0} k^2 e^{-\xi} dk + Nc_0\int_{\infty}^{0} k^4 e^{-\xi} dk$$

$$= -\frac{Pc_0}{R} - \frac{2Nc_0}{R^{5/3}3^{1/3}}\Gamma(\frac{2}{3}), \tag{6.22}$$

and

$$h_1'(0-) = Pc_1\int_{-\infty}^{0} k^2 e^{-\xi}\int_{-\infty}^{k'} e^{\xi} dk'dk + Nc_1\int_{-\infty}^{0} k^4 e^{-\xi}\int_{-\infty}^{k'} e^{\xi} dk'dk$$

$$= \frac{Pc_1}{R^2}\int_{-\infty}^{0} e^{-\xi}\int_{-\infty}^{\xi'} k^{-2} e^{\xi'} d\xi' d\xi + \frac{Nc_1}{R^2}\int_{-\infty}^{0} k^2 e^{-\xi}\int_{-\infty}^{\xi'} k^{-2} e^{\xi} d\xi' d\xi$$

$$= \frac{Pc_1}{3^{2/3}R^{4/3}}\int_{-\infty}^{0} e^{-\xi}\Gamma(\frac{1}{3},\xi)\, d\xi + \frac{Nc_1}{R^2}\int_{-\infty}^{0} \xi^{2/3} e^{-\xi}\Gamma(\frac{1}{3},\xi)\, d\xi$$

$$= O(\frac{P}{R^{4/3}}, \frac{N}{R^2}). \tag{6.23}$$

where $\Gamma(a,x) = \int_x^{\infty} u^{a-1}e^{-u}du$ $(a>0, x>0)$ is the incomplete Gamma function.

To estimate the first-order solution $h_1(k)$ at the both sides of the origin, we multiply (6.14) by e^{ξ} and integrate over $[0,k]$ for $k>0$; or integrate

over $(-\infty, k]$ for $k<0$, to find the convergent solution. Therefore we have

$$h_1 e^{\xi} = P\int_0^{k'} e^{\xi}\int_{\infty}^{k} k^2 h_0 dk dk' + N\int_0^{k'} e^{\xi}\int_{\infty}^{k} k^4 h_0 dk dk', \quad k>0$$

or

$$h_1 e^{\xi} = P\int_{-\infty}^{k'} e^{\xi}\int_{-\infty}^{k} k^2 h_0 dk dk' + N\int_{-\infty}^{k'} e^{\xi}\int_{-\infty}^{k} k^4 h_0 dk dk', \quad k<0 \qquad (6.24)$$

where h_1 satisfies the assumed condition $h_1(\pm\infty)=0$. Then, at the positive side of the origin, in terms of the normalized solution $h(0+)=c_0$, h_1 is given by

$$h_1(0+) = 0. \qquad (6.25)$$

At the negative side of the origin, h_1 is given by

$$h_1(0-) = Pc_1\int_{-\infty}^{0} e^{\xi}\int_{-\infty}^{k} k^2 e^{-\xi}\int_{-\infty}^{k'} e^{\xi} dk_1 dk dk' + Nc_1\int_{-\infty}^{0} e^{\xi}\int_{-\infty}^{k} k^4 e^{-\xi}\int_{-\infty}^{k'} e^{\xi} dk_1 dk dk'$$

$$= \frac{Pc_1}{R^2}\int_{-\infty}^{0} e^{\xi}\int_{-\infty}^{k} e^{-\xi}\int_{-\infty}^{k'} e^{\xi} k^{-2} d\xi' d\xi dk + \frac{Nc_1}{R^2}\int_{-\infty}^{0} e^{\xi}\int_{-\infty}^{k} k^2 e^{-\xi}\int_{-\infty}^{k'} k^{-2} e^{\xi} d\xi' d\xi dk$$

$$= \frac{Pc_1}{R^{4/3}3^{2/3}}\int_{-\infty}^{0} e^{\xi}\int_{-\infty}^{k} e^{-\xi}\Gamma(\frac{1}{3},\xi)\, d\xi dk + \frac{Nc_1}{R^2}\int_{-\infty}^{0} e^{\xi}\int_{-\infty}^{k} \xi^{2/3} e^{-\xi}\int_{-\infty}^{k'} \xi^{-2/3} e^{\xi} d\xi' d\xi dk$$

$$= \frac{Pc_1}{R^{5/3}3^{4/3}}\int_{-\infty}^{0} \xi^{-2/3} e^{\xi}\int_{-\infty}^{k'} e^{-\xi}\Gamma(\frac{1}{3},\xi)\, d\xi' d\xi + \frac{Nc_1}{R^{7/3}3^{2/3}}\int_{-\infty}^{0} \xi^{-2/3} e^{\xi}\int_{-\infty}^{k'} \xi^{2/3} e^{-\xi}\Gamma(\frac{1}{3},\xi)\, d\xi$$

$$= O(\frac{P}{R^{5/3}}, \frac{N}{R^{7/3}}), \quad R\gg 1. \qquad (6.26)$$

6.1.3 Asymptotics of the second-order and third-order solutions

To estimate the second-order solution h_2 in (6.10), we consider the asymptotic form of h_1 when $R\gg 1$,

$$h_1 e^{\xi} = Pc_0 \int_0^{k'} e^{\xi} \int_{\infty}^{k} k^2 e^{-\xi} dk dk' + Nc_0 \int_0^{k'} e^{\xi} \int_{\infty}^{k} k^4 e^{-\xi} dk dk'$$

$$= \frac{Pc_0}{R} \int_0^{k'} e^{\xi} (-e^{-\xi})\, dk' + \frac{Nc_0}{R^2} \int_0^{k'} k^{-2} e^{\xi} \int_{\infty}^{k} k^2 e^{-\xi} d\xi dk'$$

$$= -\frac{Pc_0}{R} k + O\left(\frac{N}{R^2}\right),$$

so that

$$h_1 \sim -\frac{Pc_0}{R} k e^{-\xi}, \qquad R\gg 1,\ k>0. \tag{6.27}$$

Thus, the derivatives of the second order solution at $k=\pm 0$, from (6.10), are

$$h_2'(0+) \sim -P \int_{\infty}^{0} k^2 \left(\frac{Pc_0}{R} k e^{-\xi}\right) dk + N \int_{\infty}^{0} k^4 \left(-\frac{Pc_0}{R} k e^{-\xi}\right) dk$$

$$= \frac{P^2 c_0}{R^{7/3} 3^{2/3}} \Gamma\left(\frac{1}{3}\right) + \frac{3NPc_0}{R^3}, \tag{6.28}$$

and

$$|h_2'(0-)| < |h_0'(0-)| = c_1, \qquad R\gg 1,\ k<0 \tag{6.29}$$

so that $h_2'(0-)$ may be neglected when R becomes large.

The second-order solution is estimated as

$$h_2 = e^{-\xi} \left[P \int_0^{k'} e^{\xi} \int_{\infty}^{k} k^2 h_1 dk dk' + N \int_0^{k'} e^{\xi} \int_{\infty}^{k} k^4 h_1 dk dk'\right]$$

$$= e^{-\xi} \cdot O\left(\frac{P^2}{R^{11/3}}, \frac{NP}{R^{13/3}}\right), \qquad R\gg 1,\ k>0 \tag{6.30}$$

which results in

$$h_3'(0+) = P\int_{-\infty}^{0} k^2 h_2 dk + N\int_{-\infty}^{0} k^4 h_2 dk = O(\frac{P^3}{R^{14/3}}, \frac{N^2 P}{R^{18/3}}). \qquad (6.31)$$

6.1.4 Estimate for the growth rate P when the flow R becomes large

Finally, taking the normalized leading-order solution with $c_0=1$, we have the solutions at $k=\pm 0$

$$h(0+) = h_0(0+) = 1,$$

$$h(0-) = h_0(0-) + h_1(0-) = \frac{c_0\Gamma(\frac{1}{3})}{R^{1/3}3^{2/3}} + O(\frac{P}{R^{5/3}}, \frac{N}{R^{7/3}}),$$

and

$$h'(0+) = h_1'(0+) + h_2'(0+) + h_3'(0+)$$

$$= -\frac{P}{R} - \frac{2N}{R^{5/3}3^{1/3}}\Gamma(\frac{2}{3}) + \frac{P^2}{R^{7/3}3^{2/3}}\Gamma(\frac{1}{3}) + \frac{3NP}{R^3} + O(\frac{P^3}{R^{14/3}}, \frac{N^2 P}{R^{18/3}}),$$

$$h'(0-) = h_0'(0-) = c_1. \qquad (6.32)$$

Substituting $\frac{h(0+)}{h'(0+)}$ and $\frac{h(0-)}{h'(0-)}$ into the eigenvalue relation (6.5) and balancing the dominant terms, we arrive at

$$2\pi P = \frac{h(0-)}{h'(0-)}e^{-i\chi} - \frac{h(0+)}{h'(0+)}e^{i\chi}$$

$$\sim \frac{Re^{i\chi}}{P + \frac{2N}{R^{2/3}3^{1/3}}\Gamma(2/3) - \frac{P^2}{R^{4/3}3^{2/3}}\Gamma(1/3) - \frac{3NP}{R^3}} + \frac{\Gamma(1/3)e^{-i\chi}}{R^{1/3}3^{2/3}}.$$

(6.33)

Use of the binomial theorem yields

$$2\pi P \sim \frac{R}{P}e^{i\chi}\{1-\frac{2N\Gamma(\frac{2}{3})}{R^{2/3}3^{1/3}P}+\frac{P\Gamma(\frac{1}{3})}{R^{4/3}3^{2/3}}+\frac{4N^2\Gamma^2(\frac{2}{3})}{R^{4/3}3^{2/3}P^2}-\frac{4NP\Gamma(\frac{2}{3})\Gamma(\frac{1}{3})}{3R^2P}$$

$$+\frac{P^2\Gamma^2(\frac{1}{3})}{R^{8/3}3^{4/3}}\}+\frac{\Gamma(\frac{1}{3})e^{-i\chi}}{R^{1/3}3^{2/3}}+O(\frac{P}{R^{5/3}}). \qquad (6.34)$$

Rewriting (6.34), by taking the dominant terms in the power-series expansion when R becomes large, and noting the fact that for the inviscid tearing mode $P \sim (\frac{R}{2\pi}e^{i\chi})^{1/2}$ (Paris and Sy, 1983) which eventually dominates the growth rate, we obtain

$$2\pi P^2 \sim Re^{i\chi}\{1+\frac{2P\Gamma(\frac{1}{3})\cos\chi}{R^{1/3}3^{2/3}}(Re^{i\chi})^{-1}-\frac{2N\Gamma(\frac{2}{3})}{PR^{2/3}3^{1/3}}+\cdots\}. \qquad (6.35)$$

Hence, the small terms in the power-series expansion may be neglected to achieve the asymptotic form of the viscous tearing mode growth rate P when $R\gg1$, given by

$$P \sim (\frac{R}{2\pi}e^{i\chi})^{1/2}+\frac{\Gamma(\frac{1}{3})\cos\chi}{2\pi R^{1/3}3^{2/3}}-\frac{N\Gamma(\frac{2}{3})}{R^{2/3}3^{1/3}}. \qquad (6.36)$$

In the inviscid limit $N=0$, the asymptotic form for large flow has been found by Bondeson and Persson (1986) to be

$$P \sim (\frac{R}{2\pi}e^{i\chi})^{1/2}+\frac{\Gamma(\frac{1}{3})\cos\chi}{2\pi R^{1/3}3^{2/3}}. \qquad (6.37)$$

This is a bench mark for testing the accuracy of the asymptotic form (6.36) for the viscous tearing mode, from which we see that the viscous contribution to the growth rate is

$$-\frac{N\Gamma(\frac{2}{3})}{R^{2/3}3^{1/3}}. \qquad (6.38)$$

The viscous term in the asymptotic form shows only a modification of the real part of the growth rate corresponding to a stabilizing effect. This may be compared with the numerical

value of the quantity V_r defined by

$$V_r =: Re(P) - \{ (\frac{R}{2\pi})^{1/2} \cos\frac{\chi}{2} + \frac{\Gamma(\frac{1}{3})\cos\chi}{2\pi R^{1/3} 3^{2/3}} \}, \qquad (6.39)$$

where $Re(P)$ is the real part of eigenvalue P obtained from numerical computations rather than the asymptotic form. The results of such a comparison are given in Table 6.1 and shown in Figure 6.1 for a large value of R and two different values of N. It is seen that, although the numerical results indicate a weak χ- dependence of the quantity V_r, the overall agreement between the analytical prediction and the numerics is quite good.

It has been found that, for large R, $P=P(R,\chi)$ is algebraically large like $R^{1/2}$ with a small destabilizing modification of order $R^{-1/3}$ when $\chi<\pi/2$, which becomes a stabilizing modification of order $R^{-1/3}$ for $\pi/2<\chi<\pi$. If $\chi=\pi$, the eigenvalue loci stay in the negative $Re(P)$ half-plane (see Figure 5.1) with a stabilizing modification of order $R^{-1/3}$. In this case the mode will approach marginal stability when $R\to\infty$. If $\chi=\pi/2$, then the growth rate of the mode will grow like $R^{1/2}$ with a stabilizing modification of order $R^{-2/3}$ from viscosity.

TABLE 6.1 A comparison between the numerical quantity V_r defined in (6.39) and the viscous contribution in the asymptotic form (6.36)

	$R=15,\ N=0.5$			$R=15,\ N=1.0$	
$\frac{\chi}{\pi}$	V_r	$-\frac{N\Gamma(2/3)}{R^{2/3}3^{1/3}}$	$\frac{\chi}{\pi}$	V_r	$-\frac{N\Gamma(2/3)}{R^{2/3}3^{1/3}}$
0.0	-0.0678	-0.0771	0.0	-0.133	-0.154
0.1	-0.068		0.1	-0.1339	
0.2	-0.069		0.2	-0.136	
0.3	-0.071		0.3	-0.139	
0.4	-0.073		0.4	-0.1426	
0.5	-0.074		0.5	-0.146	
0.6	-0.0743		0.6	-0.149	
0.7	-0.076		0.7	-0.151	
0.8	-0.076		0.8	-0.1526	
0.9	-0.077		0.9	-0.1538	
1.0	-0.0773		1.0	-0.1544	

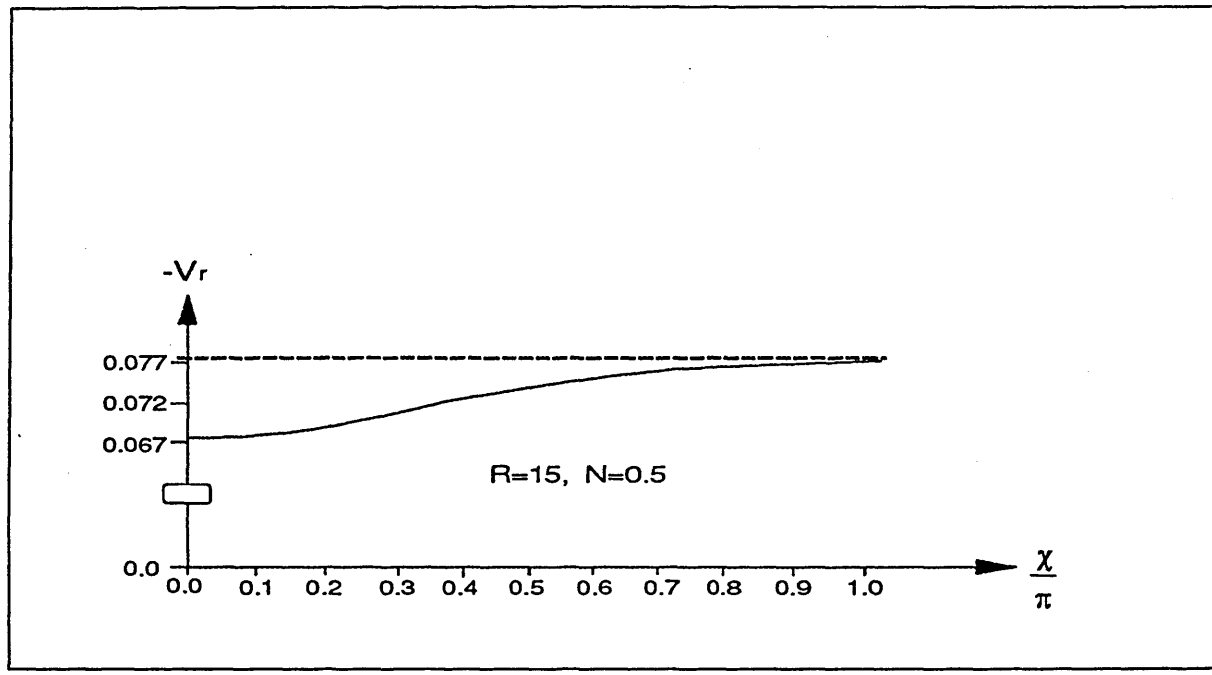

(a)

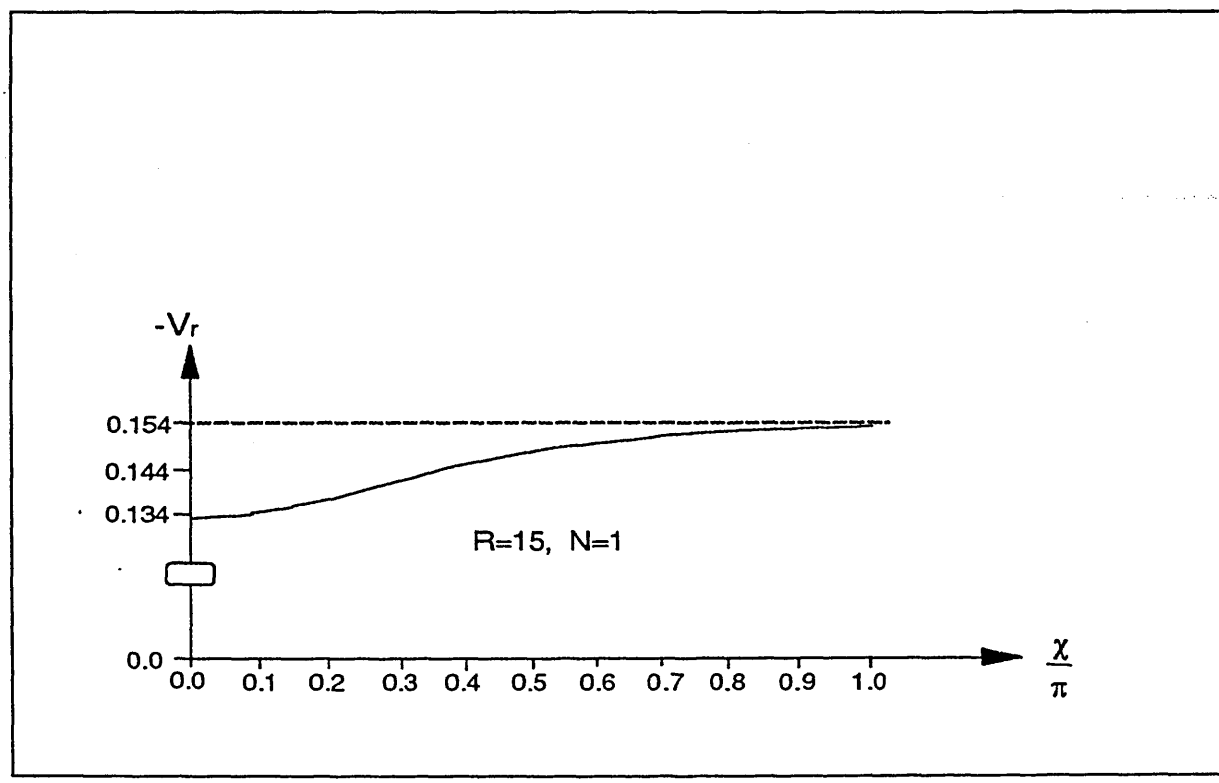

(b)

FIGURE 6.1 The numerical results (solid curve) show good agreement with the asymptotic value (dashed line) of the quantity V_r defined in (6.39) for R=15 when (a) N=0.5 and (b) N=1.0.

6.2 Large Flow Estimate for the Growth Rate P of the G-mode

In this section we perform an asymptotic estimate for the G-mode growth rate P when the flow R becomes large in the inviscid limit $N=0$. .

From (6.1) we have

$$(h'+Rk^2h)''-\frac{P}{R}h''-2P(k^2h)'=\frac{G/(F')^2-P^2k^2}{R}h. \qquad (6.40)$$

Making the perturbation expansion

$$h = h_0+h_1+h_2+h_3+\cdots, \quad R\gg 1, \qquad (6.41)$$

where the leading-order solution and the nth-order solutions satisfy the conditions

$$\begin{aligned} &h_0(\pm\infty)=h_0'(\pm\infty)=h_0''(\pm\infty)=0, \\ &h_n(\pm\infty)=h_n'(\pm\infty)=h_n''(\pm\infty)=0, \end{aligned} \qquad (6.42)$$

we now solve (6.40) perturbatively for k positive and k negative separately in the same manner as §6.1.

The transformation of (6.40) into the asymptotic recurrence relation

$$(h_0'+Rk^2h_0)''=0,$$

$$(h_n'+Rk^2h_n)''=\frac{P}{R}h_{n-1}''+2P(k^2h_{n-1})'$$

$$+\frac{G/(F')^2-P^2k^2}{R}h_{n-1}, \quad n=1,2,3,\cdots \qquad (6.43)$$

is obtained by including lower-order differential terms into the inhomogeneous term. The method has been tested in §6.1, which yields a good estimate for the viscous tearing mode growth rate. When estimating P we only use the values of h and h' at both sides of the origin $k=\pm 0$. The nth-order expansion solutions h_n, h_n' and h_n'', however, must satisfy the boundary condition that these solutions decay when $k\to\infty$.

6.2.1 Asymptotics of the leading-order solution

From the homogeneous equation in (6.43), we have, immediately, the general form of the leading-order solution for the G-mode equation

$$h_0(k) = e^{-\xi}\{c_0\int_0^k e^{\xi}dk + c_1\int_0^k ke^{\xi}dk + c_2\}, \quad \xi = \frac{R}{3}k^3. \tag{6.44}$$

Here, to simplify the analysis of the asymptotic form of h, the leading-order solution is considered, without loss of generality, to be a positive function where c_0, c_1 and c_2 are positive constants when k positive.

To decide the constants, we may discuss the associated next order solutions. On the positive k axis, the approximation of $h_0(k)$ shows that

$$h_0(k) \sim \frac{c_0e^{\xi} + c_1ke^{\xi}}{Rk^2e^{\xi}} \sim k^{-1}, \qquad k\to+\infty,$$

which follows directly from Lemma 6.1. We may prove that the first-order solution is valid only if the constants c_0, c_1 and c_2 in the leading-order solution are suitably chosen. It follows from (6.40) that integration over $[k,\infty)$ yields

$$h_1'' + R(k^2h_1)' = \frac{P}{R}h_0' + 2Pk^2h_0 - \frac{1}{R}\int_k^{\infty}\{\frac{G}{(F')^2} - P^2k^2\}h_0dk. \tag{6.45}$$

Then, $h_1''(k)$ at the origin $k=\pm0$ is given by

$$h_1''(0\pm) = \frac{P}{R}h_0'(0\pm) + \frac{1}{R}\int_{0\pm}^{\infty}\{P^2k^2 - \frac{G}{(F')^2}\}h_0dk. \tag{6.46}$$

Notice that if $c_1\neq0$ then $h_0(k)\sim k^{-1}$, as $k\to+\infty$; otherwise $h_0(k)\sim k^{-2}$, as $k\to+\infty$. From (6.46), if c_0 or c_1 isnon-zero, then the integral diverges to make $h_1''(0\pm)$ grow. Accordingly, we shall set $c_0=c_1=0$ in the leading-order solution in (6.44) to obtain

$$h_0(k) = c_2e^{-\xi}, \qquad k>0. \tag{6.47}$$

We now turn to the derivation of the asymptotic form of the solution for k negative. In terms of the coefficients c_0, $c_1\neq0$, the leading-order solution for $k<0$ is, from (6.44),

$$h_0(k) = e^{-\xi}\{c_0\int_0^{-\infty} e^{\xi}dk + c_1\int_0^{-\infty} ke^{\xi}dk + c_2 + c_0\int_{-\infty}^{k} e^{\xi}dk + c_1\int_{-\infty}^{k} ke^{\xi}dk\}$$

$$= e^{-\xi}\{-c_0\int_0^{\infty} e^{-\xi}\frac{\xi^{-2/3}}{R^{1/3}3^{2/3}}d\xi + c_1\int_0^{\infty} e^{-\xi}\frac{\xi^{-1/3}}{R^{2/3}3^{1/3}}d\xi$$

$$+ c_2 + c_0\int_{-\infty}^{k}\frac{\xi^{-2/3}}{R^{1/3}3^{2/3}}e^{\xi}d\xi + c_1\int_{-\infty}^{k}\frac{\xi^{-1/3}}{R^{2/3}3^{1/3}}e^{\xi}d\xi\}$$

$$= e^{-\xi}\{-\frac{c_0\Gamma(\frac{1}{3})}{R^{1/3}3^{2/3}} + \frac{c_1\Gamma(\frac{2}{3})}{R^{2/3}3^{1/3}} + c_2\} + O(\frac{1}{R^{1/3}3^{2/3}}, \xi^{-\frac{2}{3}}), \qquad k\to-\infty.$$

The leading-order solution $h_0(k)$ is exponentially growing when $k\to-\infty$. It may be forced to decay by eliminating the coefficient of $e^{-\xi}$: this is achieved if we set

$$-\frac{c_0\Gamma(\frac{1}{3})}{R^{1/3}3^{2/3}} + \frac{c_1\Gamma(\frac{2}{3})}{R^{2/3}3^{1/3}} + c_2 = 0.$$

Thus the solution for $k<0$ is given by

$$h_0(k) = e^{-\xi}\{c_0\int_{-\infty}^{k} e^{\xi}dk + c_1\int_{-\infty}^{k} ke^{\xi}dk\}, \qquad k<0. \tag{6.48}$$

To express $h_0(k)$ and its derivatives at $k=0\pm$, we may take the normalized leading-order solution with $c_2=1$, so that

$$h_0(0+) = 1,$$

$$h_0'(0+) = h_0''(0+) = 0; \tag{6.49}$$

and

$$h_0(0-) = \frac{c_0\Gamma(\frac{1}{3})}{R^{1/3}3^{2/3}} - \frac{c_1\Gamma(\frac{2}{3})}{R^{2/3}3^{1/3}},$$

$$h_0'(0-) = c_0, \quad h_0''(0-) = c_1. \tag{6.50}$$

Note that $h_0(0+)$ is constant (independent of R) which satisfies the boundary condition $h(0+)=1$, so that the next order solutions $h_1(0+)$, $h_2(0+)$, $h_3(0+)$, ···, which are very small compared to $h_0(0+)$, may be ignored when R is large. For the same reason we ignore $h_1''(0-)$, $h_2''(0-)$ and $h_3''(0-)$ in the order balancing algebra.

6.2.2 Asymptotics of the first-order solution

In the usual manner for asymptotically estimating the first-order solutions of (6.40), double integration of (6.43) with $n=1$, over $[k,\infty)$, yields

$$h_1'+Rk^2h_1 = \frac{P}{R}h_0 + \frac{2P}{R}\int_\infty^k h_0 d\xi - \frac{1}{R}\int_\infty^k\int_\infty^{k'} \{\frac{G}{(F')^2} - P^2k^2\} h_0 dk dk'. \tag{6.51}$$

We may estimate h_1' and h_1'' at $k=0+$ by substituting the zero-order solution $h_0=e^{-\xi}$ to find

$$h_1'(0+) = \frac{P}{R} - \frac{2P}{R} - \frac{G}{R^3(F')^2}\int_\infty^0 (\frac{3}{R})^{-4/3}(\xi')^{-2/3}\int_\xi^\infty e^{-\xi}\xi^{-2/3}d\xi d\xi' + \frac{P^2}{R^2}\int_\infty^0\int_k^\infty e^{-\xi}d\xi dk$$

$$= -\frac{P}{R} + \frac{G}{R^{5/3}(F')^2}\int_0^\infty \frac{\Gamma(\frac{1}{3},\xi)}{3^{4/3}\xi^{2/3}}d\xi - \frac{P^2}{R^2}\int_0^\infty e^{-\xi}dk$$

$$= -\frac{P}{R} + \frac{G}{R^{5/3}(F')^2}\int_0^\infty \frac{\Gamma(\frac{1}{3},\xi)}{3^{4/3}\xi^{2/3}}d\xi - \frac{P^2}{R^{7/3}3^{2/3}}\Gamma(\frac{1}{3}); \tag{6.52}$$

and

$$h_1''(0+) = -\frac{1}{R}\int_0^\infty \{\frac{G}{(F')^2} - P^2k^2\} e^{-\xi}dk$$

$$= \frac{P^2}{R^2} + \frac{G}{R^{4/3}3^{2/3}(F')^2}\Gamma(\frac{1}{3}). \tag{6.53}$$

From (6.51), upon multiplication by the integrating factor e^{ξ}, we obtain

$$(h_1 e^{\xi})' = \frac{P}{R} + \frac{2P}{R} e^{\xi} \int_{\infty}^{k} e^{-\xi} d\xi - \frac{e^{\xi}}{R} \int_{\infty}^{k'} \int_{k}^{\infty} \{ \frac{G}{(F')^2} - P^2 k^2 \} e^{-\xi} dk dk'$$

$$= \frac{P}{R} - \frac{2P}{R} - \frac{G}{(F')^2 R^{5/3} 3^{4/3}} e^{\xi} \int_{\infty}^{k} \xi^{-\frac{2}{3}} \Gamma(\frac{1}{3}, \xi)\, d\xi + \frac{P^2}{R^2} e^{\xi} \int_{\infty}^{k} e^{-\xi} dk$$

$$= -\frac{P}{R} + \frac{G}{(F')^2 R^{5/3} 3^{4/3}} e^{\xi} \int_{k}^{\infty} \xi^{-\frac{2}{3}} \Gamma(\frac{1}{3}, \xi)\, d\xi$$

$$- \frac{P^2}{R^{7/3} 3^{2/3}} e^{\xi} \Gamma(\frac{1}{3}, \xi), \qquad (6.54)$$

Integration of (6.54) over $[0, k)$, we have

$$h_1 e^{\xi} = -\frac{P}{R} k + \frac{G}{(F')^2 R^{5/3} 3^{4/3}} \int_{0}^{k} e^{\xi} \int_{\xi}^{\infty} \xi^{-\frac{2}{3}} \Gamma(\frac{1}{3}, \xi)\, d\xi dk - \frac{P^2}{R^{7/3} 3^{2/3}} \int_{0}^{k} e^{\xi} \Gamma(\frac{1}{3}, \xi)\, dk$$

$$= -\frac{P}{R} k + \frac{G}{(F')^2 R^{8/3} 3^{4/3}} \int_{0}^{k} k^{-2} e^{\xi} \int_{\xi'}^{\infty} \xi^{-\frac{2}{3}} \Gamma(\frac{1}{3}, \xi)\, d\xi' d\xi - \frac{P^2}{R^{10/3} 3^{2/3}} \int_{0}^{k} k^{-2} e^{\xi} \Gamma(\frac{1}{3}, \xi)\, d$$

$$= -\frac{P}{R} k + \frac{G}{(F')^2 R^2 3^2} \int_{0}^{\xi} \xi^{-\frac{2}{3}} e^{\xi} \int_{\xi'}^{\infty} \xi^{-\frac{2}{3}} \Gamma(\frac{1}{3}, \xi)\, d\xi' d\xi - \frac{P^2}{R^{8/3} 3^{4/3}} \int_{0}^{\xi} \xi^{-\frac{2}{3}} \Gamma(\frac{1}{3}, \xi)\, d\xi$$

$$= -\frac{P}{R} k + O(\frac{G}{(F')^2 R^2}, \frac{N}{R^{8/3}}), \quad R \gg 1.$$

The above presentation appears complicated as the integrals contain the incomplete Gamma function. However, the calculation in obtaining the asymptotic form is much simplified in the large flow approximation, as the higher order terms are negligible when R becomes large. This then yields the leading asymptotic behaviour of $h_1(k)$ when R is large

$$h_1(k) \sim -\frac{P}{R} k e^{-\xi}, \qquad R \gg 1. \qquad (6.55)$$

For negative k, the first-order solution is obtained in a similar way as for k positive,

by substituting

$$h_0(k) = e^{-\xi}\{\frac{C_0}{R^{1/3}3^{2/3}}\int_{-\infty}^{k}\xi^{-2/3}e^{\xi}d\xi + \frac{C_1}{R^{2/3}3^{1/3}}\int_{-\infty}^{k}\xi^{-1/3}e^{\xi}d\xi\},$$

for $k<0$, into (6.51) to find

$$h_1'(0-) = \frac{P}{R}h_0(0-) + \frac{2P}{R}\int_{-\infty}^{0}h_0 d\xi - \frac{1}{R}\int_{-\infty}^{0}\int_{k}^{-\infty}\{\frac{G}{(F')^2} - P^2k^2\}h_0 dk dk'$$

$$= \frac{P}{R}\{\frac{c_0\Gamma(\frac{1}{3})}{R^{1/3}3^{2/3}} - \frac{c_1\Gamma(\frac{2}{3})}{R^{2/3}3^{1/3}}\} + \frac{2c_0P}{R^{7/3}3^{2/3}}\int_{0}^{-\infty}e^{\xi'}\int_{-\infty}^{\xi}e^{\xi}(\frac{3}{R}\xi)^{-\frac{2}{3}}d\xi d\xi' + O(\frac{P}{R^{5/3}})$$

$$= \frac{c_0P\Gamma(\frac{4}{3})}{R^{1/3}3^{2/3}} - \frac{c_1P\Gamma(\frac{2}{3})}{R^{5/3}3^{1/3}} + O(\frac{P}{R^{5/3}}). \qquad (6.56)$$

Multiplying (6.51) by e^{ξ}, and integrating over $(-\infty, k]$ for $k<0$, we then obtain

$$h_1e^{\xi} = \frac{P}{R}\int_{-\infty}^{k}\{c_0\int_{-\infty}^{k}e^{\xi}\frac{\xi^{-2/3}}{R^{1/3}3^{2/3}}d\xi + c_1\int_{-\infty}^{k}e^{\xi}\frac{\xi^{-1/3}}{R^{2/3}3^{1/3}}d\xi\}e^{\xi}dk$$

$$+\frac{2P}{R}\int_{-\infty}^{k}e^{\xi}\int_{-\infty}^{k'}e^{\xi'}\{c_0\int_{-\infty}^{k}e^{\xi}\frac{\xi^{-2/3}}{R^{1/3}3^{2/3}}d\xi + c_1\int_{-\infty}^{k}e^{\xi}\frac{\xi^{-1/3}}{R^{2/3}3^{1/3}}d\xi\}d\xi' dk$$

$$-\frac{1}{R}\int_{-\infty}^{k}\int_{-\infty}^{k'}\int_{k}^{-\infty}(\frac{G}{(F')^2} - P^2k^2)\{c_0\int_{-\infty}^{k}e^{\xi}\frac{\xi^{-2/3}}{R^{1/3}3^{2/3}}d\xi + c_1\int_{-\infty}^{k}e^{\xi}\frac{\xi^{-1/3}}{R^{2/3}3^{1/3}}d\xi\}dk dk' dk.$$

Term-by-term, scaling the integrand yields

$$h_1e^{\xi} = \frac{Pc_0}{R^{4/3}3^{2/3}}\int_{-\infty}^{k}\Gamma(\frac{1}{3},\xi)e^{\xi}dk + \frac{Pc_1}{R^{5/3}3^{1/3}}\int_{-\infty}^{k}\Gamma(\frac{2}{3},\xi)e^{\xi}dk$$

$$+\frac{2Pc_0}{R^{4/3}3^{2/3}}\int_{-\infty}^{k}e^{\xi}\int_{-\infty}^{\xi}e^{\xi}\Gamma(\frac{1}{3},\xi)d\xi + \frac{2Pc_1}{R^{5/3}3^{1/3}}\int_{-\infty}^{k}e^{\xi}\int_{-\infty}^{\xi}e^{\xi}\Gamma(\frac{2}{3},\xi)d\xi dk$$

$$-\frac{G'}{R^{4/3}3^{2/3}}\int_{-\infty}^{k}\int_{-\infty}^{k'}\int_{-\infty}^{k}\left[c_0\Gamma\left(\frac{1}{3},\xi\right)+c_1\frac{3^{1/3}}{R^{1/3}}\Gamma\left(\frac{2}{3},\xi\right)\right]dkdk'dk$$

$$+\frac{P^2}{R^{4/3}3^{2/3}}\int_{-\infty}^{k}\int_{-\infty}^{k'}\int_{-\infty}^{k}k^2\left[c_0\Gamma\left(\frac{1}{3},\xi\right)+c_1\frac{3^{1/3}}{R^{1/3}}\Gamma\left(\frac{2}{3},\xi\right)\right]dkdk'dk$$

$$=\frac{Pc_0}{R^{5/3}3^{4/3}}\int_{-\infty}^{k}\Gamma\left(\frac{1}{3},\xi\right)e^{\xi}\xi^{-\frac{2}{3}}d\xi+\frac{Pc_1}{R^{2}3^{2/3}}\int_{-\infty}^{k}\Gamma\left(\frac{2}{3},\xi\right)e^{\xi}\xi^{-\frac{1}{3}}d\xi$$

$$+\frac{2Pc_0}{R^{5/3}3^{2/3}}\int_{-\infty}^{\xi}e^{\xi}\xi^{-\frac{2}{3}}\int_{-\infty}^{\xi'}e^{\xi}\Gamma\left(\frac{1}{3},\xi\right)d\xi'd\xi+\frac{2Pc_1}{R^{2}3^{2/3}}\int_{-\infty}^{\xi}e^{\xi}\xi^{-\frac{1}{3}}\int_{-\infty}^{\xi'}e^{\xi}\Gamma\left(\frac{2}{3},\xi\right)d\xi'd\xi$$

$$-\frac{G'}{R^{7/3}3^{8/3}}\int_{-\infty}^{\xi}\xi^{-\frac{2}{3}}\int_{-\infty}^{\xi'}\xi^{-\frac{2}{3}}\int_{\xi}^{-\infty}\xi^{-\frac{2}{3}}\left[c_0\Gamma\left(\frac{1}{3},\xi\right)+c_1\frac{3^{1/3}}{R^{1/3}}\Gamma\left(\frac{2}{3},\xi\right)\right]d\xi d\xi'd\xi$$

$$+\frac{P^2}{R^{3}3^{2}}\int_{-\infty}^{\xi}\xi^{-\frac{2}{3}}\int_{-\infty}^{\xi'}\xi^{-\frac{2}{3}}\int_{\xi}^{-\infty}\left[c_0\Gamma\left(\frac{1}{3},\xi\right)+c_1\frac{3^{1/3}}{R^{1/3}}\Gamma\left(\frac{2}{3},\xi\right)\right]d\xi d\xi'd\xi.$$

Therefore, we have

$$h_1(0-)=\frac{Pc_0}{R^{5/3}3^{4/3}}\int_{-\infty}^{0}\Gamma\left(\xi,\frac{1}{3}\right)\xi^{-\frac{2}{3}}e^{\xi}d\xi+O\left(\frac{P}{R^2}\right)$$

$$=O\left(\frac{P}{R^{5/3}}\right),\qquad R\gg 1. \tag{6.57}$$

6.2.3 Asymptotics of the second and third-order solutions

We observe that the scaling of the n^{th} order solution with the flow parameter R is dependent upon integrals of the recurrence relation, in (6.51). Considering the second-order equation

$$h_2' + Rk^2 h_2 = \frac{P}{R} h_1 + \frac{2P}{R} \int_{\infty}^{k} h_1 d\xi - \frac{1}{R} \int_{\infty}^{k'\infty} \int_{k} \{ \frac{G}{(F')^2} - P^2 k^2 \} h_1 dk dk' \quad (6.58)$$

when $k>0$, we have

$$h_2'(0+) = \frac{2P}{R} \int_{\infty}^{0} h_1 d\xi - \frac{1}{R} \int_{\infty}^{0} \int_{k}^{\infty} \{ \frac{G}{(F')^2} - P^2 k^2 \} h_1 dk dk'$$

$$\sim -\frac{2P^2}{R} \int_{\infty}^{0} k e^{-\xi} d\xi + \frac{G}{(F')^2 R} \int_{\infty}^{0} \int_{k}^{\infty} \frac{P}{R} k e^{-\xi} dk dk' - \frac{P^3}{R^2} \int_{\infty}^{0} \int_{k}^{\infty} k^3 e^{-\xi} dk dk'$$

$$= \frac{2P^2}{R^2} \int_{0}^{\infty} (\frac{3}{R})^{1/3} \xi^{1/3} e^{-\xi} d\xi + \frac{GP}{(F')^2 R^2} \int_{\infty}^{0} \frac{\xi^{-2/3}}{R^{1/3} 3^{2/3}} \int_{k}^{\infty} \frac{\xi^{-2/3}}{R^{2/3} 3^{1/3}} e^{-\xi} d\xi d\xi'$$

$$- \frac{P^3}{R^{11/3}} \int_{\infty}^{0} \xi^{-2/3} \int_{k}^{\infty} \xi^{-2} e^{-\xi} d\xi d\xi'$$

$$= \frac{2P^2}{R^{7/3} 3^{2/3}} \Gamma(\frac{1}{3}) + O(\frac{GP}{(F')^2 R^3}, \frac{P^3}{R^{11/3}}), \qquad R \gg 1. \quad (6.59)$$

Inserting $h_1'(0+)$ into (6.43) when $n=2$ at $k=0+$, then yields

$$h_2''(0+) = \frac{P}{R} h_1'(0+) - \frac{1}{R} \int_{0}^{\infty} \{ \frac{G}{(F')^2} - P^2 k^2 \} h_1 dk$$

$$= \frac{P}{R} \{ -\frac{P}{R} + \frac{G}{(F')^2 R^{5/3} 3^{4/3}} \int_{0}^{\infty} \xi^{-\frac{2}{3}} \Gamma(\xi, \frac{1}{3}) d\xi - \frac{P^2}{R^{7/3} 3^{2/3}} \Gamma(\frac{1}{3}) \}$$

$$+ \frac{P}{R^2} \int_{0}^{\infty} (\frac{G}{(F')^2} - P^2 k^2) k e^{-\xi} dk$$

$$= -\frac{P^2}{R^2} - \frac{2P^3}{R^{10/3} 3^{2/3}} \Gamma(\frac{1}{3}) + O(\frac{G}{(F')^2 R^{13/6}}), \qquad R \gg 1. \quad (6.60)$$

Again the calculation in obtaining the asymptotic form is much simplified for large flow approximation, as the higher order terms are negligible when R becomes large.

From the result of (6.55) we may derive the second-order solution by multiplying (6.58)

by the integrating factor e^{ξ} to find

$$(h_2 e^{\xi})' = \frac{P}{R} h_1 e^{\xi} + \frac{2P}{R} e^{\xi} \int_{\infty}^{k} h_1 d\xi - \frac{e^{\xi}}{R} \int_{\infty}^{k'\infty} \int (\frac{G}{(F')^2} - P^2 k^2) h_1 dk dk' .$$

Then

$$h_2 e^{\xi} \sim -\frac{P^2}{R^2} \int_0^k k dk - \frac{2P^2}{R^2} \int_0^k e^{\xi} \int_{\infty}^{k} k e^{-\xi} d\xi dk$$

$$+ \int_0^k \frac{e^{\xi}}{R} \int_{\infty}^{k'\infty} \int (\frac{G}{(F')^2} - P^2 k^2) \frac{P}{R} k e^{-\xi} dk dk' dk$$

$$= -\frac{P^2}{2R^{8/3} 3^{-2/3}} \xi^{\frac{2}{3}} - O(\frac{1}{R^{5/3}}) , \qquad R \gg 1$$

so that

$$h_2 \sim -\frac{P^2 3^{2/3}}{2R^{8/3}} \xi^{\frac{2}{3}} e^{-\xi} , \qquad R \gg 1 . \tag{6.61}$$

Similarly, the third-order solution at $k=0+$ in (6.43) is given by

$$h_3''(0+) = \frac{P}{R} h_2'(0+) - \frac{1}{R} \int_0^{\infty} (\frac{G}{(F')^2} - P^2 k^2) h_2 dk . \tag{6.62}$$

Substituting (6.59) and (6.61) into (6.62), we then finally have

$$h_3''(0+) = \frac{2P^3}{R^{10/3} 3^{2/3}} \Gamma(\frac{1}{3}) + \frac{G}{2(F')^2 R^3}$$

$$- \frac{1}{R^{8/3} 3^{1/3}} \Gamma(\frac{2}{3}) + O(\frac{1}{R^{8/3}}) . \tag{6.63}$$

6.2.4 Determination of the eigenvalue and concluding remarks

Collecting together the results for $h(0+)$, $h(0-)$, $h'(0+)$, $h'(0-)$

and $h''(0+)$, $h''(0-)$, in (6.49), (6.50), (6.52), (6.53), (6.56), (6.59), (6.60) and (6.63) we finally obtain the expansion of h and its derivatives at $k=0\pm$ for $R\gg1$ in the form

$$h(0+) = 1,$$

$$h(0-) = c_0\frac{\Gamma(\frac{1}{3})}{R^{1/3}3^{2/3}} - c_1\frac{\Gamma(\frac{2}{3})}{R^{2/3}3^{1/3}} + O(\frac{P}{R^{5/3}});$$

$$h'(0+) = -\frac{P}{R} + \frac{P^2\Gamma(\frac{1}{3})}{R^{7/3}3^{2/3}} + \frac{2P}{R^{8/3}3^{1/3}}\Gamma(\frac{2}{3}) + O(\frac{G}{R^{5/3}}),$$

$$h'(0-) = c_0 + c_0\frac{P\Gamma(\frac{1}{3})}{R^{4/3}3^{2/3}} + O(\frac{P}{R^{5/3}}); \qquad (6.64)$$

and

$$h''(0+) = \frac{G}{(F')^2R^{4/3}3^{2/3}}\Gamma(\frac{1}{3}) - \frac{P^2}{R^{8/3}3^{1/3}}\Gamma(\frac{2}{3}) + O(\frac{G}{R^3}),$$

$$h''(0-) = c_1.$$

The growth rate P may now be estimated by balancing the leading order terms in (6.64), followed by substitution into the eigenvalue relation

$$2\pi P = \frac{h(0-)}{h'(0-)}e^{-i\chi} - \frac{h(0+)}{h'(0+)}e^{i\chi}, \quad -\pi<\chi\leq\pi.$$

The ratios $h(0-)/h'(0-)$ and $h(0+)/h'(0+)$ are obtained as

$$\frac{h(0-)}{h'(0-)} = \{\frac{c_0\Gamma(\frac{1}{3})}{R^{1/3}3^{2/3}} - \frac{c_1\Gamma(\frac{2}{3})}{R^{2/3}3^{1/3}}\}/\{c_0 + c_0\frac{P\Gamma(\frac{1}{3})}{R^{4/3}3^{2/3}}\}$$

$$\sim \{\frac{\Gamma(\frac{1}{3})}{R^{1/3}3^{2/3}} - \frac{c_1\Gamma(\frac{2}{3})}{c_0R^{2/3}3^{1/3}}\}\cdot\{1-\frac{P\Gamma(\frac{1}{3})}{R^{4/3}3^{2/3}}\}, \qquad (6.65)$$

and

$$\frac{h(0+)}{h'(0+)} = -\frac{R}{P\{1-\frac{P}{R^{4/3}3^{2/3}}\Gamma(\frac{1}{3}) - \frac{2}{R^{5/3}3^{1/3}}\Gamma(\frac{2}{3})\}}, \qquad (6.66)$$

where the higher order terms in the binomial expansion are negligible when R is sufficiently large, and therefore have been neglected. Substituting (6.65) and (6.66) into the eigenvalue relation yields

$$2\pi P \sim \frac{R}{P}e^{i\chi} + \frac{2\Gamma(\frac{1}{3})}{R^{1/3}3^{2/3}}\cos\chi$$

$$+\{\frac{2\Gamma(\frac{2}{3})}{PR^{2/3}3^{1/3}} - \frac{P\Gamma^2(\frac{1}{3})}{R^{5/3}3^{4/3}}\}e^{i\chi} - \frac{c_1\Gamma(\frac{2}{3})}{c_0R^{2/3}3^{1/3}}e^{-i\chi}. \qquad (6.67)$$

To eliminate $c_1e^{-i\chi}/c_0$ in (6.67), the second-order jump condition in (6.57) needs to be employed to obtain the approximation

$$2\pi\frac{G}{(F')^2} = \frac{h''(0+)}{h'(0+)}e^{i\chi} - \frac{h''(0-)}{h'(0-)}e^{-i\chi}, \qquad (6.68)$$

where, from (6.64)

$$\frac{h''(0+)}{h'(0+)} = -\frac{R}{P}\{\frac{G}{(F')^2R^{4/3}3^{2/3}}\Gamma(\frac{1}{3}) - \frac{P^2}{R^{8/3}3^{1/3}}\Gamma(\frac{2}{3})\}$$

$$\cdot\{1+\frac{P}{R^{4/3}3^{2/3}}\Gamma(\frac{1}{3}) + \frac{2}{R^{5/3}3^{1/3}}\Gamma(\frac{2}{3}) + O(\frac{P^2}{R^{8/3}})\}$$

$$\sim -\frac{G\Gamma(\frac{1}{3})}{(F')^2PR^{1/3}3^{2/3}}\{1-\frac{3^{1/3}P^2\Gamma(\frac{2}{3})(F')^2}{GR^{4/3}\Gamma(\frac{1}{3})}\}, \qquad (6.69)$$

and

$$\frac{h''(0-)}{h'(0-)} = \frac{c_1}{c_0}\{1-\frac{P\Gamma(\frac{1}{3})}{R^{4/3}3^{2/3}}+O(\frac{P^2}{R^{8/3}})\}$$

$$\sim \frac{c_1}{c_0}\{1-\frac{P\Gamma(\frac{1}{3})}{R^{4/3}3^{2/3}}\}. \qquad (6.70)$$

Thus, from (6.68), (6.69) and (6.70), we have

$$-\frac{c_1}{c_0}e^{-i\chi} \sim \{2\pi\frac{G}{(F')^2}+\frac{G\Gamma(\frac{1}{3})}{(F')^2PR^{1/3}3^{2/3}}[1-\frac{3^{1/3}P^2\Gamma(\frac{2}{3})}{G(F')^2R^{4/3}\Gamma(\frac{1}{3})}]e^{i\chi}\}$$

$$\cdot\{1+\frac{P\Gamma(\frac{1}{3})}{R^{4/3}3^{2/3}}\}. \qquad (6.71)$$

Combining (6.67) and (6.71), then yields

$$2\pi P \sim \frac{R}{P}e^{i\chi}+\frac{2\Gamma(\frac{1}{3})}{R^{1/3}3^{2/3}}\cos\chi+\{\frac{2\Gamma(\frac{2}{3})}{PR^{2/3}3^{1/3}}-\frac{P\Gamma^2(\frac{1}{3})}{R^{5/3}3^{4/5}}\}e^{i\chi}$$

$$+\frac{\Gamma(\frac{2}{3})}{R^{2/3}3^{1/3}}\{2\pi\frac{G}{(F')^2}+2\pi\frac{GP\Gamma(\frac{1}{3})}{(F')^2R^{4/3}3^{2/3}}+\frac{G\Gamma(\frac{1}{3})}{(F')^2PR^{1/3}3^{2/3}}e^{i\chi}-\frac{P\Gamma(\frac{2}{3})}{R^{5/3}3^{1/3}}e^{i\chi}\}$$

$$=\frac{R}{P}e^{i\chi}+2\frac{\Gamma(\frac{1}{3})}{R^{1/3}3^{2/3}}\cos\chi+2\pi\frac{G\Gamma(\frac{2}{3})}{(F')^2R^{2/3}3^{1/3}}$$

$$+2\pi\frac{GP\Gamma(\frac{1}{3})\Gamma(\frac{2}{3})}{3(F')^2R^2}+O(\frac{1}{R^{7/6}}). \qquad (6.72)$$

Neglecting high order R terms in (6.72), we conclude that

$$2\pi P^2 \sim Re^{i\chi} + 2\frac{P\Gamma(\frac{1}{3})}{R^{1/3}3^{2/3}}\cos\chi + 2\pi\frac{GP\Gamma(\frac{2}{3})}{(F')^2R^{2/3}3^{1/3}}$$

$$= Re^{i\chi}\{1 + 2\frac{P\Gamma(\frac{1}{3})}{R^{1/3}3^{2/3}}\cos\chi\,(Re^{i\chi})^{-1} + 2\pi\frac{GP\Gamma(\frac{2}{3})}{(F')^2R^{2/3}3^{1/3}}(Re^{i\chi})^{-1}\}, \tag{6.73}$$

so that

$$P \sim (\frac{R}{2\pi}e^{i\chi})^{\frac{1}{2}}\{1 + \frac{P\Gamma(\frac{1}{3})}{R^{1/3}3^{2/3}}\cos\chi\,(Re^{i\chi})^{-1} + \frac{\pi GP\Gamma(\frac{2}{3})}{(F')^2R^{2/3}3^{1/3}}(Re^{i\chi})^{-1}\}$$

$$= (\frac{R}{2\pi}e^{i\chi})^{\frac{1}{2}} + (\frac{R}{2\pi}e^{i\chi})(Re^{i\chi})^{-1}\frac{\Gamma(\frac{1}{3})\cos\chi}{R^{1/3}3^{2/3}}$$

$$+ (\frac{R}{2\pi}e^{i\chi})(Re^{i\chi})^{-1}\frac{\pi G\Gamma(\frac{2}{3})}{(F')^2R^{2/3}3^{1/3}}.$$

Thus, the final form of the asymptotic estimate for the G-mode growth rate for large flow is given by

$$P \approx (\frac{R}{2\pi}e^{i\chi})^{\frac{1}{2}} + \frac{\Gamma(\frac{1}{3})\cos\chi}{2\pi R^{1/3}3^{2/3}} + \frac{G\Gamma(\frac{2}{3})}{2(F')^2R^{2/3}3^{1/3}}, \quad R\gg 1. \tag{6.74}$$

This shows that the leading order effect of the gravitational term is either destabilizing (when $G>0$) or stabilizing (when $G<0$). The validity of the approximation (6.74) can be tested from the numerical results by comparing the G-term contribution to (6.74), namely

$$\frac{G\Gamma(\frac{2}{3})}{2(F')^2R^{2/3}3^{1/3}} \tag{6.75}$$

with the numerical value of the quantity G_r defined by

$$G_r =: Re(P) - \{ (\frac{R}{2\pi})^{\frac{1}{2}} \cos\frac{\chi}{2} + \frac{\Gamma(\frac{1}{3})\cos\chi}{2\pi R^{1/3} 3^{2/3}} \}, \qquad (6.76)$$

where $Re(P)$ is the numerically obtained value of the eigenvalue P in (6.5). The results for two different values of R over the range $0 \le \chi \le \pi$ are given in Table 6.2 and shown in Figure 6.2. It is seen that a good agreement has been obtained for $0 \le \chi \le \pi$.

The growth rate $P = P(R, \chi, G)$ grows algebraically like $R^{1/2}$ for large R (which corresponds to the tearing mode branch) but possesses a destabilizing modification (when $G > 0$) scaling like $R^{-2/3}$ from the G-mode branch. Consequently, in contrast to the tearing mode where increasing flow results in an increased growth rate, the gravitational contribution to P is seen to *decrease* as R increases. This can be made more apparent when we consider the case $\chi = \pi$, which effectively eliminates the tearing mode. In this case, we find from (6.74)

$$P \approx i(\frac{R}{2\pi})^{\frac{1}{2}} - \frac{\Gamma(\frac{1}{3})}{2\pi R^{1/3} 3^{2/3}} + \frac{G\Gamma(\frac{2}{3})}{2(F')^2 R^{2/3} 3^{1/3}},$$

so that, as R increases, the tearing mode stabilising term of $O(R^{-1/3})$ eventually dominates the gravitational term of $O(R^{-2/3})$. This behaviour is confirmed by the numerical results; see Figure 4.10, where the locus of $\chi = \pi$ approaches the imaginary axis when R increases no matter weather G small or large. In conclusion, we confirm that when the flow R becomes large the tearing mode eventually dominates the resistive MHD instability of the plane plasma slab.

TABLE 6.2 A comparison between the numerical quantity G_r defined in (6.76) and the G-term contribution in the asymptotic form (6.74)

	$R=6,\ G'=0.1$			$R=7,\ G'=0.1$	
$\frac{\chi}{\pi}$	G_r	$\frac{G'\Gamma(\frac{2}{3})}{2R^{2/3}3^{1/3}}$	$\frac{\chi}{\pi}$	G_r	$\frac{G'\Gamma(\frac{2}{3})}{2R^{2/3}3^{1/3}}$
0.0	0.0306	0.0284	0.0	0.0277	0.0256
0.1	0.0302		0.1	0.0271	
0.2	0.0289		0.2	0.0260	
0.3	0.0274		0.3	0.0250	
0.4	0.0267		0.4	0.0240	
0.5	0.0269		0.5	0.0240	
0.6	0.0278		0.6	0.0250	
0.7	0.0288		0.7	0.0262	
0.8	0.0293		0.8	0.0265	
0.9	0.0290		0.9	0.0262	
1.0	0.0281		1.0	0.0256	

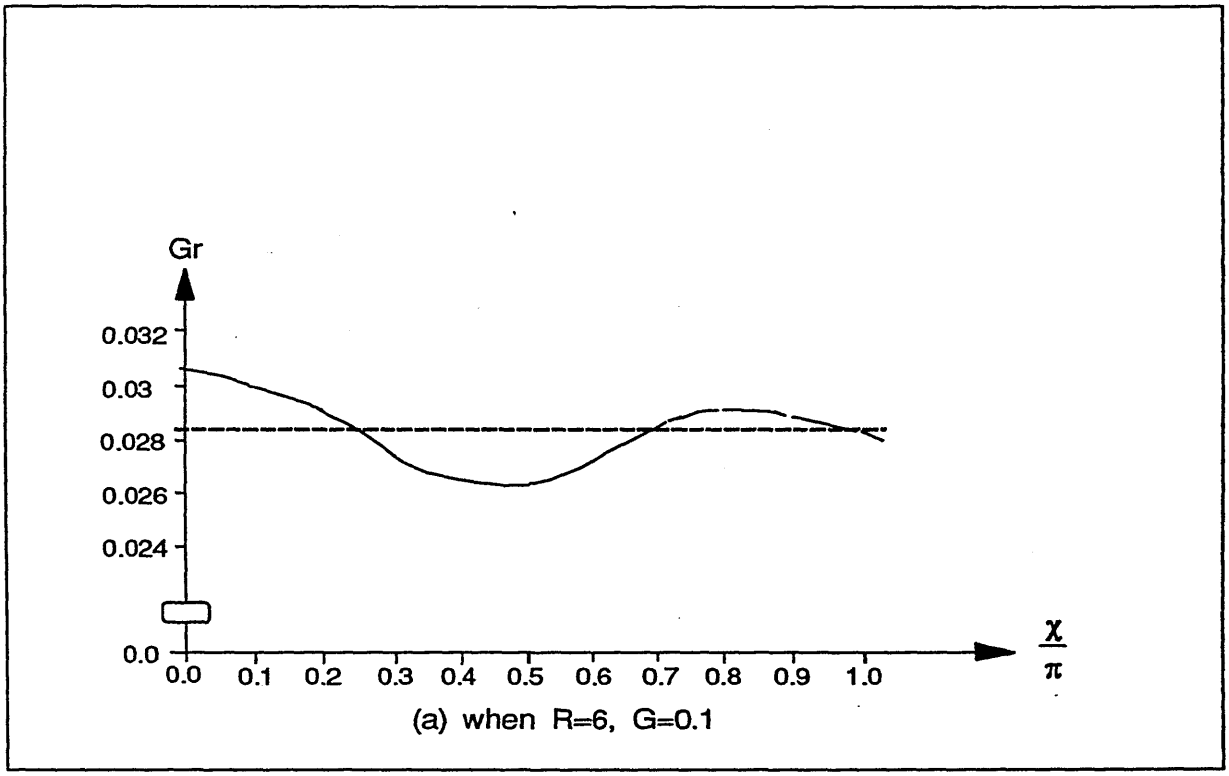

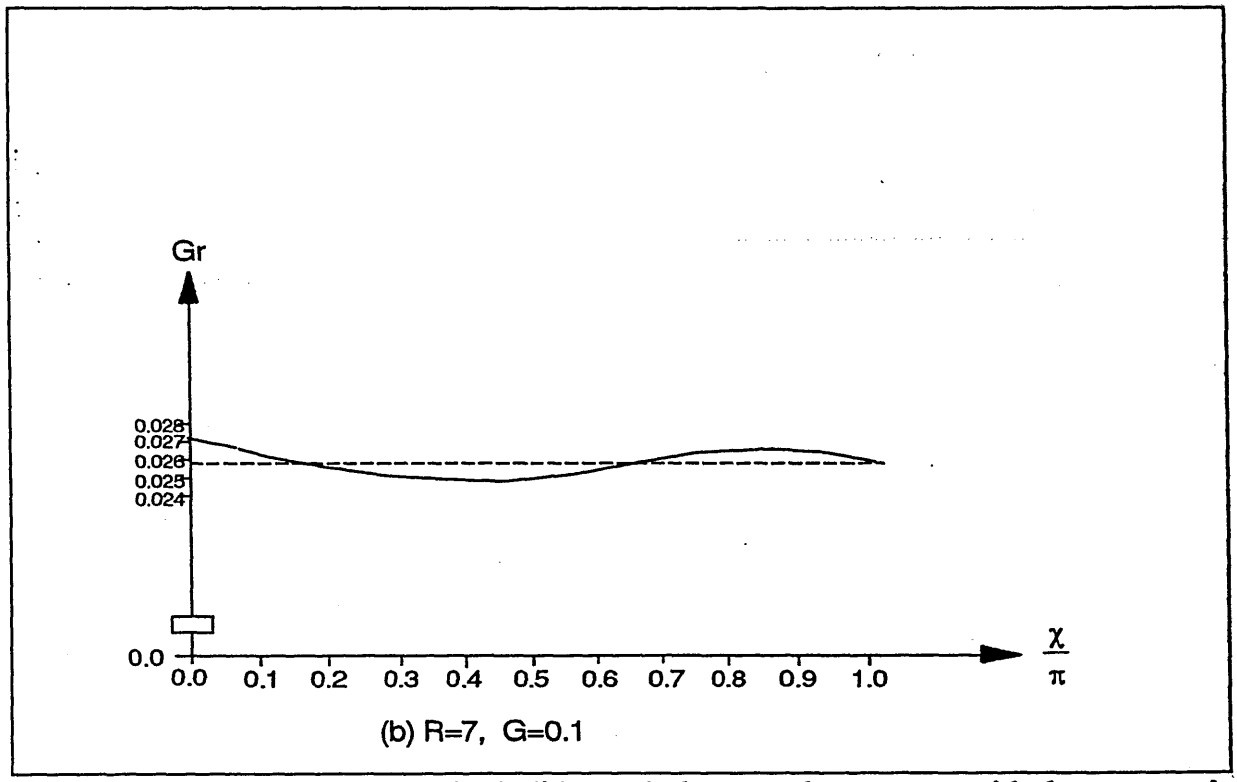

FIGURE 6.2 The numerical results (solid curve) show good agreement with the asymptotic value (dashed line) of the quantity G_r defined in (6.76) as a function of χ / π when (a)R=6,G'=0.1 and (b)R=7,G'=0.1.

CHAPTER VII
CONCLUSIONS

Introduction

In the previous chapters a combination of analytic-numerical investigations on the effects of flow along the confining equilibrium sheared magnetic field has been described in the linear regime. The instabilities studied are the resistive tearing and gravitational interchange modes when the equilibrium flow is chosen to scale like $\eta^{1/5}$ (see §2.2). This ordering excludes the Kelvin-Helmholtz instability which is important in the Alfvénic regime. In the limit of high magnetic Lundquist number, the method adopted is the standard division of the current layer into a narrow boundary layer centred about the resonant surface and an outer infinite conductivity region. The external solution, in the constant- Ψ approximation, is not affected by the flow in the present ordering. The external matching quantity is thereby taken to be the parameter χ, which is independent of R and is decided by the global equilibrium field structure. The effects of a sheared equilibrium flow on the visco-resistive tearing mode and G-mode have been studied numerically by calculating the eigenvalue of the boundary-layer equation and asymptotically for large flow perturbation. Both stabilizing and destabilizing effects are found.

7.1 The Stabilizing and Destabilizing Effects of Flow

In the absence of a gravitational term, it has been found that the introduction of a plasma shear flow along the magnetic field destabilizes the tearing mode. Modes which are predicted to be stable in the usual no flow case, corresponding to $\Delta'<0$ (or $|\chi|>\pi/2$), can be driven unstable by sufficiently large flow in the sub-Alfvénic regime. We have investigated in some detail the dependence of this destabilisation on the parameters which describe the flow and viscosity.

The inclusion of the effects of a gravitational term is complicated by the fact that it is not

possible to completely separate the resistive G-mode from the tearing mode, so that a certain amount of mode mixing is unavoidable. The variation of the instability growth rate in the presence of an unfavourable gravitational term, $G>0$, has been determined as a function of the other parameters of the boundary-layer equation. The principal conclusion is that, while an equilibrium shear flow has a destabilizing effect on the tearing mode, the effect of the flow on the G-mode is, surprisingly, a stabilizing one. In particular, we have determined qualitatively the marginal stability condition which corresponds to the value of the parameters (R, G, χ) for which the eigenvalue locus of the growth rate P crosses over from the region $Re(P)<0$ to $Re(P)>0$ in the complex P-plane.

The computational procedure for the tearing-G mode problem with flow consists of increasing the flow parameter R from zero in small increments. It was therefore necessary to first consider the flowless case $(R=0)$ before dealing with the case with flow $(R\neq 0)$. The results for the two cases are summarised as follows:

(i) When $R=0$. We need to understand the dependence of the eigenvalue P on G and χ in the flowless case. The classical instability condition for the tearing mode is $\Delta'>0$, which is $|\chi|<\pi/2$. Otherwise, if $|\chi|\geq\pi/2$, the mode is stable with P situated on the ray $arg(P)=4\pi/5$.

If $|\chi|<\pi/2$ and $G>0$, the growth rate P increases with G so that the mode becomes more unstable; when $G<0$, P increases from negative values approaching zero with increasing $|G|$, and $|G|\neq 0$, there is another branch of P. A real-root branch increases positively with increasing $G>0$, and a stable complex-root branch situated in the negative half P-plane with $Re(P)<0$ approaches the origin as $G\to\infty$. When G is decreased negatively, we cannot find a real-root branch, but the complex-root branch approaches the rays $arg(P)=\pm 2\pi/3$, as $G\to-\infty$.

(ii) When $R\neq 0$. We obtained the eigenvalue pattern with the effects of flow for both the inviscid and viscid cases.

In the inviscid case, the stable tearing mode (i.e. $\chi>\pi/2$) can be driven unstable if the flow R is sufficiently large; while the unstable tearing mode (i.e. $|\chi|<\pi/2$) becomes more unstable under the influence of flow. The unstable G-mode can become stable when we consider the effects of flow for a certain degree of tearing stability (i.e. certain values of $|\chi|>\pi/2$). However, it is found that the stabilizing effect of flow on the unstable G-

mode only effectively exist before the flow R exceeds the marginal stable value R_m (see §4.2.3), thereby shows only a short range in the stable region. A full degree of stabilizing effect of flow on the mixed tearing-G-mode has been found; nevertheless, the dominant behaviour of the destabilizing effects of flow on the tearing mode remain unchanged.

To support our numerical analysis, we also carried out an asymptotic calculation to determine the growth rate dependence for large values of the flow parameter R but still within the ordering given in §2.2. Our results indicate that in the inviscid case the estimate for the tearing-G mode is

$$P \sim \left(\frac{R}{2\pi} e^{i\chi}\right)^{\frac{1}{2}} + \frac{\cos\chi\,\Gamma(\frac{1}{3})}{2\pi R^{1/3} 3^{2/3}} + \frac{G\Gamma(\frac{2}{3})}{(F')^2 R^{2/3} 3^{1/3}} . \qquad (7.1)$$

This analysis confirms the numerical results in Chapter 4, namely that the contribution to the growth rate P arising from the gravitational term is a decreasing function of R and that, when $|\chi| < \pi$, the tearing mode eventually dominates. This behaviour physically may be explained by the fact that small flow slows down the perpendicular interchange but speeds up the field line reconnection when the flow becomes large in the sub-Alfvénic regime.

The study on the effects of viscous flow explores some new results of instability exchange between the stable branch and the unstable branch. The stable or unstable branches are identified by whether the eventual position of the loci for fixed χ are in the stable region $(Re(P) < 0)$ or otherwise when R becomes large. The level crossing in the loci pattern has been analysed to illustrate the discontinuous instability loci growing behaviour. For certain values of viscosity N, the flow R can drive the unstable branch into the stable region thereby showing a stabilizing effect, while showing a destabilizing effect by driving the stable branch into the unstable region. Increasing viscosity N, we found that there are switches between the stable branch and unstable branch through the bifurcation points. Therefore the stable branch can be changed to become unstable by exchanging with the unstable branch, and vice versa. The loci discontinuity may be smoothed out by further increasing the viscosity N and the pattern shows lower $Re(P)$ and $Im(P)$; compare the inviscid case. Both the asymptotic and numerically estimated growth rates for the viscous tearing mode agree with that obtained by Paris and Sy (1983) for the leading term and Bondeson and Persson (1986) for the first two terms as

$$P \sim \left(\frac{R}{2\pi} e^{i\chi}\right)^{\frac{1}{2}} + \frac{\cos\chi\,\Gamma\left(\frac{1}{3}\right)}{2\pi R^{1/3} 3^{2/3}} - \frac{N\Gamma\left(\frac{2}{3}\right)}{R^{2/3} 3^{1/3}}, \qquad (7.2)$$

where the third-term is the asymptotic form of the viscous contribution obtained in §6.1.

7.2 Discussion on Further Studies

It is impossible to indicate, or with the best of ability, to solve all of the problems arising in resistive instability theory. We therefore discuss some possible directions for future studies.

The magnetohydrodynamic model is found to be a good approximation for many plasma physics problems. For example, the Rayleigh-Taylor instability in inertial confinement; the sawtooth oscillation instability in Tokamaks; the Kelvin-Helmholtz instability and the effects of nonlinear flow and a more realistic plasma viscosity on the visco-resistive modes. The straightforward consequences resulting from the recent G-mode may be:

(i) the effects of Alfvénic flows on the tearing-G mode;

(ii) the modification of the external solution to the matching condition Δ' for Alfvénic flows and the use of a nonconstant- Ψ solution to the boundary-layer equations.

Both the "constant- Ψ " tearing mode, which has a growth rate that scales as $S^{-3/5}$, and the "nonconstant- Ψ " tearing mode $[\Delta' > (\alpha S)^{1/3}]$, which has a growth rate that scales as $S^{-1/3}$, have been found in the flowless case. Chen and Morrison found that the shear flow has a significant influence on both the internal resistive boundary layer and the external ideal region in the Alfvénic regime, in which the matching quantity Δ' is dependent of the shear flow. Therefore it is necessary to further investigate the viscous G-mode when we consider the lower-order terms [i.e. $R^{*\prime\prime} W \sim \rho W'' \sim (\rho R^*)' W \sim \delta^{-4}$] in the normalization of the boundary-layer equations (2.32) and (2.33). Also, the nonconstant- Ψ for the external solution should be considered. The relative boundary-layer equations in the Alfvénic regime then become

$$\frac{1}{\alpha^2 S^2}\left[(P+iR^*)W'' - i\rho R^{*\prime\prime} W - N^* W^{(4)}\right] - F^2 W + \frac{GW}{P+iR^*}$$

$$= (P+iR^*)F\Psi - F''\Psi,$$

$$\Psi'' = (p+iR^*)\Psi + FW. \qquad (7.3)$$

It was found by Einaudi and Rubini (1986, 1989) and Chen and Morrison (1990 a,b) that large flow stabilises the tearing mode. This has not been studied in the viscous G-mode so that more detailed investigation is necessary for shear Alfvénic flows. The remaining questions are: (i) Does the shear flow in the Alfvénic regime stabilize the tearing-G modes, as was predicted for the tearing mode? (ii) How does the Kelvin-Helmholtz instability behave in considering the gravitational interchange? (iii) Does the viscosity enhance instability (Einaudi and Rubini, 1989; and Chen and Morrison, 1990b) for the Alfvénic G-mode?

Finally, the nonlinear effects of flow may be considered for the visco-G mode as follows:

$$\left(\frac{\partial}{\partial t} + \underline{V}\cdot\nabla_\perp\right)\omega = \underline{B}\cdot\nabla j + \mu\nabla_\perp^2\omega + \rho g,$$

$$\frac{\partial\Psi}{\partial t} = \underline{B}\cdot\nabla\phi - \eta j + E_z(t), \qquad (7.4)$$

where Ψ is the flux function, $\underline{B}=\nabla\Psi\times\underline{z}+B_z\underline{z}$ is the magnetic field and $\underline{V}=\nabla\phi\times\underline{z}$ is the velocity, ϕ is the stream function, $\omega=-\nabla_\perp^2\phi$ and $j=-\nabla_\perp^2\Psi$ are the toroidal vorticity and the plasma current, respectively, E_z is the transformer toroidal electric field, $\nabla_\perp=\nabla-\underline{z}\frac{\partial}{\partial z}$, and g is the centrifugal (or gravitational) force.

This equation when $g=0$ has been investigated by Persson and Bondeson (1990), Persson (1991) and Wessen and Persson (1991) for the tearing-mode stability in a cylindrical plasma with equilibrium flows.

REFERENCES

1. Furth, H.P., Killeen, J. and Rosenbluth, M.N. Finite-resistive instabilities of a sheet pinch. Physics of Fluids 6, 459 (1963).

2. Paris, R.B. and Sy, W.N-C. Influence of equilibrium shear flow along the magnetic field on the resistive tearing instability. Physics of Fluids 26, 2966 (1983).

3. Bondeson, A. and Persson, M. Resistive tearing modes in the presence of equilibrium flows. Physics of Fluids 29, 2997 (1986).

4. Chen, F. Introduction to Plasma Physics, Plenum Press (1974).

5. Bateman, G. MHD Instabilities, MIT Press, Cambridge, Massachusetts (1978).

6. Jeffrey, A. Magnetohydrodynamics, Oliver and Boyd (1966).

7. Paris, R.B. Lecture Notes on Resistive Instabilities in MHD, Ann Phys. Fr. 9, 347 (1984).

8. Einaudi, G. and Rubini, F. Resistive instabilities in a flowing plasma: I. Inviscid case. Physics of Fluids 29, 2563 (1986).

9. Einaudi, G. and Rubini, F. Resistive instabilities in a flowing plasma: II. Effects of viscosity. Physics of Fluids B1, 2224 (1989).

10. Chen, X.L. and Morrison, P.J. Resistive tearing instability with equilibrium shear flow. Physics of Fluids B2, 495 (1990).

11. Chen, X.L. and Morrison, P.J. The effect of viscosity on the resistive tearing mode with the presence of shear flow. Physics of Fluids B2, 2575 (1990).

12. Bender, C.M. and Orszag, S.A. Advanced Mathematical Methods for Scientists and Engineers. McGraw-Hill (1978).

13. Whittaker, E.T. and Watson, G.N. Modern Analysis, Cambridge University Press (1965).

14. Drazin, P.G. and Reid, W.H. Hydrodynamic Stability, Cambridge University Press (1981).

15. Chandrasekhar, S. Hydrodynamic and Hydromagnetic Stability. Oxford University Press (1961).

16. Lin, C.C. The Theory of Hydrodynamic Stability. Cambridge University Press (1967).

17. Persson, M. and Bondeson, A. Oscillating magnetic islands in a rotating plasma. Physics of Fluids, B2, 2315 (1990).

18. Persson, M. Suppression of magnetic islands by plasma rotation. Nuclear Fusion 31, 382 (1991).

19. Paris, R.B., Wood, A.D. and Stewart, S. The effects of equilibrium flow on the resistive tearing mode. Physics of Fluids B2, (1993).

20. Paris, R.B. and Wood, A.D. The exponentially-improved asymptotics for the gamma function. J. Comp. Appl. Math. 41, 135-143, (1992).

21. Wessen, K.P. and Persson, M. Tearing mode stability in a cylindrical plasma with equilibrium flows. Plasma Physics, 45, 267 (1991).

22. Erdélyi, A. (Ed.) Table of Integral Transforms, 1, 118, (1953).

23. Berry, M.V. Uniform asymptotic smoothing of Stokes' discontinuities. Proc. Roy. Soc. London Ser. A 422, 7-21, (1989).

24. Rayleigh, Lord. Investigation of the character of the equilibrium of an incompressible heavy fluid of variable density. Proc. London Math. Soc. 14, 170-7, (1883b).

25. Rayleigh, Lord. On the question of the stability of the flow of fluids. Phil. Mag.(5) 34, 59-70 (1892a).

26. Lin, C.C. On the stability of two-dimensional parallel flows. Quart. Appl. Math. 3, 117-42, 218-34 and 277-301 (1945).

27. Kármán, T. von. Some aspects of the turbulence problem. Proceedings 4th International Congress on Applied Mechanics, Cambridge, England, 54-91 (1934).

28. Hofmann, I. Resistive tearing modes in a sheet pinch with shear flow. Plasma physics, 17, 143-157 (1975).

29. Dobrott, D., Prager, S.C. and Taylor, J.B. Influence of equilibrium flows on the tearing modes. Physics of Fluids, 20, 1850, (1977).

30. Dobrowolny, M. and Paravano, A. Nuovo Cimento 49, 137, (1979).

LIST OF SYMBOLS

η	resistivity
$\underline{j}$	current density
ρ	density of plasma
$\underline{E}$	electrical field
$\underline{B}$	magnetic field
T_e	electron temperature
K	Boltzmann's constant
$\underline{V}$	velocity of plasma flow
m_i	ion mass
m_e	electron mass
n_i	ion number
n_e	electron number
$\underline{V_i}$	ion velocity
$\underline{V_e}$	electron velocity
e	electric charge
g	gravitational acceleration
$\overline{p}$	pressure
c	speed of light
ν	kinematic viscocity
$\underline{W}$	vorticity
a	dimension
τ_R	resistive diffusion time scale
τ_H	hydromagnetic time scale
V_A	hydromagnetic wave speed
τ_g	gravitational interchange time scale
S	Lundquist (magnetic Reynolds) number
S_R	Reynolds number
L	characteristic length

$\underline{k}$	wave number
$\underline{B_0}$	unperturbed field
$\underline{V_0}$	unperturbed velocity
$\mu_\perp$	perpendicular coefficient of viscocity
ρ	perturbed density $= \rho_1 / \langle \rho \rangle$
$\underline{B_1}$	perturbed field
$\underline{V_1}$	perturbed velocity
ω	growth rate
F	magnetic shear $= (\underline{k} \cdot \underline{B_0}) / kB$
Ψ	dimensionless field $= B_{y1}/B$
W	dimensionless velocity $= -ik\tau_R V_{y1}$
α	dimensionless wave number $= ka$
G	dimensionless gravitational term $= -g\rho_0' \tau_H^2 / \rho_0$
N	dimensionless viscous term $= 4\pi\mu_\perp / \eta$
$V_\perp$	perpendicular diffusion flow
δ	boundary layer thickness
Ψ_1	perturbed field component $= B_{y1}/B$
p	dimensionless growth rate $= \omega\tau_R$
Δ'	jump condition at the origin
Δ'_{ext}	external jump condition
Δ'_{int}	internal jump condition
H	complex function $= W + iR^{*\prime}/F'$
P	normalized growth rate
R^*	normalized shear flow $= \tau_R (\underline{k} \cdot \underline{V_0})$
R	rescaled shear flow gradient $= R^{*\prime} \Delta^{-3/5} (\alpha S F')^{-4/5}$,
Δ	rescaling quantity
χ	instability degree of tearing mode $\Delta e^{i\chi} = \Delta' - i\pi F''/F'$
θ	variable in normalized differential equation
$h(k)$	Fourier transform of $H(\theta)$
$\delta(k)$	Dirac delta function
$U(k)$	unit step function

$\langle\rho\rangle$	the characteristic scaling of ρ
B	the characteristic scaling of $\underline{B}$
P^*	the conjugate of P
Λ	eigenvalue in the flowless eigenvalue relation (3.12)
Λ_0	lowest eigenvalue of Λ
G'	rescaled G-term $=G/(F')^2$
$S(\theta)$	Stokes multiplier
R_0	destabilizing turning point of R
R_m	marginal value of R
NF	eigenvalue loci in the no flow case
AP	eigenvalue loci emanating from the accumulating point
BW	Butterfly Wing shape pattern
V_r	numerical value of viscous contribution to P
G_r	numerical value of G-term contribution to P

APPENDIX

In the following appendix we list two programs of the G-mode with and without flow which are written in FORTRAN-77:

(i) **A fourth-order system.** The program for calculating of visco-G mode when $R=0$;

(ii) **MHD.** The program for calculating of visco-G mode when $R\neq 0$.

```
      A 4-th Order System (with t/m) to compute Vis-G mode (when R=0)
      implicit complex(z)
      implicit real(x,y)
      parameter (bl=5060,npoint=501)
      real*4 r,pr,pi,g,nn,ki
      common r,pr,pi,g,nn,ki
      data nout/60/,py/3.14159265898/
      dimension x(npoint),xt(npoint),y(4,npoint),p(2,4),u(2),q(2,4),v(2),
     1  bloc(bl),ss(npoint),tt(npoint),
     1  zzf(npoint),zf(2),f(2),zff(npoint),rr(npoint),zy(npoint),
     1  f1(npoint),f2(npoint),f3(npoint),f4(npoint)
      external calcul,d01gae

      write(6,*)'r,pr,pi,g,nn,ki,x1,h'
      read(5,*)r,pr,pi,g,nn,ki,x1,h

      write(nout,994)
      write(nout,995)r,pr,pi,g,nn,ki,x1,h
      do 300 itr=1,6
      type*,'iteration=',itr
      zp1=cmplx(pr,pi)
      do 20 ii=1,2
      idy=4
      idp=2
      idq=2
      n=4
      ip=2
      iq=2

c--   bl=n*(2+max(ip,iq)+2*n)--- 108  +npoint*(n+1)*(max(ip,iq))
c     condition at x(0)
      do 2 i=1,2
      do 2 j=1,4
2     p(i,j)=0.0

      p(1,1)=1.
      p(2,2)=1.

c     condition at x(x1) (- condition 5)
      do 5 i=1,2
      do 5 j=1,4

      q(i,j)=0.
      u(i)=0.
      v(i)=0.
5     continue
      q(1,1)=1.
      q(2,2)=1.
      H=0.002
      lt=1
c     ax=1.-x1**2
c     y1=x1/ax

      do 40 k=1,npoint
      x(k)=(k-251)*x1/250.
40    continue

      call adllh2(n,npoint,x,idy,y,ip,idp,p,u,iq,idq,q,v,H,lt,bloc,calcul)
      do 41 k=1,npoint

      xt(k)=x(k)/(1.-x(k)*x(k))
      zy(k)=cmplx(y(1,k),y(2,k))
41    continue
c--   call gino
```

```
--      call t4010
--      call piccle
--      call graf(ss,tt,100,0)
--      call ginend
--      call devend
-       return

        zi=(0.,1.)
        zp=cmplx(pr,pi)
        ifail=0
        do 111 i=1,npoint

        f1(i)=xt(i)*y(1,i)*(1.+x(i)**2)/((1.-x(i)**2)**2)
11      continue
        call d01gae(x,f1,501,xx1,er,ifail)
        f(ii)=pr-(cos(ki*py)-xx1)/py
        zf(ii)=cmplx(f(ii),0.)
0       df1=real(zf(ii))
        df2=aimag(zf(ii))
        df=sqrt(df1**2+df2**2)

        if(ii.eq.2) goto 120
        if(df-(1.e-5))301,301,104
.04     write(nout,109)itr,df,pr,pi
.09     format(i4,5x,3f14.6)
        zpd=(1.e-4,0.)
        pr=pr+1.e-4
        pi=pi+0.
20      continue
120     zfd=(zf(2)-zf(1))/zpd
        zp=zp1-zf(1)/zfd
        type*,'zp,df',zp,df
        pr=real(zp)
        pi=aimag(zp)
300     continue
301     type*,'df',df,zp
        write(nout,996)
        do 302 k=1,npoint
302     write(nout,997)xt(k),(y(i,k),i=1,2)
        stop

994     format(5x, ' R     PR     PI     G      N     Chi    X1     H ')

995     format(8f7.3)
996     format(5x,'   Xt          Yr            DYr    ')
997     format(5f14.6)
998     format(4f14.6)
        end


        subroutine calcul(a,vs,x,n)
        implicit complex(z)
        real*4 x,y,ki,nn,nt
        dimension a(n,1),vs(1)
        common r,pr,pi,g,nn,ki
        data py/3.14159265898/
c-      TYPE *,'A ',A
c-      TYPE *,'VS ',VS
c-      TYPE *,'X ',X
c-      TYPE *,'N ',N

        do 14 i=1,4
        do 14 j=1,4
        a(i,j)=0.
```

```
      continue
      type*,'zp',pr,pi
      zi=(0.,1.)
      xt=x/(1.-x**2)
      a(1,2)=1.
      a(2,3)=1.
      a(3,4)=1.
      s=12.*x*(3.+x**2)/(1.-x**4)
      a1=pr*(1.+x**2)**2/(nn*(1.-x**2)**4)
      a2=-12.*(3.*(x**6)+16.*(x**4)+31.*(x**2)-2.)/((1.-x**4)**2)
      aa=a1+a2
      b1=12.*x*(x**8+6.*(x**6)+16.*(x**4)+58.*(x**2)-17.)/((1.-x**4)**3)
      b2=-2.*pr*x*(3.+x**2)*(1.+x**2)/(nn*((1.-x**2)**5))
      bb=b1+b2
      nt=((1.-x**2)**8)/((1.+x**2)**4)
      cc=(g/pr-xt**2)/(nt*nn)
      d1=24.*pr*xt*(xt**4-10.*(xt**2)+5.)/(nt*((1.+xt**2)**5))
      d2=2.*(pr**2)*xt*(3.-xt**2)/(nt*nn*((1.+xt**2)**3))
      d3=-((pr+g)*xt/(1.+xt**2)+sin(ki*py)/py)/(nn*nt)
      dd=d1+d2+d3
      a(4,1)=cc
      a(4,2)=bb
      a(4,3)=aa
      a(4,4)=s
      do 10 i=1,4
      vs(i)=0.0
10    continue
      vs(4)=dd
      type*,'vs',vs(4)
      return
      end
```

```
      program mhd
      implicit complex(z)
      parameter (bl=4800,npoint=91)
      real*4 r,pr,pi,g,s,kt,ki,prr,prl,pr2
      common r,pr,pi,g,s,c
      data nout/60/,py/3.14159265898/
      dimension x(npoint),kt(npoint),y(6,91),p(2,6),u(2),q(4,6),v(4),
     1  pp(4,6),uu(4),qq(2,6),vv(2),bloc(bl),tt(91),a(91),b(91),
     1  aa(91),bb(91),ab(91),yy(6,91),at(91),bt(91),zf(2)
      external calcul,t4010,piccle,graf,ginend,devend,cal1044
      write(6,*)'r,pr,pi,g,vn,ki,x1,h1,x2,h2'
      read(5,*)r,pr,pi,g,s,ki,x1,h1,x2,h2
332   write(nout,105)
      write(nout,106)r,pr,pi,g,s,ki
      write(nout,108)
      do 300 itr=1,6
      type*,'iteration number=',itr
      do 20 ii=1,2
      idy=6
      idp=2
      idq=4
      n=6
      ip=2
      iq=4
      c=1.
      do 1 i=1,2
      do 1 j=1,6
1     p(i,j)=0.
      p(1,2)=1.
      p(2,5)=1.
      u(1)=sin(ki*py)
      u(2)=-cos(ki*py)
      do 4 i=1,4
      do 4 j=1,6
      q(i,j)=0.
      v(i)=0.
4     continue
      q(1,1)=1.
      q(2,2)=1.
      q(3,4)=1.
      q(4,5)=1.
      h=h1
      lt=1
      do 30 k=1,npoint
      x(k)=(k-1)*x1/(npoint-1)
      ab(k)=x(k)/(1.-x(k))
30    continue
      call adllh2(n,npoint,x,idy,yy,ip,idp,p,u,iq,idq,q,v,h,lt,bloc,calcul)
      do 31 k=1,npoint
      a(k)=x(k)
      b(k)=yy(1,k)

31    continue
      b11=yy(1,1)
      b21=yy(2,1)
      b31=yy(3,1)
      b41=yy(4,1)
      b51=yy(5,1)
      b61=yy(6,1)

      idp=4
      idq=2

      ip=4
```

```
      iq=2

c     condition at x(0)
      do 2 i=1,4
      do 2 j=1,6
2     pp(i,j)=0.0
      pp(1,2)=1.
      pp(2,5)=1.
      pp(3,2)=-2.
      pp(3,3)=1.
      pp(4,5)=-2.
      pp(4,6)=1.
      uu(1)=sin(ki*py)
      uu(2)=cos(ki*py)
      uu(3)=b31-2.*b21
      uu(4)=b61-2.*b51+2.*py*g
c     condition at x(npoint) (when k- and pr-, condition 5)
      do 5 i=1,2
      do 5 j=1,6

      qq(i,j)=0.

      vv(i)=0.
5     continue
      qq(1,1)=1.
      qq(2,4)=1.

      c=-1.
      h=h2
      do 40 k=1,npoint
      x(k)=(k-1)*x2/(npoint-1)
      kt(k)=x(k)/(1.-x(k))
40    continue
      call adllh2(n,npoint,x,idy,y,ip,idp,pp,uu,iq,idq,qq,vv,
     1 H,lt,bloc,calcul)

      k1=x2/(1.-x2)
      b1=b11-y(1,1)+2.*py*pi
      b4=b41-y(4,1)-2.*py*pr
      zf(ii)=cmplx(b1,b4)
      df=sqrt(b1**2+b4**2)
      if(ii.eq.2) goto 120

      if(df-(1.e-4))301,301,104
104   write(nout,109)itr,df,pr,pi
109   format(i4,5x,3f16.6)
      zp =cmplx(pr,pi)
      zpd=(.001,.001)
      pi=pi+.001
      pr=pr+.001
20    continue
      type*,'zf(1),zf(2)',zf(1),zf(2)
120   zfd=(zf(2)-zf(1))/zpd

      zp=zp-zf(1)/zfd
      pr=real(zp)
      pi=aimag(zp)
      type*,'zp',zp
300   continue
      if(g-0.0)301,301,302
301   prl=pr-((abs(r)/2./py)**(1./2.))*cos(ki*py/2.)
     1 -1.2879*cos(ki*py)/2./py/(abs(r)**(1./3.))
      type*,'prl',prl
      goto 303
```

```
302     prl=pr-((abs(r)/2./py)**(1./2.))*cos(ki*py/2.)
     1  -1.2879*cos(ki*py)/2./py/(abs(r)**(1./3.))
        prr=prl-0.9374*g/2./(abs(r)**(2./3.))

        type*,'prl=',prl
        type*,'prr=',prr
303     write(nout,110)itr,df,pr,pi
110     format(i4,5x,3f16.6)
        write(nout,996)
105     format(5x,'    R       Re(P)       Im(P)        G
     1     N       Chi')
106     format(4x,6f10.4)
108     format(1x,'ITER            DF             Re(P)        Im(P)')

        do 41 k=npoint,1,-1
41      write(nout,997)c*kt(k),(y(i,k),i=1,2),(y(j,k),j=4,5)
        do 42 k=1,npoint,2
42      write(nout,998)ab(k),(yy(i,k),i=1,2),(yy(j,k),j=4,5)

        stop


996     format(5x,' k              Re(Y)          Re(DY)
     1    Im(Y)          Im(DY) ')
997     format(1x,f8.4,4f16.8)
998     format(1x,f8.4,4f16.8)
        end

        subroutine calcul(a,vs,x,n)
        dimension a(n,1),vs(1)
        common r,pr,pi,g,s,c

        real*4 r,pr,pi,g,s,c
        do 14 i=1,6
        do 14 j=1,6
        a(i,j)=0.
14      continue
        ax=1.-x
        cc=c*r*ax**6

        a(1,2)=1.
        a(2,3)=1.
        a(3,1)=(4.*c*r*pr*x/ax+g-2.*r*r-(pr*pr-pi*pi)*x*x/(ax**2)
     1  +4.*c*r*s*x**3/(ax**3)-s*pr*x**4/(ax**4))/cc
        a(3,2)=(2.*c*r*pr*x*x-4.*r*r*x*ax+2.*r*r*x*x*ax-2.*pr*ax**3
     1  -6.*c*r*ax**4+c*r*s*x**4/(ax**2))/cc
        a(3,3)=(6.*c*r*ax**3+pr*ax**2-r*r*x*x)*ax**2/cc
        a(3,4)=(2.*pr*x/ax-4.*c*r+s*x**3/(ax**3))*x*pi/(ax*cc)
        a(3,5)=2.*pi*(ax**3-c*r*x*x)/cc
        a(3,6)=-pi*ax**4/cc
        a(4,5)=1.
        a(5,6)=1.
        a(6,1)=-a(3,4)
        a(6,2)=-a(3,5)
        a(6,3)=-a(3,6)
        a(6,4)=a(3,1)
        a(6,5)=a(3,2)
        a(6,6)=a(3,3)
        do 10 i=1,6
        vs(i)=0.0
10      continue
        return
        end
```